UC Berkeley
UC Berkeley Electronic Theses and Dissertations

Title
The extension of bound state electronic structure methods to molecular resonances

Permalink
https://escholarship.org/uc/item/15s4j57t

Author
White, Alec Frederick

Publication Date
2017

Peer reviewed|Thesis/dissertation

eScholarship.org Powered by the California Digital Library
University of California

The extension of bound state electronic structure methods to molecular resonances

by

ALEC FREDERICK WHITE

A dissertation submitted in partial satisfaction of the

requirements for the degree of

Doctor of Philosophy

in

Chemistry

in the

Graduate Division

of the

University of California, Berkeley

Committee in charge:

Professor Martin P. Head-Gordon, Chair
Professor K. Birgitta Whaley
Professor David Graves

Spring 2017

The extension of bound state electronic structure methods to molecular resonances

Copyright 2017
by
ALEC FREDERICK WHITE

Abstract

The extension of bound state electronic structure methods to molecular resonances

by

ALEC FREDERICK WHITE

Doctor of Philosophy in Chemistry

University of California, Berkeley

Professor Martin P. Head-Gordon, Chair

In this thesis, we present our work in pursuit of black-box, *ab initio* methods for computing positions and widths of molecular resonances. The method of complex basis functions is efficiently implemented and applied in the context of various electronic structure approximations. Within the static exchange approximation, basis set effects are investigated and the method is applied to a series of N-containing heterocycles. The extension to Hartree-Fock theory allows for more accurate calculations. These methods have been applied to several small molecules, and the computation of properties within this framework is discussed. The application of complex basis functions to shape and Feshbach resonances at correlated levels of theory including Møller-Plesset perturbation theory at second order and equation of motion coupled cluster singles and doubles is also investigated from a practical perspective, and the prospect of using these methods for computing accurate potential energy surfaces is explored. Finally, we describe some theoretical and practical aspects of computing positions and widths of low-energy shape resonances by analytic continuation in the coupling constant. We find that the properties of attenuated Coulomb potentials make them ideal for such calculations.

Contents

List of Figures

List of Tables

Acknowledgments

This thesis would not have been possible without the support of many people. My two advisors, Martin Head-Gordon and Bill McCurdy, always offered helpful advice while allowing me the freedom to work on a variety of interesting topics. Leslie Silvers always made sure I was paid on time, and the US Department of Energy provided this funding via the SciDAC program. I am also grateful for scientific discussions with Thomas Rescigno, Robert Lucchese, Eleonora Luppi, and Anna Krylov.

Additionally, I need to thank my family: Kellie, David, Margot, and Nicole. Without them I would never have made it to this point. My girlfriend, Lisa Alexander, is largely responsible for making graduate school an enjoyable experience along with my friends and coworkers: Brant Abeln, Julian Azar, Luke Bertels, Noelle Catarineu, Kristi Closser, Leonel Cosio, Mickael Delcey, Scott Ellis, Evgeny Epifanovsky, Zhengting Gan, Brad Ganoe, Grace Ge, Matt Goldey, Jerome Gonthier, Loren Greenman, Diptarka Hait, Samia Hamed, Andreas Hauser, Dan Haxton, Chiara Heide, Paul Horn, Nate Karnovsky, Monatrice Lam, Royce Lam, Donghyun Lee, Joonho Lee, Susi Lehtola, Daniel Levine, Michelle Leuenberger, Matthias Loipersberger, Erum Mansoor, Sam Manzer, Yuezhi Mao, Narbe Mardirossian, Nick Mayhall, Jacob Olshansky, Katherine Oosterbaan, Julien Panetier, Aurora Pribram-Jones, Roberto Peverati, Srimukh Prasad, Walter Ralston, Eloy Ramos-Cordoba, Jake Seeley, Mark Shapero, Alex Shearer, Dave Small, Tamar Stein, David Stuck, Eric Sundstrom, Jonathan Thirman, Udi Tsivion, Jean Van Buren, Jon Weisberg, Jon Witte, Shane Yost.

Chapter 1

Introduction

1.1 Molecular resonances in chemistry and physics

Metastable states, or resonances, have played an important role in nuclear, atomic and molecular physics. These states possess a finite lifetime and are properly described using the language of scattering theory. The scattering experiment is of fundamental importance to our understanding of physics, and resonances, which are temporarily bound states of the projectile and target, lead to conspicuous features in the scattering observables.

The first direct observation of resonances in electron-molecule scattering by Schulz[1] marked the beginning of the formal study of molecular resonances[2]. This field is particularly rich because the typical lifetime of a molecular resonance can be comparable to timescales associated with the motion of the nuclei. This means that these states can play a role in chemical reactions. Resonances have been implicated as intermediates in various physical processes including the quenching of plasmas[3], the formation of molecules in interstellar space[4], and radiation damage to DNA[5]. Furthermore, the development of attosecond lasers[6] has spurred some recent interest in the field, because the energies of these laser systems, typically in the XUV range, is such that most molecules will be excited to metastable states that lie energetically above the cation[7].

Despite their importance, reliable computation of energies and lifetimes of molecular resonances is not yet routine. The goal of the work presented here is the development of black-box, systematically improvable, computational methods for molecular resonances.

1.2 The quantum theory of resonances

It is beyond the scope of this work to give a complete discussion of resonances in the quantum theory of scattering. We confine ourself to those points that are important to the body of this thesis. More detail including a general discussion of scattering theory can be found in the textbooks of Taylor[8] and Newton[9].

1.2.1 Resonances in scattering theory

In the theory of scattering due to a well-behaved, short-range potential, the S-matrix provides a map from initial states to final states that completely determines all observable aspects of the scattering process. For the spherical potential, elastic scattering problem, the S-matrix is a single-channel quantity indexed by the angular momentum quantum number l. It is related to the scalar partial wave phase shift ($\delta_l(k)$) as

$$S_l(k) = e^{2i\delta_l(k)} \tag{1.1}$$

where k is the magnitude of the wavenumber associated with the projectile. The corresponding solution to the Schrödinger equation is associated with an energy $E = \hbar^2 k^2/2m$ and behaves asymptotically as

$$u_l(r) \sim e^{-i(kr-l\pi/2)} - e^{i(kr-l\pi/2)+2i\delta_l(k)} \qquad [r \to \infty]. \tag{1.2}$$

The partial wave S-matrix for a given l is a function of k with a well-defined analytic structure. In particular, if the S-matrix has a pole at momentum k, then it has a pole at $-k^*$ and zeros at $-k$ and k^*. Furthermore, at the S-matrix pole, the solution has the simple asymptotic form

$$u_l(r) \sim e^{ikr} \qquad [r \to \infty]. \tag{1.3}$$

This is discussed in detail in Chapters 12 and 13 of Taylor[8]. The relationship between the poles of the S-matrix and the scattering states implies a physical interpretation. For example, those states on the positive imaginary axis are associated with a negative energy and must, by Equation 1.3, decay exponentially. These poles can therefore be associated with bound states. The properties of the S-matrix imply constraints on the locations of the poles such that all possible poles of the S-matrix can be placed in one of 4 categories:

(1) k on the positive imaginary axis

(2) k on the negative imaginary axis

(3) Re $k > 0$, Im $k < 0$

(4) Re $k < 0$, Im $k < 0$

As we have just stated, poles of type (1) are associated with bound states. Poles of type (2) are associated with so-called "virtual states." We will not discuss these states further, but a good discussion can be found in [10]. Poles of type (4) are reflections of those of type (3) and have little physical importance due to distance from the positive real axis. As we will see, the poles of type (3) are associated with resonances, or quasi-bound states.

The poles of type (3) occur at energies

$$E = E_r - i\Gamma/2, \tag{1.4}$$

with $E_r, \Gamma > 0$. The properties of the S-matrix also imply that there is a zero at $E_r + i\Gamma/2$. We can write an expression that parameterizes $S_l(E)$ near such a pole in a manner consistent with this structure and the unitarity of the S-matrix:

$$S_l(E) = e^{2i\delta_l^0(E)} \frac{E - (E_r + i\Gamma/2)}{E - (E_r - i\Gamma/2)}. \tag{1.5}$$

The quantity $\delta_l^0(E)$ is called the background phase shift and parameterizes the variations in the S-matrix not due to the pole. We will assume that the background phase shift is a slowly varying function of energy. This is generally a very good approximation in the vicinity of a pole. Using Equation 1.1, we may solve for the total phase shift:

$$\delta_l(E) = \delta_l^0(E) + \delta_l^R(E) \qquad \delta_l^R(E) \equiv \arctan\left[\frac{\Gamma/2}{E_r - E}\right]. \tag{1.6}$$

Assuming that the background phase shift is zero, we may compute the partial wave cross section as

$$\sigma_l(k) = \frac{4\pi}{k^2}(2l+1)\sin^2\delta_l(k) = \frac{4\pi}{k^2}(2l+1)\frac{\Gamma^2/4}{(E-E_r)^2 + \Gamma^2/4}. \tag{1.7}$$

This function is sharply peaked about $E = E_r$ which implies that poles just off the real energy axis are associated with peaks in the cross section. In the case that the background phase shift is large, we can say more generally that these poles are associated with sharp features in the cross section.

It remains to show that these sharp features can be associated with a temporarily bound, or metastable, state. From an analysis of wavepacket dynamics[11], it can be shown that the time-delay, Δt, is related to the phase shift as

$$\Delta t = 2\hbar \frac{d\delta}{dE}. \tag{1.8}$$

The relationship between the S-matrix and the phase shift given in Equation 1.1 then implies that

$$\Delta t = -i\hbar \frac{dS}{dE} S^*. \tag{1.9}$$

For the case of resonant scattering described in Equation 1.6 the time delay has the form

$$\Delta t = \frac{\hbar\Gamma}{(E - E_r)^2 + 1/4\Gamma^2} + 2\hbar \frac{d\delta_l^0}{dE} \tag{1.10}$$

and is clearly peaked about the resonance energy. A peak in the time-delay implies a temporarily bound complex of projectile and target. This is how resonances appear in the elementary theory of potential scattering. The extension to multichannel collision theory introduces some complications but retains the essential features (see Chapter 2 of Ref. [12], Chapter 18 of Ref. [8], and Ref. [13]).

1.2.2 Resonances as quasi-stationary states

Consider the solution to the radial Schrödinger equation at an S-matrix pole given in Equation 1.3. For a resonance, the pole of type (3) occurs at a complex momentum with a positive real part and a negative imaginary part

$$k = k^R - ik^I. \tag{1.11}$$

This implies a solution that behaves asymptotically as

$$u_l(r) \sim e^{ik^R r} e^{k^I r} \qquad [r \to \infty] \tag{1.12}$$

which diverges exponentially. It is clear that this is not really a physically realizable quantum state, but if we define a "resonance wavefunction" as

$$\phi_{\text{res}}(r) = \frac{u_l(r)}{r}, \tag{1.13}$$

where u_l has the asymptotic behavior given in Equation 1.12, then we may write the time-dependent wavefunction associated with this state as

$$\psi_{\text{res}}(r,t) = \phi_{\text{res}}(r) e^{-iE_r t/\hbar} e^{-i\Gamma t/2\hbar}. \tag{1.14}$$

This is called a Gamow state or occasionally a Siegert state. It is a solution to the Schrödinger equation with pure outgoing wave boundary conditions given in Equation 1.3 in contrast to the physical boundary conditions of Equation 1.2.

These Gamow states are odd solutions to the Schrödinger equation in that they diverge exponentially for any time as $r \to \infty$ and they decay exponentially for any point in space as $t \to \infty$. They correspond to a "density" of the form

$$|\psi_{\text{res}}(r,t)|^2 = |\phi_{\text{res}}(r)|^2 \, e^{-\Gamma t/\hbar}, \tag{1.15}$$

and only in a limit where both r and t go to infinity can we think of particle number of these states as a conserved quantity. Nevertheless, this heuristic analysis shows that we may think of resonances as corresponding to solutions to the time-independent Schrödinger equation. In this context, they correspond to *quasi*-stationary solutions which decay in time with a characteristic lifetime of

$$\tau = \frac{\hbar}{\Gamma}. \tag{1.16}$$

1.2.3 The Siegert energy

We have now shown how, starting from language of elementary scattering theory, we may think of resonances as temporarily bound states and quasi-stationary states. In either case, we can associate with the resonance a complex energy called a Siegert energy:

$$E = E_r - i\Gamma/2. \tag{1.17}$$

The Siegert energy is the location of a pole of the S-matrix and the imaginary part encodes the time-decay of the associated Gamow state. We can also connect this complex energy to a simple perturbative treatment of a bound state coupled to a continuum by a matrix element V_{fi}. In this case we can use, for example, Fermi's golden rule to write the rate of transitions as

$$\Gamma = 2\pi |V_{fi}|^2 \delta(E_f - E_i). \tag{1.18}$$

This width leads to an exponential decay in the simplest picture of time-dependence. In this picture, the probability density decays in time as

$$P(r,t) = P(r,0) e^{-\Gamma t/\hbar} \tag{1.19}$$

which can be thought of as arising from a probability amplitude of the form

$$\psi(r,t) = \phi_{\text{res}}(r) e^{-i(E_r - i\Gamma/2)t/\hbar}. \tag{1.20}$$

The result is a state with an effectively complex energy that decays exponentially in time exactly as the Gamow state. This offers another interpretation of a resonance as a bound state coupled to a continuum.

The Siegert energy is a powerful way to mathematically encode the properties of a resonance. However, it is worth considering the limitations of this parameterization. In particular, we have assumed that the resonance is close to the real axis (long-lived) and that the background scattering is small. If this assumption is not valid, then the Siegert energy will not be a useful parameterization without more information about the background scattering processes. Furthermore, in the case of nearby resonances, the Siegert energy gives no direct information about interference-type effects associated with the two resonances.

1.2.4 Molecular resonances

Electronic resonances in molecular systems are considerably more complicated due to the many electronic and nuclear degrees of freedom of the target. They can be observed in both electron scattering and photo-ionization experiments[2] and they are often observed indirectly in the cross-sections for various kinds of molecular fragmentation[14, 15].

Resonances in a many-body system can be loosely divided into two classes: shape resonances and Feshbach resonances. Shape resonances decay by a one-particle, tunneling mechanism, while Feshbach resonances decay by a mechanism involving more than 1 degree of freedom. Molecular resonances are usually easy to place in one of these two categories, because they be can be described as adding an electron to one or more "parent states" of the associated target molecule. Resonances that lie energetically above at least one parent will be shape resonances in general. Resonances that are lower in energy than their parent states can only decay by a mechanism involving a change in the target state and are therefore Feshbach resonances. The distinction between shape and Feshbach resonances is shown schematically in Figure 1.1. Though these concepts are not always well defined, most molecular resonances can be classified in this way.

1.3 Molecular electronic structure theory

In order to compute the properties of molecular resonances, we use the ideas of the previous section in the context of the many-body molecular electronic problem. In atomic units, the electronic Hamiltonian for a system of N electrons and M nuclei

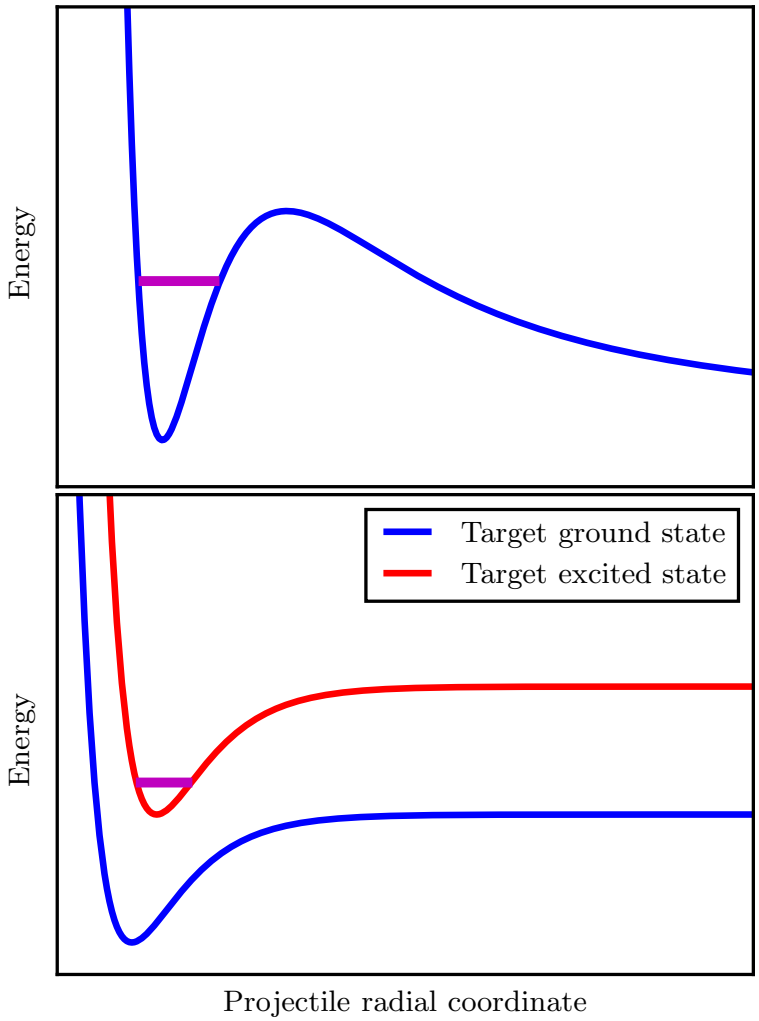

Figure 1.1: Schematic representation of the difference between shape (top) and Feshbach (bottom) resonances. The position of the resonance is shown in magenta. A shape resonance can decay by a 1-particle tunneling mechanism, while the Feshbach resonance can only decay by correlated de-excitation of the target.

is given, within the Born-Oppenheimer approximation, by

$$H = -\frac{1}{2}\sum_{i=1}^{N}\boldsymbol{\nabla}_i^2 + \sum_{i=1}^{N}\sum_{j=i+1}^{N}\frac{1}{|\mathbf{r}_i - \mathbf{r}_j|} - \sum_{i=1}^{N}\sum_{\alpha=1}^{M}\frac{Z_\alpha}{|\mathbf{r}_i - \mathbf{R}_\alpha|} + V_{\mathrm{nn}}, \tag{1.21}$$

where Z_α is the charge of the αth nucleus and V_{nn} is the nuclear-nuclear repulsion. An exact solution to this problem scales as the exponential of the number of electrons. An exact solution is therefore impractical for all but the smallest systems. The approximate solution of this equation is the subject of molecular electronic structure theory, and the basics are described in various monographs[16, 17]. In this section, we will describe those points of direct importance to this work.

1.3.1 Mean-field states and the orbital picture

The typical zero-order picture of a many-fermion system is one in which each particle occupies a single-particle state according to an effective single-particle Hamiltonian that includes electron-electron interactions at the mean-field level. These single particle wavefunctions are called orbitals, and the energy to ionize the system by removing a particle from a particular orbital is the associated orbital-energy. More formally, such a mean-field state can be obtained for a system of electrons by minimizing the energy of a single Slater determinant. This simple wavefunction properly accounts for the anti-symmetry of the wavefunction with respect to the interchange of any pair of electronic coordinates, but it only includes the electron-electron interaction in an approximate sense. These orbitals are solutions to the single particle Schrödinger-like equation,

$$f(i)\phi_i(\mathbf{r}) = \epsilon_i\phi_i(\mathbf{r}), \tag{1.22}$$

where the Fock operator for the ith electron, $f(i)$, is defined such that

$$f(i)\phi_j(\mathbf{r}_i) = -\frac{1}{2}\boldsymbol{\nabla}_i^2\phi_i(\mathbf{r}) - \sum_{\alpha=1}^{M}\frac{Z_\alpha}{|\mathbf{r}_i - \mathbf{R}_\alpha|}\phi_i(\mathbf{r}) + \sum_{j=1}^{N}\langle\phi_i\phi_j|\,|\phi_i\phi_j\rangle\,. \tag{1.23}$$

Our notation for the matrix elements of the electron-electron repulsion operator is standard and described in many places (see for example Chapter 2 of Szabo and Ostlund[16]). Note that the operator depends on the single particle orbitals, so this equation must be solved self-consistently. In practice, this is done in a finite basis of single particle functions $\{\chi_\mu(\mathbf{r})\}$ which are usually Gaussians, and the solution to this problem is obtained from the Roothaan-Hall equations:

$$\mathbf{FC} = \mathbf{SC}\epsilon. \tag{1.24}$$

Here the bold indicates a matrix quantity and the coefficient matrix gives the expansion coefficients for the orbitals in the 1-particle basis set:

$$\phi_i(\mathbf{r}) = \sum_\mu C_i^\mu \chi_\mu(\mathbf{r}). \tag{1.25}$$

ϵ is a diagonal matrix of orbital energies, and the overlap matrix, $\mathbf{S}$ is simply

$$S_{\mu\nu} = \langle \chi_\mu |\, \chi_\nu \rangle \,. \tag{1.26}$$

In computational chemistry, this is called the Hartree-Fock method. For closed shell systems, the wavefunctions are usually further constrained such that all occupied orbitals are doubly occupied with electrons of opposite spin. This is called restricted Hartree-Fock (RHF). For open-shell systems, the determinant of maximum m_s may be described by constraining most orbitals to be doubly occupied with the open-shell orbitals singly occupied. This is called restricted open-shell Hartree-Fock (ROHF). Allowing an entirely different set of orbitals for different spins is called unrestricted Hartree-Fock (UHF). These are the most common variants of Hartree-Fock, though others exist. We will further discuss some features of the computational realization of this method is Section 1.3.3. Density functional theory(DFT)[18], which will not be described here, is also based on the orbital picture and shares many computational features with Hartree-Fock.

The single-orbital picture suffers from an incomplete description of the electron-electron interaction, but nevertheless provides a valuable, easy to interpret wavefunction that is the starting point for most more sophisticated theories. Despite its limitations, the orbital picture is more than just a computational tool; it is the basis upon which chemists build their understanding of complicated, many-electron systems.

1.3.2 Electron correlation

Electron correlation is broadly defined as those pieces of the energy and wavefunction that are missing from the Hartree-Fock determinant. In a finite basis, the correlation energy can be more precisely stated as the difference between the full configuration interaction (FCI) energy and the Hartree-Fock energy. The FCI energy is obtained by minimizing the energy of a wavefunction expanded in all possible configurations. It is the exact energy within a finite 1-particle basis set. The correlation energy can be obtained approximately, and the three most common approximations are truncated configuration interaction (CI), Møller-Plesset perturbation theory, and coupled cluster theory.

The idea of truncating CI expansions by excitation level comes from the representation of the exact (FCI) wavefunction as

$$|\Psi\rangle = |\Psi_0\rangle + \sum_{ia} c_i^a |\Psi_i^a\rangle + \sum_{i<j,a<b} c_{ij}^{ab} \left|\Psi_{ij}^{ab}\right\rangle \dots \tag{1.27}$$

where $|\Psi_0\rangle$ is the Hartree-Fock determinant. This ansatz is discussed in Chapter 4 of Szabo and Ostlund[16]. By truncating this expansion at a certain point, we are left with a tractable, linear-variational problem. The correlation energy for an arbitrary CI expansion is easily shown to be

$$\begin{aligned} E_c &= \langle\Psi_0| H - E_0 |\Psi\rangle & (1.28)\\ &= \sum_{ia} c_i^a \langle\Psi_0| H |\Psi_i^a\rangle + \sum_{i<j,a<b} c_{ij}^{ab} \left\langle\Psi_0\right| H \left|\Psi_{ij}^{ab}\right\rangle. & (1.29) \end{aligned}$$

The singles term usually vanishes due to Brillouin's theorem leaving only the doubles term. Truncation at the level of double excitations to give a CI with singles and doubles (CISD) wavefunction is usually sufficient to recover the majority of the correlation energy for small molecules. The advantages of this method stem from its simple, linear-variational wavefunction ansatz. These include a variational energy and a simple extension to excited states. Unfortunately, such expansions suffer from a lack of size consistency. Given two non-interacting subsystems, A and B, size-consistency is the property that

$$E(AB) = E(A) + E(B), \tag{1.30}$$

and this is not true in general for energies computed from truncated CI wavefunctions. This means that the quality of the method will deteriorate as the system size is increased.

We may also account for the correlation energy using perturbation theory. Many different types of perturbation theory are possible, but the most successful has been Møller-Plesset[19] perturbation theory which partitions the Hamiltonian as

$$H = F + \phi \qquad \phi \equiv H - F. \tag{1.31}$$

Here we have used F as the many-body Fock operator. At first order, we simply recover the Hartree-Fock energy, while at second order, we get the first contribution to the correlation energy:

$$E^{(2)} = -\sum_{ia} \frac{|F_i^a|^2}{\epsilon_a - \epsilon_i} - \frac{1}{4} \sum_{ijab} \frac{|\langle ab| |ij\rangle|^2}{\epsilon_a + \epsilon_b - \epsilon_i - \epsilon_j}. \tag{1.32}$$

The term involving the Fock operator is usually zero due to Brillouin's theorem. Unlike truncated CI, Møller-Plesset perturbation theory at 2nd order (MP2) *is* size-consistent. Unfortunately, the accuracy of the method is limited by the low order perturbation theory, and it is very difficult to use this theory to obtain accurate excited state energies. This theory is discussed in detail in Chapter 6 of Szabo and Ostlund[16] and Chapter 14 of Helgaker[17].

The coupled cluster method, in its modern formulation, is based on an exponential ansatz (see Chapter 13 of Helgaker[17]),

$$|\Psi\rangle = e^T |\Phi_0\rangle , \tag{1.33}$$

where $|\Phi_0\rangle$ is the Hartree-Fock determinant and T is the cluster operator. If we use μ to index all possible excitations, then the cluster operator can be written as

$$T = \sum_\mu t_\mu \hat{\tau}_\mu \tag{1.34}$$

where τ_μ is an operator that generates the μth excited determinant when acting on the Hartree-Fock reference. Grouping excitations by singles, doubles, triples, etc. we can write T as

$$T = T_1 + T_2 + T_3 + \ldots \tag{1.35}$$

This non-linear expansion contains enough parameters to recreate the full-CI wavefunction, but at an even greater cost. We can generate computationally tractable theories by truncating T at a given excitation level. Truncating at doubles, $T = T_1 + T_2$, is called coupled cluster singles and doubles (CCSD), while truncating at the triples level, $T = T_1 + T_2 + T_3$, is called coupled cluster singles, doubles, and triples (CCSDT). Determining the T-amplitudes in a variational manner is not practical, even for truncated CC. In practice the energy and amplitudes are determined from the projected Schrödinger equation after left-multiplication by e^{-T}:

$$\left\langle \Phi_0 \right| \bar{H} \left| \Phi_0 \right\rangle = E \qquad \left\langle \Psi_\mu \right| \bar{H} \left| \Phi_0 \right\rangle = 0 \qquad \bar{H} \equiv e^{-T} H e^T. \tag{1.36}$$

Truncated coupled cluster approximations are not variational when determined in this way, but they are size-consistent. Furthermore, a powerful excited state method can be obtained from the equation-of-motion formalism which leads to a CI-like ansatz on top of a CC ground state[20, 21]. The wavefunction has the form

$$|\Psi_{\mathrm{EOM}}\rangle = R e^T |\Phi_0\rangle , \tag{1.37}$$

where R is a sum of excitation operators,

$$R = \sum_\mu r_\mu \hat{\tau}_\mu. \tag{1.38}$$

The amplitudes can be determined from the solution of a linear-variational (CI-like) problem.

These methods are all acceptable in situations where the correlation energy that we wish to compute is due to a large number of determinants making small contributions to the exact wavefunction. This "dynamic" correlation is well described by these methods which all tacitly assume that the Hartree-Fock determinant is the most important. However, there is another type of correlation. "Non-dynamic" or "static" correlation is due to multiple determinants entering the FCI expansion with large or even equal weight. In this situation, the single-reference methods that we have just described break down. The most common solution to this problem is to partition the orbital space into a space that is doubly occupied in all important determinants, a space that is unoccupied in all determinants, and an active space in which the FCI problem is explicitly solved. This procedure combined with orbital optimization is called the complete-active-space self-consistent field (CASSCF) method[22]. Though often effective in practice, this method is very limited in scope, difficult to use, and tends to neglect dynamic correlation. The development of methods to address systems with strong non-dynamic correlation effects is a subject of current research.

1.3.3 Computational implementation

In order for any of these methods to be usable in practice, an efficient implementation is of paramount importance. The technology to efficiently evaluate the electron repulsion integrals, accelerate the convergence of non-linear optimizations, and efficiently contract very large tensors has proven critical in making large molecular calculations practical.

Most of the time in an HF or DFT calculation is spent evaluating the 6-dimensional electron-repulsion integrals:

$$\langle \mu\nu |\, \lambda\sigma \rangle = \int d^3r_1 \int d^3r_2 \chi^*_\mu(\mathbf{r}_1)\chi^*_\mu(\mathbf{r}_2)\frac{1}{r_{12}}\chi_\lambda(\mathbf{r}_1)\chi_\sigma(\mathbf{r}_2). \tag{1.39}$$

Gaussian basis functions are almost always used because there exists a variety of recurrence based approaches to evaluate the integrals in an efficient manner[23]. While the naïve scaling of the computation is the number of basis functions to the 4th power, the sparsity[24] and/or low-rank properties of the ERI tensor can be leveraged to create lower-scaling and/or computationally more efficient schemes.

The expense of any HF/DFT calculation can also be significantly decreased by developing methods to accelerate the convergence of the iterative optimization of the wavefunction. Techniques for non-linear optimization,[25] as well as the direct

inversion of the iterative subspace method of Pulay[26, 27] have been instrumental in decreasing the cost of such calculations. The solution of the CCSD equations must also be accomplished iteratively, and can be accelerated in similar ways. The iterative solution of large eigenproblems or large linear systems that appear in CI/CC methods can be viewed in similar terms, and development of iterative, memory-efficient schemes for these problems has enabled calculations on increasingly large systems[28].

Finally, for CI/CC calculations the ability to efficiently multiply large tensors while encoding the appropriate space, spin, and permutational symmetry will largely determine the efficiency of the implementation[29]. Software frameworks for accomplishing exactly these goals have been developed over the last several years for a variety of different architectures[30, 31].

1.3.4 Challenges for molecular resonances

The electronic structure of molecular resonances presents several computational difficulties even without considering the continuum nature of such states. They are usually open-shell, sometimes high in energy relative to the ground state, and they can sometimes decay into multiple channels. In order to accurately describe the electronic structure of such states, we require a balanced treatment of a potentially large number of open-shell states having different number of electrons. The mean-field picture is rarely sufficient for such a problem, and electron correlation effects are important to obtain even qualitative accuracy. Because of this difficulty, it is important that any practical method for computing the properties of molecular resonances is able to effectively utilize the accuracy and efficiency of existing bound state quantum chemistry infrastructure.

1.4 Computational methods for molecular resonances

Existing methods, including those further described in this work, can be loosely divided into 4 classes of methods. Scattering methods directly solve the full scattering problem with the goal of computing scattering observables like cross-sections. Stabilization techniques use the behavior of continuum eigenvalues in bound state calculations to determine the positions, and sometimes widths of resonances. Generalized complex coordinate methods compute Siegert energies as the eigenvalues of some effective, non-Hermitian Hamiltonian. Methods based on extrapolation, or analytic continuation of bound state energies can compute positions and sometimes

widths of low-lying resonances from purely bound state calculations. It would be impossible to include a detailed explanation of each, so we confine ourselves to a brief description of the advantages and disadvantages of each class of method.

1.4.1 Scattering methods

Methods that directly compute scattering observables have a long history in quantum mechanics. For the molecular problem at low energies, the most useful such methods are the R-matrix method[12, 32], the Schwinger multichannel method[33], and the complex Kohn method[34]. Each of these methods has its own set of advantages and disadvantages, but their unifying advantage is the direct computation of observable cross-sections. In the case that one wants to directly compute these observables, there is little choice but to use such a method. Unfortunately, these methods are generally quite expensive, difficult to converge with respect to the basis set/discretization, and can suffer from numerical artifacts.

1.4.2 Stabilization

Stabilization calculations, originally suggested in the molecular context by Taylor[35, 36], rely on the fact that a resonance corresponds to a peak in the density of states of the continuum. This means that as some parameter is varied, the continuum roots will stabilize and there will be avoided crossings at the location of the resonance. An analytic continuation of these avoided crossings can allow for computation of the position and widths of molecular resonances.[37–39] Unfortunately, the analytic structure of the problem leads to several difficulties, and it can be hard to obtain results that are not dependent on the specifics of the procedure[40].

1.4.3 Complex coordinate methods

Complex coordinate methods are related to the theorems of Balslev, Aguilar and Combes[41, 42], and Simon[43]. These theorems state that, for an ensemble of particles interacting via coulomb potentials, scaling the coordinate of the Hamiltonian by a complex number $e^{i\theta}$ results in the following:

1. the bound spectrum is unchanged

2. the continuum is rotated into the lower-half plane by an angle of 2θ

3. for large enough θ, new eigenvalues are "uncovered" and these appear at the Siegert energies (poles of the S-matrix) and correspond to square-integrable eigenfunctions.

While not formally applicable to the molecular problem in the Born-Oppenheimer approximation, the appropriate extension, termed "exterior complex scaling" was developed by Barry Simon[44]. The difficulty of numerically accomplishing exterior complex scaling has spurred the development of a host of related methods with the goal of computation. These include an application of complex scaling to finite-basis matrix elements[45], complex basis functions[46], and smooth exterior scaling[47]. These methods have the great advantage that they attempt to compute a square-integrable function and can be applied within the context of bound-state electronic structure theory. Unfortunately, the non-Hermitian formalism can lead to numerical difficulties, and the implementation is often non-trivial.

A highly related method is based on the addition of a complex absorbing, usually negative-imaginary, potential (CAP or sometimes NEP)[48–51]. These methods can be shown to be related to smooth-exterior scaling[52], and share many features of other complex-coordinate methods. The CAP method has the advantage that implementation in quantum chemistry codes is fairly straightforward, but care must be taken so that the addition of the CAP does not effect the problem in unphysical ways.

1.4.4 Analytic continuation methods

Finally, there are methods based on analytic continuation of bound state energies. In this class of methods, a short-range potential is added to the Hamiltonian to make the resonance bound, and the bound state energies are analytically continued to determine the complex, resonance energy at zero coupling strength[53–55]. The analytic continuation is an inherently unstable procedure for higher energy resonances, but it has the advantages that very little code development is required and any bound state method can be used.

1.5 Outline

The body of this thesis is concerned with the development of *ab initio* approaches to compute positions and widths of molecular resonances. The first three chapters describe the theory, efficient implementation, and application of complex basis function methods in the context of different levels of approximate electronic structure theory. The final chapter describes work towards a practical analytic continuation

technique for computing positions and widths of low-energy shape resonances. Chapters 2,3, and 5 have appeared as journal articles in the Journal of Chemical physics. Chapter 4 has been submitted.

1.5.1 Chapter 2

The method of complex basis functions for computing positions and widths of molecular shape resonances is revisited. An open-ended and efficient implementation is described. The basis set requirements of the complex basis are investigated within the computationally inexpensive static-exchange approximation, and the results of this investigation lead to a hierarchy of basis sets for complex basis function calculations on small molecules. These basis sets are then applied in static-exchange calculations on some larger molecules with multiple low energy shape resonances: carbon tetrafluoride, benzene, pyridine, pyrimidine, pyrazine, and s-triazine. The results indicate that more sophisticated methods using complex basis functions are worth pursuing in the search for accurate and computationally feasible methods for computing resonance energies in molecular systems. The content of this chapter has been published in the Journal of Chemical Physics (AF White, M Head-Gordon, and CW McCurdy, *J. Chem. Phys.* **142** 054103 (2015))[56].

1.5.2 Chapter 3

This work describes the implementation and applications of non-Hermitian self-consistent field (NH-SCF) theory with complex basis functions for the *ab initio* computation of positions and widths of shape resonances in molecules. We utilize both the restricted open-shell and the previously unexplored spin-unrestricted variants to compute Siegert energies of several anionic shape resonances in small diatomic and polyatomic molecules including carbon tetrafluoride, which has been the subject of several recent experimental studies. The computation of general molecular properties from a non-Hermitian wavefunction is discussed, and a density-based analysis is applied to the $^2B_1$ shape resonance in formaldehyde. Spin-unrestricted NH-SCF is used to compute a complex potential energy surface for the carbon monoxide anion which correctly describes dissociation. The content of this chapter has been published in the Journal of Chemical Physics (AF White, CW McCurdy, and M Head-Gordon *J. Chem. Phys.* **143** 074103 (2015))[57].

1.5.3 Chapter 4

The method of complex basis functions is applied to molecular resonances at correlated levels of theory. Møller-Plesset perturbation theory at second order and equation-of-motion electron attachment coupled-cluster singles and doubles (EOM-EA-CCSD) methods based on a non-Hermitian self-consistent-field reference are used to compute accurate Seigert energies for shape resonances in small molecules including N_2^-, CO^-, CO_2^-, and CH_2O^-. Analytic continuation of complex θ-trajectories is used to compute Seigert energies, and the θ-trajectories of energy differences are found to yield more consistent results than those of total energies. The ability of such methods to accurately compute complex potential energy surfaces is investigated, and the possibility of using EOM-EA-CCSD for Feshbach resonances is explored in the context of e-helium scattering. The content of this chapter has been submitted for publication in the Journal of Chemical Physics as "Second order Møller-Plesset and coupled cluster singles and doubles methods with complex basis functions for resonances in electron-molecule scattering" by Alec F. White, Evgeny Epifanovsky, C. William McCurdy, and Martin Head-Gordon.

1.5.4 Chapter 5

The computation of Siegert energies by analytic continuation of bound state energies has recently been applied to shape resonances in polyatomic molecules by several authors. We critically evaluate a recently proposed analytic continuation method based on low order (type III) Padé approximants as well as an analytic continuation method based on high order (type II) Padé approximants. We compare three classes of stabilizing potentials: Coulomb potentials, Gaussian potentials, and attenuated Coulomb potentials. These methods are applied to a model potential where the correct answer is known exactly and to the $^2\Pi_g$ shape resonance of N_2^- which has been studied extensively by other methods. Both the choice of stabilizing potential and method of analytic continuation prove to be important to the accuracy of the results. We conclude that an attenuated Coulomb potential is the most effective of the three for bound state analytic continuation methods. With the proper potential, such methods show promise for algorithmic determination of the positions and widths of molecular shape resonances. The content of this chapter has been published in the Journal of Chemical Physics (AF White, M Head-Gordon, and CW McCurdy *J. Chem. Phys.* **146** 044112 (2017))[58].

Chapter 2

Complex basis functions: Implementation and applications within the static exchange approximation

2.1 Introduction

Over the past 40 years, complex coordinate methods have proven to be useful for the computation of Siegert energies of atomic and molecular resonances[52, 59–61]. Originally motivated by the theorems of Aguilar, Balslev and Combes[41, 42], and Simon[43], these methods involve some analytic continuation of the Hamiltonian to generate a non-Hermitian effective Hamiltonian that includes in its spectrum discrete, complex, Siegert energies corresponding to square-integrable eigenfunctions.

Unfortunately, the extension of the mathematically rigorous techniques to the molecular problem in the Born-Oppenheimer (fixed-nuclei) approximation, is not straightforward. Of the many suggested solutions to this problem, the most popular method has been to add to the molecular Hamiltonian a complex-absorbing-potential (CAP)[48–51]. This method is related to complex scaling[62, 63] and simple to apply, but suffers from a significant dependence of the complex-energies on the form of the CAP and a perturbation of the bound state energies[64]. These issues have been largely overcome in recent work using a density matrix approach[65], however calculations with CAPs have indicated that the application of this method to Feshbach resonances is not straightforward[66, 67].

The complex basis function technique of McCurdy and Resigno[46] does not suf-

fer from the same problems, but is difficult to implement in an efficient manner. Even so, many older calculations[68–74] as well as some more recent calculations by Honigmann *et al*[75–78] have demonstrated the practicality of the method. Specifically, the method of complex basis functions has been shown to provide a description of molecular resonances including polarization effects in the context of complex restricted open-shell Hartree-Fock (ROHF)[70, 71, 73, 76]. Calculations using a multiconfigurational self-consistent field (MCSCF)[74] or multi-reference configuration interaction (MRCI)[75–78] wavefunction are capable of describing correlation and are therefore applicable to Feshbach resonances. However, these previous applications have been limited to atoms and diatomic molecules and there has been no systematic investigation of the basis set requirements of this method. In fact, despite the numerous complex-coordinate and CAP methods, there are only a few investigations of the basis set requirements. Specifically, there has been recent work on the basis set requirements of CAP methods[79], construction of Gaussian basis sets for Rydberg and resonance states of helium[80], and on construction of complex STO-NG basis sets for photoionization calculations of atoms and diatomic molecules[81].

In the present study, an efficient implementation of the method of complex basis functions within the static-exchange approximation is used to explore the basis set requirements of the method, and some applications to shape resonances in larger molecules are presented.

In the static-exchange (SE) approximation, the orbitals of the target are assumed to be frozen, but exchange effects are taken into account. It is the simplest approximation that could be expected to yield qualitatively correct results for low-energy shape resonances. SE calculations have been used to generate guesses for ROHF calculations employing complex basis functions[71], but the static-exchange energies are not reported. The SE approximation is not particularly useful for quantitative estimates of Siegert energies, but its simplicity makes it ideal for investigations of basis set convergence. Also, as the fastest method, it will always be the only practical method for the largest systems.

2.2 The Method of Complex Basis Functions

The method of complex basis functions, originally introduced by McCurdy and Recigno[46], uses the unscaled molecular Hamiltonian in a basis set including Gaussian functions with complex exponents. The justification originally given is that a matrix element of the complex scaled Hamiltonian over basis functions of a real valued coordinate can be equivalently written as a matrix element of unscaled Hamiltonian over basis functions with a complex coordinate. In a Gaussian basis this is

asymptotically equivalent to using basis functions with complex exponents. This method is equivalent to analytic continuation of the matrix elements of the Hamiltonian which was shown by Moiseyev and Corcoran[45] to effectively avoid the non-analyticities introduced by complex scaling in the Born-Oppenheimer approximation.

Another justification can be made by applying the complex variational principle[82–84] to the exterior scaled molecular electronic Hamiltonian $\tilde{H}$. The spectrum of the exterior scaled, non-dilatation-analytic, molecular electronic Hamiltonian has been rigorously shown to mimic the behavior of the spectra of complex scaled dilatation-analytic Hamiltonians[44]. Applying the complex variational principle to the exterior scaled Hamiltonian we get that:

$$\frac{(\psi|\tilde{H}|\psi)}{(\psi|\psi)} = E_{\text{trial}}. \tag{2.1}$$

This provides a stationary approximation to the true Siegert energy, where the rounded brackets indicate that the c-product[83], where the bra is not complex conjugated, is used, and $|\psi)$ is some c-normalizable trial function. A change of variables followed by a contour distortion reveals one may just as well search for stationary points of the functional

$$\frac{(\tilde{\psi}|H|\tilde{\psi})}{(\tilde{\psi}|\tilde{\psi})} = E_{\text{trial}} \tag{2.2}$$

where $|\tilde{\psi})$ is also just a c-normalizable function. Note that the transformation is also applied to the denominator so as to absorb the Jacobian of the transformation into the new trial function $|\tilde{\psi})$. In this sense, the method of complex basis functions can be viewed as a finite basis approximation to exterior complex scaling, a point that was argued by Morgan and Simon[85].

In theory, any c-normalizable basis can be used, but in practice Gaussian basis sets are a practical choice because the Gaussian product theorem greatly simplifies the computation of multicenter integrals. In order to reproduce as closely as possible the correct asymptotic form of the matrix elements of the exterior scaled Hamiltonian, a mixed one-electron basis set of tight real Gaussians and diffuse Gaussians with complex exponents will be used. The complex Gaussians have the form

$$\begin{aligned} \phi_\theta(r) &= N(\theta)(x - A_x)^l (y - A_y)^m (z - A_z)^n \\ &\times \exp\left[-\alpha e^{-2i\theta}(\boldsymbol{r} - \boldsymbol{A})^2\right] \end{aligned} \tag{2.3}$$

where θ mimics the rotation angle in traditional complex scaling, and $N(\theta)$ is a normalization factor. Although the problem has been reduced to a finite basis set

expansion, the requirements of this complex basis have the potential to be complicated and problem dependent. It then becomes necessary, as in traditional complex scaling calculations, to do a variational search in an auxiliary parameter. This one-electron basis is convenient because it has much in common with the basis sets of electronic structure theory including manageable analytic schemes for computing two-electron integrals.

In the simplest approximation, molecular anions can be described by the static-exchange Hamiltonian

$$H = h_{\text{core}} + 2J - K \tag{2.4}$$

where orbitals of the N electron target are fixed, and the density is used to generate J and K. The core orbitals are assumed to be doubly occupied and can be generated with a restricted Hartree-Fock (RHF) calculation in a basis of purely real functions. The matrix representation of H in the basis of particle configurations including complex basis functions is diagonalized to get approximations to the Seigert energies of the $N + 1$ electron state. This simple method reduces to building a Fock matrix using a real N-electron density in a basis including complex basis functions, then diagonalizing the virtual block to get new, complex, virtual orbital energies which correspond to complex energies of the $N+1$ electron state. If the full Fock matrix is diagonalized, the first N orbital energies should correspond to the ionization energies needed to access various $N-1$ electron states. These energies should closely approximate the real occupied orbital energies obtained in the initial N electron calculation since they are not self-consistent. The static-exchange approximation is generally a quite poor approximation, but the low cost of the method allows for a detailed study of basis set requirements and application to shape resonances in some larger molecules.

An example of this method applied to N_2^- is shown in Figure 2.1. In this case the full Fock matrix was diagonalized in a basis including complex Gaussians to get energies of $N - 1$ and $N + 1$ electron states. The process was repeated for θ going from 0.5^o to 30^o in intervals of 0.5^o. Detailed plots of the behavior of continuum, bound, and resonance roots are shown in Figure 2.2. The low energy continuum roots are rotated into the lower half plane at an angle of approximately θ as in complex scaling. The energies of the $N-1$ electron states which are all bound remain mostly real with the small imaginary part attributable to basis-set incompleteness. The well-characterized $^2\Pi_g$ shape resonance stands out clearly from the continuum, and the stationary point is easily identified with the Siegert energy.

Though the stationary points are almost always recognizable from visual inspection, a method to identify them consistently and precisely is desirable. This is accomplished via analytic continuation of the energy of the resonance as a function of θ[71].

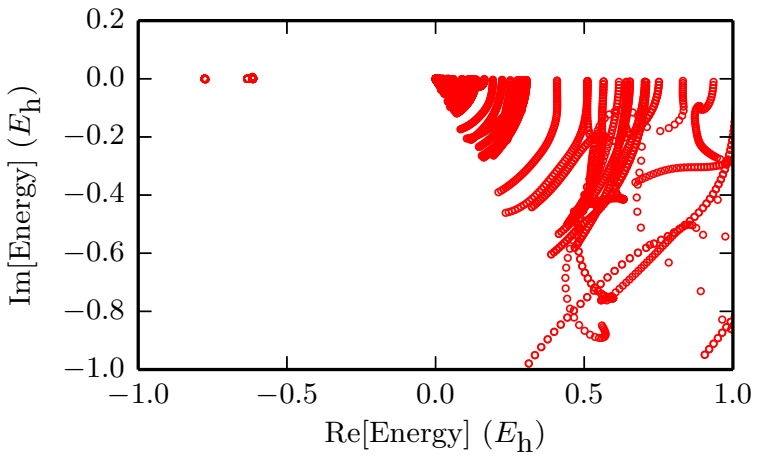

Figure 2.1: Theta trajectories for N_2^- in the caug-cc-pVTZ(cm+) basis.

The "point method" of Schlessinger[86] is used to construct a rational interpolant that goes through all the available points. This interpolant is constructed from a continued fraction representation that is equivalent to an [N/M] Pade Approximant given $N + M + 1$ energy points. The continued fraction has the form

$$C(\theta) = \frac{E(\theta_1)}{1+}\frac{a_1(\theta-\theta_1)}{1+}\cdots\frac{a_n(\theta-\theta_n)}{1} \tag{2.5}$$

where the coefficients a_i are determined from the conditions that the function passes through the specified points. The derivative of the continued fraction can be found analytically, and the zeros of this function can be computed using Newton's method. In this way, the variational stationary point with respect to the scaling parameter can be found by fitting the complex energies from any variational calculation performed at a series of θ values to a Pade approximant and numerically finding the solution of

$$\left.\frac{dE_{\text{trial}}(\theta)}{d\theta}\right|_{\theta_s} = 0. \tag{2.6}$$

The value of θ_s found in this way can be complex-valued, corresponding to an overall real scaling of the complex exponents. Allowing θ to obtain a complex value has been shown to be important in finding the truly stationary point[87], but in practice the imaginary parts of the optimal θ are found to be generally less than 0.05. An example of the application of this method to N_2^- is shown in Figure 2.3. The stationary point was computed from the θ-trajectory in the caug-cc-pVTZ(cm+) basis (○) which will

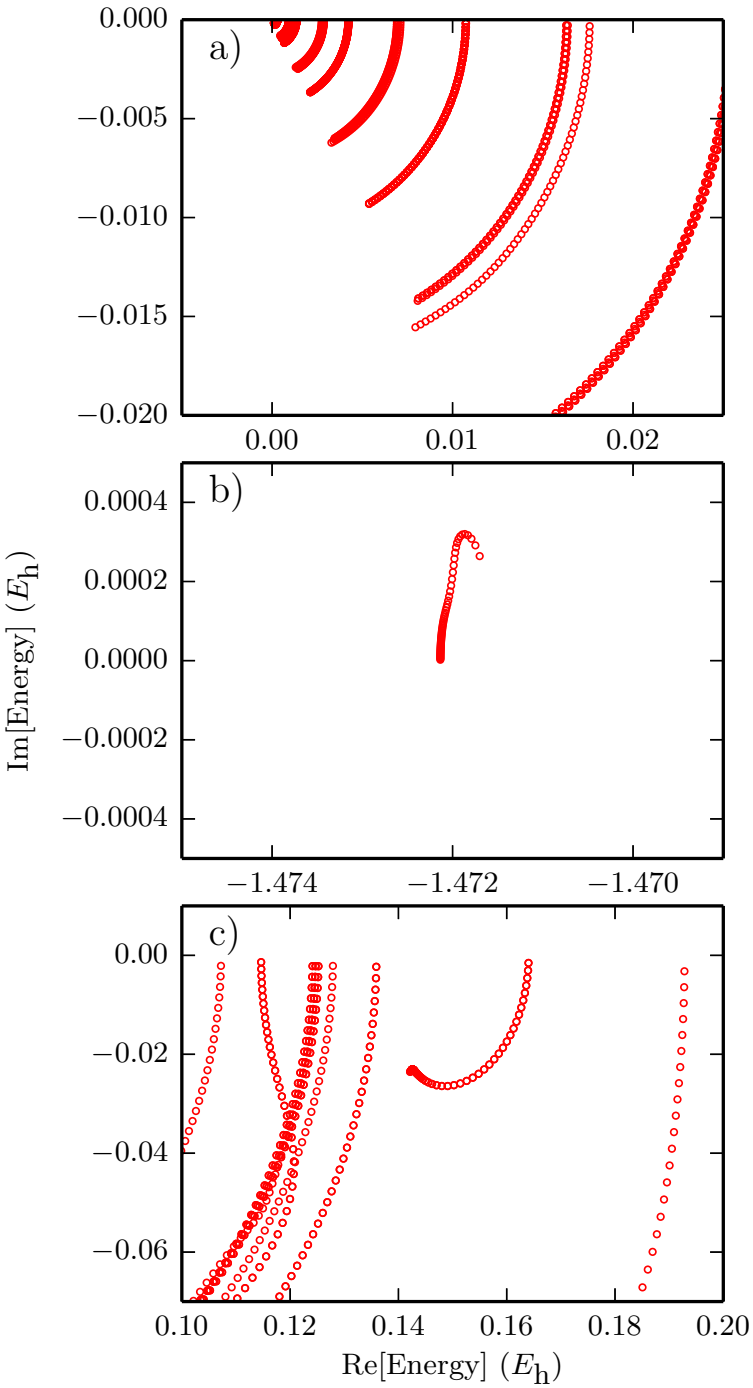

Figure 2.2: Detailed plots of continuum (a), bound (b), and resonance (c) eigenvalues from Fig 2.1.

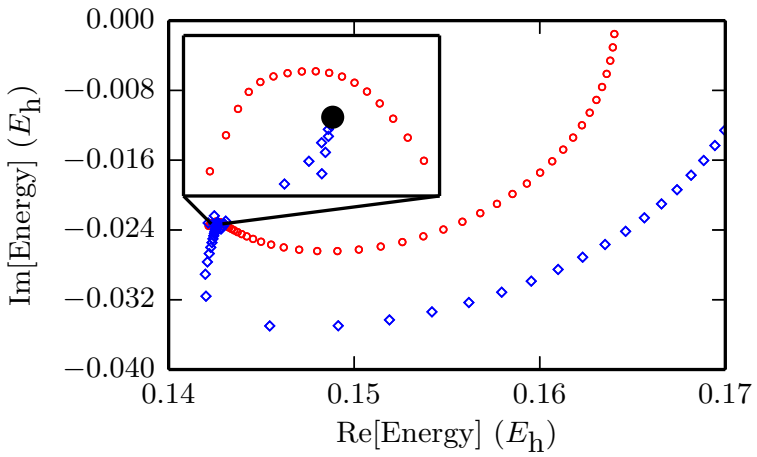

Figure 2.3: Plot of resonance theta trajectory (○), stationary point (●), and theta trajectory with optimized exponents (◇). The optimized exponents correspond to an optimal value of $\theta = 0.408 + i0.040$.

be described in Section 2.4. Given the approximation to the stationary θ_s found in this way, the complex exponents in the basis were scaled so that the resulting curve (◇) should pass through the stationary point. This result shows the validity of this analytic continuation method. In practice, this method is assumed to give an accurate value for the stationary energy if the computed stationary energy and θ-value lie close to the actual trajectory.

The wavefunction corresponding to the complex SE energy is of course square integrable and is not unlike the orbitals obtained from bound state calculations. However, because of the complex normalization, the magnitude of the wavefunction does not integrate to one, and it is instead the real part of the complex density

$$\rho(\mathbf{x}) = (\phi|\mathbf{x})(\mathbf{x}|\phi) = \phi(\mathbf{x})^2 \tag{2.7}$$

that will integrate to 1. The normalization also guarantees that the imaginary part of the density is traceless. These quantities are visualized for a typical case (one component of the π_g resonance orbital, N_2, c-aug-cc-pVTZ(cm+) basis) at the stationary value of θ in Figure 2.4. In the valence region, the wavefunction resembles a π_g antibonding orbital. At larger distances the oscillations characteristic of complex-scaled wavefunctions become apparent. These oscillations are shown in more detail in Figure 2.5. Despite the prominent oscillations in real and imaginary parts of the wavefuctions, the real part of the density has only very small oscillations and largely resembles the density of a real bound state orbital.

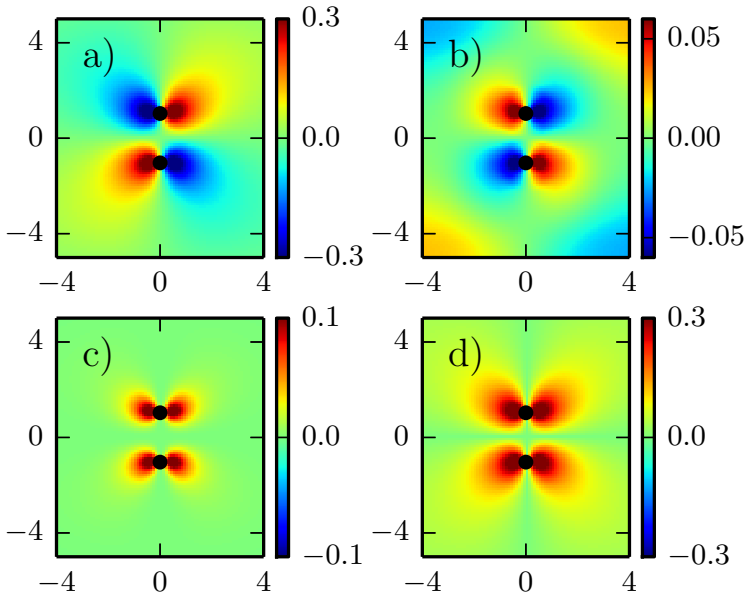

Figure 2.4: Contour plots in the xz-plane of the real part (a), imaginary part (b), and magnitude (d) of the resonance orbital as well as the real part of the resonance density (c). The atomic centers are denoted by (•), and the z-axis is the molecular axis. Both axes are in atomic units (a_0)

2.3 Implementation

The static-exchange method using complex basis functions has been implemented in the Q-Chem electronic structure package[88]. The Armadillo C++ linear algebra library was used for all matrix operations[89].

The basis set representation of the Hamiltonian in a c-orthonormal complex basis requires one- and two-electron integrals common to standard electronic structure methods. The one-electron integrals are computed using general explicit formulas originally given by Taketa et al[90] These formulas are also valid for Gaussian basis functions with complex exponents, α, provided that $\mathrm{Re}[\alpha] > 0$.

The computation of the two-electron integrals, also called electron repulsion integrals (ERIs), can be computed in the same manner as in standard electronic structure codes. Unlike in previous implementations of complex basis functions, the integrals are computed directly and never explicitly stored as is common in modern electronic structure programs. The recursion relations common in ERI evaluation are in general the same for basis functions with complex exponents. The Head-Gordon Pople

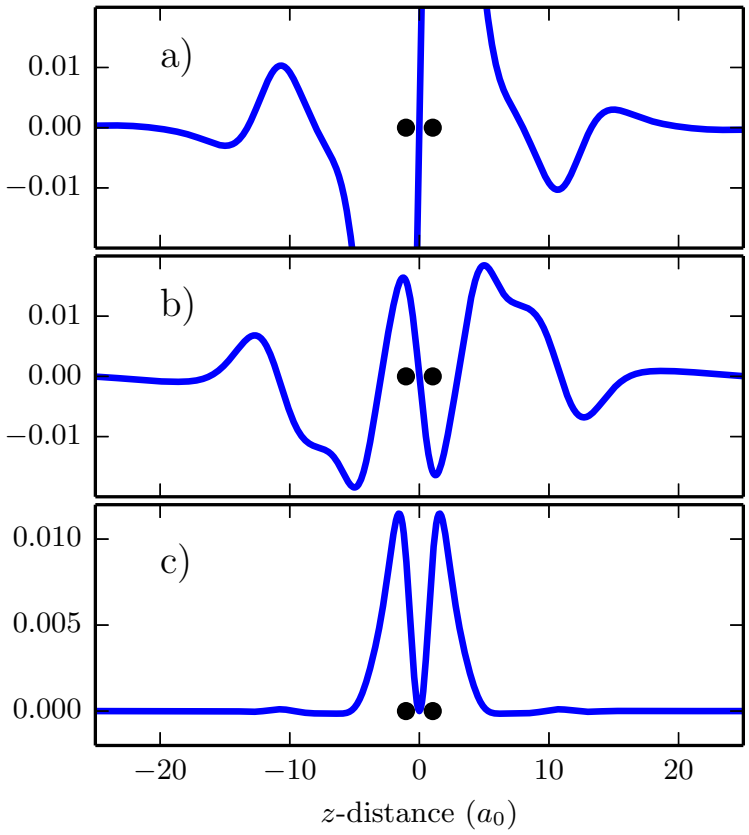

Figure 2.5: Plots along the line $x = 2, y = 0$ a_0 of the real part (a) and imaginary part (b) of the xz-component of the resonance orbital, and the real part of the complex density (c). The positions of the atomic centers along the z-axis are denoted by (•)

(HGP)[91] method and one path (operator, contraction, momentum, and density or OCLD) of the COLD-PRISM[92] method, both implemented in Q-Chem, were appropriately modified for complex arithmetic. These evaluation schemes are both based on the recurrence relations of Obara and Saika[93] and additionally on those of McMurchie and Davidson[94] in the case of the COLD-PRISM. These recurrences have the same analytic form when exponents are complex as long as $\mathrm{Re}[\alpha] > 0$.

As in the real case, the first step in ERI evaluation is the computation of the Boys function,

$$F_m(T) = \int_0^1 t^{2m} e^{-Tt^2} dt \tag{2.8}$$

where the index m runs from 0 to $l_a + l_b + l_c + l_d$ and T depends on the exponents

and centers of the 4 basis functions. For basis functions with complex exponents, T is complex. In the case of real basis functions, this step is often accelerated using Chebyshev interpolation[95]; however, an interpolation scheme for complex F as a function of complex T is necessarily two-dimensional and is significantly more difficult. Instead, the Boys functions is computed on the fly when it is evaluated for complex T. For small values of T ($|T| < 10$), F is computed for the maximum required m according to

$$F_m(T) = \frac{1}{2}e^{-T}\Gamma\left(m+\frac{1}{2}\right)\sum_{n=0}^{\infty}\frac{T^n}{\Gamma(m+n+3/2)} \tag{2.9}$$

where the sum is truncated when the terms become negligible. The Boys function for the remaining values of m is computed by recursion:

$$F_{m-1}(T) = \frac{1}{2m-1}[2TF_m(T) + e^{-T}]. \tag{2.10}$$

For large T ($|T| \geq 10|$), the downward recursion becomes unstable, so $F_0(T)$ is computed by the explicit formula,

$$F_0(T) = \frac{1}{2}\sqrt{\frac{\pi}{T}}\mathrm{erf}\left(\sqrt{T}\right) \tag{2.11}$$

and recursion is used to compute F for the remaining values of m:

$$F_{m+1}(T) = \frac{(2m+1)F_m(T) - e^{-T}}{2T}. \tag{2.12}$$

After the Boys function has been computed for a given shell-quartet of integrals, the application of the recursion relations proceeds as in the real case. This implementation is sufficiently general so as to also allow for Hermitian calculations using complex basis functions. The algorithm described here provides at least 11 significant figures in the relevant regions of the complex plane, and an algorithm capable of providing machine accuracy has been described elsewhere[96].

In the Hermitian case it is common to ignore certain shell-quartets that can be shown to be negligible due to the so-called Schwarz bound[24], but for a non-Hermitian calculation this bound does not apply because the ERIs are not positive definite.

The implementation of the required matrix manipulations is straightforward, though some care must be taken with notions of orthogonality and unitarity. In the complex, bi-orthogonal space relevant to the problem, complex-orthogonal (c-product preserving) matrices replace unitary matrices. In all relevant cases, the

eigenvectors of a complex-symmetric matrix can be made c-orthonormal so that the matrix of eigenvectors is complex-orthogonal. However, if two eigenvalues lie close together, there is no guarantee that the eigenvectors found by a general non-symmetric eigensolver will have this property. Therefore, a modified Gram-Schmidt method that utilizes the c-product must be used to ensure that the matrix of eigenvectors obtained from a complex-symmetric matrix are complex-orthogonal.

2.4 Basis Sets

The reduction of the scattering problem to a variational search within a basis set is undoubtedly a simplification of the problem, but the requirements and convergence properties of the c-normalizable basis set are not known. It is therefore of great practical importance to explore the basis set requirements of a typical molecular shape resonance and construct a hierarchy of basis sets for general applications.

2.4.1 Requirements for a complex basis

In previous applications of complex basis functions, knowledge of the symmetry of the resonance was generally used to pick the basis set on a case by case basis[71, 72]. While this method can be successful, it is difficult to apply in cases where the symmetry of the resonance is not known or the molecule has low symmetry. This method also precludes using the same basis set to describe multiple resonances. In addition to being sufficiently general to describe resonances of different symmetry, an ideal hierarchy of basis sets would be computationally practical, converge to the basis set limit, and have a well-defined relationship with the real basis sets of quantum chemistry that have already been optimized for bound states.

As in many types of basis set calculations, linear dependence in the basis can be a problem. This is a particular difficulty for complex basis function calculations, because the matrix playing the role of the metric is not a Hermitian matrix. Also, any analytic continuation scheme will suffer if basis functions are discarded in a discontinuous manner. Ideally, linear dependence should be avoided.

A further problem is that there is no guarantee that the complex energy will have only one stationary point as a function of θ. This is not necessarily surprising, because θ is a highly non-linear parameter. However, the basis set should be large enough that artificial stationary points associated with basis set incompleteness are avoided.

In practice these requirements will be impossible to satisfy for all systems. In the following sections, the $^2\Pi_g$ resonance in N_2^- at an inter-nuclear distance of 1.094Å is

used as a typical example of a molecular shape resonance. The basis set requirements of this system are explored in detail and simple generalizations are made about basis sets for general molecular resonances. In all cases, the static-exchange energies were computed for $\theta = 0^\circ$ to $\theta = 30^\circ$ at intervals of 0.5°. The analytic continuation scheme described earlier is used to precisely find the stationary point in the complex plane.

2.4.2 The role of diffuse complex functions

In order to explore the role of diffuse complex basis functions in the description of the resonance, shells of d-functions on the center of the molecule or shells of p-functions on each nitrogen were added one by one. In both cases, an even-tempered set of functions with a spacing of 2.3 and starting at 1.75×10^2 is used. The most diffuse exponent in this series is $\alpha = 1.24 \times 10^{-4}$. Table 2.1 shows the resonance energy with added complex functions using 6-31G* as the real basis. As expected, tight functions alone do not allow for any description of the resonance, and it is only with functions with exponents on the order of 1 that the resonance can be found at all. In both cases, the resonance energy converges, and functions beyond a certain diffuseness are not necessary. However the energies with p-functions and with d-functions converge to slightly different values. This can be attributed to the tight p-functions which may be necessary to describe the resonance near the nuclei.

The same calculations were performed in the cc-pVQZ real basis set and the results are also shown in Table 2.1. For this particular resonance, there is relatively little change in the limiting results as the real basis is changed from 6-31G* to cc-pVQZ. Similar conclusions can be drawn about the relevant range of exponents necessary for describing the resonance, but in the larger basis, the calculations involving p-functions and those involving d-functions converge to almost the same energy. This is likely because the real basis is much closer to completeness, and adding tight p-functions is redundant.

This importance of the tight complex functions is examined by systematically removing the shells of tight functions. The results for 6-31G* and for cc-pVQZ are shown in Table 2.2. As expected, the tight d-functions are not necessary for describing the resonance, and the tight p-functions are only necessary in the case of an incomplete real basis. In other words, only the diffuse functions need be complex. This makes physical sense because the functions with complex exponents are necessary to implicitly apply correctly decaying outgoing wave boundary conditions in the asymptotic region where only diffuse functions are significantly non-zero.

# of shells	6-31G*				cc-pVQZ			
	d-functions		p-functions		d-functions		p-functions	
	Re[E]	Im[E]	Re[E]	Im[E]	Re[E]	Im[E]	Re[E]	Im[E]
7	4.6810	-0.0196			4.2293	-0.0001		
8	4.6837	-0.0157	4.5570	-0.0043	4.2259	-0.0147	4.1875	-0.0339
9	4.6790	-0.0149	4.5550	-0.0099	4.2265	-0.0204	4.1831	-0.0147
10	3.9172	-0.5155	3.7876	-0.5816	3.8171	-0.6080	3.7750	-0.5298
11	3.8808	-0.5662	3.8503	-0.6390	3.8120	-0.7023	3.8721	-0.6071
12	3.8489	-0.5778	3.8449	-0.5999	3.8228	-0.6372	3.8329	-0.6072
13	3.8799	-0.6000	3.8499	-0.6023	3.8299	-0.6306	3.8440	-0.6126
14	3.8859	-0.6099	3.8507	-0.6033	3.8534	-0.6197	3.8461	-0.6151
15	3.8874	-0.6134	3.8509	-0.6037	3.8545	-0.6200	3.8466	-0.6160
16	3.8878	-0.6147	3.8509	-0.6038	3.8534	-0.6208	3.8468	-0.6164
17	3.8879	-0.6151	3.8510	-0.6039	3.8534	-0.6209	3.8468	-0.6165
18	3.8880	-0.6153	3.8510	-0.6039	3.8534	-0.6210	3.8468	-0.6165

Table 2.1: Energy of the $^2\Pi_g$ resonance in N_2 as more shells of functions are added to the center (d-functions) or to the two Nitrogen atoms (p-functions). The real basis is 6-31G* or cc-pVQZ.

# of shells	6-31G*				cc-pVQZ			
	d-functions		p-functions		d-functions		p-functions	
	Re[E]	Im[E]	Re[E]	Im[E]	Re[E]	Im[E]	Re[E]	Im[E]
18	3.8880	-0.6153	3.8510	-0.6039	3.8534	-0.6210	3.8468	-0.6165
17	3.8880	-0.6151	3.8511	-0.6029	3.8534	-0.6210	3.8467	-0.6156
16	3.8880	-0.6144	3.8482	-0.6008	3.8534	-0.6210	3.8456	-0.6120
15	3.8880	-0.6123	3.8625	-0.5488	3.8534	-0.6210	3.8507	-0.5888
14	3.8878	-0.6065	3.9110	-0.4755	3.8534	-0.6209	3.8270	-0.5922
13	3.8866	-0.5912	3.8925	-0.5100	3.8533	-0.6209	3.8311	-0.5949
12	3.8757	-0.5560	3.8806	-0.5322	3.8528	-0.6202	3.8289	-0.6123
11	3.8619	-0.5687	3.8680	-0.5504	3.8523	-0.6193	3.8592	-0.6260
10	3.8354	-0.5988	3.8376	-0.5967	3.8513	-0.6173	3.8532	-0.6168
9	3.9209	-0.5921	3.9195	-0.5928	3.8399	-0.6120	3.8410	-0.6114
8	3.8225	-0.5561	3.8238	-0.5555	3.8039	-0.6361	3.8042	-0.6354

Table 2.2: Energy of the $^2\Pi_g$ resonance in N_2 as tight functions are removed. The real basis is 6-31G* and cc-pVQZ.

2.4.3 The role of the even-tempered spacing

The role of the even-tempered spacing is explored in the 6-31G* and cc-pVQZ basis sets (Table 2.3). The even-tempered spacing of the added complex functions was systematically changed, and the number of shells was changed as well so that the exponents span roughly the same range. The largest exponent was 1.75×10^2 in all cases, and the smallest exponent is shown in Table 2.3.

The two most striking effects are that the energies in the smaller basis are more sensitive to the even-tempered spacing than the energies in the larger basis, and that the energies computed with complex d-functions are much more sensitive than those computed with complex p-functions. The first of these effects is easily attributable to the incompleteness of the real basis. The second is likely due to the fact that for the d-functions centered in the middle of the molecule, the even-tempered spacing affects the behavior near the two nitrogen centers. This accounts for the oscillatory behavior of the energy as the even-tempered spacing is changed. The basis set is clearly starting to break down around an even-tempered spacing of 2.8, and the spacing of 2.3 that was used in the previous calculations is relatively conservative.

2.4.4 General scheme: caug-cc-pVXZ(cm+) basis sets

In general, the angular momentum requirements of the basis set will be highly problem-dependent. A flexible one-electron basis set should therefore contain complex functions on multiple centers so that functions of very high angular momentum can be avoided. Something akin to Dunning's scheme of adding diffuse functions to each center[97] is necessary so that the complex part of the basis is flexible enough to describe molecular resonances of different character. However, this protocol will often be accompanied by problems with linear dependence that can be avoided by a single center expansion. For this reason, it seems advisable to combine atom-centered and center of mass complex basis functions to define a viable basis set.

In this section, a general scheme for complex basis sets for small molecules is presented. This scheme, which will be referred to as the caug-cc-pVXZ(cm+) (X = D,T,Z,...), consists of the real correlation consistent basis sets[98], each angular momentum augmented by a shell of complex functions with diffuse of on each center. Additionally, diffuse complex functions with maximum angular momentum equal to the maximum angular momentum of the real basis are added on the center of mass. The atomic centered diffuse functions have the same exponents as the corresponding aug-cc-pVXZ[97] basis set but scaled by the complex number $e^{-2i\theta}$. The diffuse functions on the center of mass are even-tempered, and start at one even-tempered spacing more diffuse than the most diffuse atom-centered function.

spacing	# of shells	min. exponent	6-31G*				cc-pVQZ			
			d-functions		p-functions		d-functions		p-functions	
			Re[E]	Im[E]	Re[E]	Im[E]	Re[E]	Im[E]	Re[E]	Im[E]
2.0	21	1.67E-04	3.9652	-0.6177	3.8443	-0.6020	3.8503	-0.6219	3.8448	-0.6245
2.1	20	1.32E-04	3.8540	-0.6858	3.8454	-0.6095	3.8512	-0.6302	3.8441	-0.6264
2.2	19	1.20E-04	3.9177	-0.6781	3.8330	-0.6041	3.8379	-0.6232	3.8414	-0.6280
2.3	18	1.24E-04	3.8880	-0.6153	3.8493	-0.5989	3.8534	-0.6210	3.8468	-0.6165
2.4	17	1.44E-04	3.9819	-0.6141	3.8382	-0.6214	3.8210	-0.6191	3.8405	-0.6411
2.5	16	1.88E-04	3.8161	-0.5814	3.8316	-0.5866	3.8472	-0.6156	3.8316	-0.6023
2.6	16	1.04E-04	3.7830	-0.6030	3.8576	-0.5855	3.8360	-0.6617	3.8398	-0.6110
2.7	15	1.60E-04	3.9430	-0.5933	3.8647	-0.5850	3.8404	-0.6131	3.8719	-0.6188
2.8	14	2.68E-04	3.7497	-0.6779	3.8621	-0.5629	3.8365	-0.6123	3.8122	-0.6521
2.9	14	1.71E-04	3.7493	-0.7132	3.8205	-0.6684	3.8770	-0.6776	3.8129	-0.6706
3.0	14	1.10E-04	3.7589	-0.7482	3.8601	-0.6863	3.8911	-0.6752	3.8275	-0.6953
3.2	13	1.52E-04	3.8589	-0.5229	3.7144	-0.5637	3.8161	-0.6162	3.8097	-0.5811
3.4	12	2.49E-04	3.8812	-0.8710	3.6648	-0.6613	3.9321	-0.6563	3.9324	-0.6885
3.6	12	1.33E-04	3.8138	-0.5460	3.9349	-0.4971	3.9490	-0.6439	3.9524	-0.6583

Table 2.3: Energy of the $^2\Pi_g$ resonance in N_2 as the even tempered spacing of the added complex functions is changed. The real basis sets are 6-31G* and cc-pVQZ. The even tempered series was extended so that the exponents are of more than sufficient diffuseness based upon the results of section 2.4.2.

In the following calculations, an even-tempered spacing of 2.3 was used for all center of mass functions. The DZ basis was augmented with 7 shells of s-functions, 7-shells of p-functions, and 6-shells of d-functions. The TZ basis also includes 5 shells of f-functions, and the QZ basis additionally includes 4 shells of g-functions. These are very large basis sets and are probably larger than necessary in terms of both the even-tempered spacing and the diffuseness of the center of mass functions. However, despite the large number of basis functions including some very diffuse functions, linear dependence is not a problem when these basis sets are used for small molecules.

Table 2.4 shows resonance energies of N_2^- (Π_g), CO_2 (Π_u), and formaldehyde (B_1). Since the symmetry of these resonances are known, the caug-cc-pVXZ(cm+) basis sets are not the most efficient choice, since they are based on the presumption that the symmetry of the resonance is not known *a priori*. Furthermore, the simple nature of these resonances means that even the smallest of these basis sets offers a good descriptions of the resonance with the possible exception of CO_2. Indeed the reasonable energy of the Π_u resonance of CO_2 in the caug-cc-pVDZ(cm+) basis is a bit surprising since the atomic centered p-functions would be expected to provide only a limited description of a diffuse π_u orbital. The important point is that these basis sets offer a systematic way to examine the convergence of a Siegert energy with respect to basis set size in the context of the method of complex basis functions. The QZ basis used here is by far the largest basis set hitherto employed in this kind of calculation.

For larger molecules, the center of mass is less important, and this basis set scheme is likely not ideal. Something akin to a double or triple augmentation on each center would likely be most effective, but linear dependence is a serious problem for such a scheme, and an effective method for dealing with linear dependence will likely be necessary to perform reliable calculations on large, asymmetric molecules.

2.5 Applications

In this section, Siegert energies are calculated using the method described above for more complicated molecules with multiple resonances. These energies are compared with literature and experiment and some features of the method are explored.

2.5.1 Overlapping resonances in carbon tetrafluoride

Carbon tetrafluoride has been observed to have two low energy shape resonances of A_1 and T_2 symmetry. A summary of older experimental results can be found in

Basis	N_2		CO_2		CH_2O	
	Re[E]	Im[E]	Re[E]	Im[E]	Re[E]	Im[E]
caug-cc-pVDZ(cm+)	3.9752	-0.6363	5.5268	-0.2972	2.6848	-0.8078
caug-cc-pVTZ(cm+)	3.8818	-0.6301	5.5035	-0.3435	2.6459	-0.7887
caug-cc-pVQZ(cm+)	3.8413	-0.6215	5.4733	-0.3500	2.5775	-0.8170
geometry	N≡N(1.094Å)		C=O(1.16Å)		CH(1.11Å), C=O(1.205Å), H-C-H(116.2º)	

Table 2.4: SE energies of resonances in N_2, CO_2 and formaldehyde as the basis size is increased

Ref. [99]. More recently, CF_4 has been the subject of some studies of orientation effects in dissociative electron attachment processes that may proceed through these resonances[100, 101].

The resonance energies of the two lowest shape resonances of CF_4 (C-F = 1.33Å) are reported in Table 2.5 along with other calculations from the literature. The complex basis function results show the T_2 resonance position to be lower in energy than that of the A_1 resonance which is in agreement with most of the previous theoretical and experimental results. The best theoretical treatment to date is the Schwinger multichannel calculations of Ref [102] in the static-exchange plus polarization (SEP) approximation. The method goes beyond the static-exchange approximation, but the Schwinger method requires a basis set representation of the potential that can introduce an unknown amount of error. The complex basis function calculations reported here are the only calculations to date that provide any idea of convergence to the basis set limit. Based on the energies in the different caug-cc-pVXZ basis sets, it is likely that these energies are within 0.05 eV of the basis set limit. This provides a valuable benchmark for evaluating different basis sets and methods.

2.5.2 Low energy resonances of some nitrogen-containing heterocycles

In this section, we compare energies of some low energy shape resonances in benzene and a series of nitrogen-containing hetercycles (pyridine, pyrimidine, pyrazine, s-triazine). This series of molecules was first studied in detail by Pisanias et al.,[106] and later by Nenner and Schulz[107], who suggested that pyrazine, s-triazine, and possibly pyrimidine have bound anions while benzene and pyridine have only low energy resonances. These results are shown in Table 2.6; note that the energies of bound anions are from polarography experiments and not directly from scattering experiments. Shortly afterward, Mathur and Hasted[108, 109] reported observing low energy temporary anions in benzene, pyrimidine, and pyrazine (see Table 2.7) in apparent contradiction to the results of Nenner and Schulz. There has since been conflicting reports on the sign of the electron affinity of pyrazine as noted by Song et al.[110], who also noted that clusters of various sizes and components will have bound anions even if the gas phase monomer does not.

CCSD(T) calculations in the aug-cc-pVTZ basis were performed on the neutral and anionic forms of these molecules at geometries optimized at the DFT-ωB97X-V level of theory. The results of these calculations are shown in Table 2.8. These results strongly suggest that these anions are unbound, but have limited quantitative value since these EAs will converge to 0 as the basis set size is increased. This justifies the

reference	T_2 resonance		A_1 resonance		method/basis
	Position	Width	Position	Width	
Huo[103]	6.6	4.1	11.7	22.8	Schwinger Variational(SE)
Modelli et al[104]	8.95	-	8.70	-	Multiple Scattering-Xα
Modelli et al[104]	8.58	-	8.98	-	Continuum Multiple Scattering-Xα
Winstead et al[105]	11.5	-	13.0	-	Schwinger Multichannel (SE)
Varella et al[102]	9.9	-	11.0	-	Schwinger Multichannel (SEP)
this work	10.6301	2.0553	12.7184	2.0902	caug-cc-pVDZ(cm+)
this work	11.0816	1.9737	12.0561	1.9617	caug-cc-pVTZ(cm+)
this work	11.0410	1.9090	12.1620	1.9621	caug-cc-pVQZ(cm+)

Table 2.5: Calculated positions and widths (eV) of low energy shape resonances in CF_4. Static-exchange plus polarization is abbreviated SEP.

Benzene	Pyridine	pyrimidine	pyrazine	s-triazine
1.14	0.62	0.0	-0.4	-0.45
	1.20	0.77	0.87	
4.85	4.58	4.24	4.10	4.0

Table 2.6: Positions (eV) of the lowest three resonances/anions of benzene, pyridine, pyrimidine, pyrazine, and s-triazine from Ref. [107]

Benzene	Pyridine	pyrimidine	pyrazine
1.086	0.79	0.33	0.08
	1.15	0.82	0.92

Table 2.7: Positions (eV) of the lowest two resonances of benzene, pyridine, pyrimidine, and pyrazine as reported in Ref. [108] and [109]

	Benzene	Pyridine	Pyrimidine	Pyrazine	s-Triazine
vertical		1.0390	0.6766	0.3987	0.4685
adiabatic	0.7878	0.8246	0.4183	0.1417	0.2015

Table 2.8: Vertical and adiabatic electron affinities (eV) calculated with CCSD(T) in the aug-cc-pVTZ basis. The "vertical" EA's were determined from calculations both done at the geometry of the neutral while for the "adiabatic" EA, the anion geometry was optimized separately.

use of scattering/complex-coordinate methods for these states.

The results in the static-exchange approximation are shown in Table 2.9. In two cases, multiple stationary points were found from the same θ-trajectory. The reported value is the stationary point that occurs at a complex θ that is closest to values of the θ actually used in the computation. In practice however, these multiple stationary points lie quite close together. An example of this behavior is shown in Figure 2.6. The two stationary points are viable from the θ-trajectory, but differ by an amount that is significantly less than either the error from the static-exchange approximation or from basis set incompleteness. It is likely that these molecules represent close to the upper limit of the usefulness of basis sets including center of mass functions. A double or triple augmentation on each atomic center would likely provide a more complete and more efficient representation of the resonances.

Despite the crudeness of the static-exchange approximation, these energies reproduce the qualitative trends of the experimental data. This is demonstrated in

benzene(e_{2u}, b_{2g})		pyridine(b_1, a_2, b_1)		pyrimidine(a_2, b_1, b_1)		pyrazine(b_{3u}, a_u, b_{2g})		s-triazine(e'', a_2')'	
Re[E]	Im[E]	Re[E]	Im[E]	Re[E]	Im[E]	Re[E]	Im[E]	Re[E]	Im[E]
3.1301	-0.2647	2.6493[1]	-0.1861	2.3639	-0.1430	2.1014	-0.1877	2.2702[1]	-0.0814
		3.0235	-0.2260	2.7557	-0.1681	2.8270	-0.1661		
9.4337	-1.2197	9.2772	-1.1519	8.9607	-0.9640	8.8174	-0.8005	8.1209	-0.6744

Table 2.9: Complex energies (eV) of the lowest three resonances of benzene, pyridine, pyrimidine, pyrazine, and s-triazine in the static-exchange approximation. The basis set is caug-cc-pVDZ(cm+).

[a]multiple stationary points

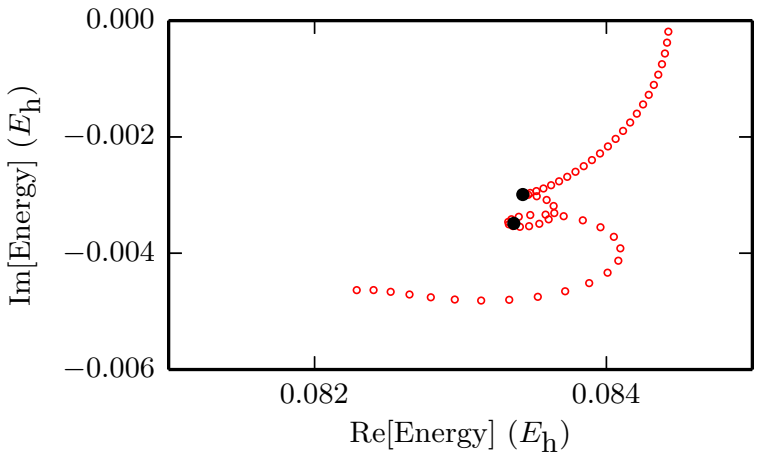

Figure 2.6: Example of multiple stationary points (•) for the lowest energy resonance of s-triazine.

present work				
benzene	pyridine	pyrimidine	pyrazine	s-triazine
0.4808	0.0000	-0.2854	-0.5479	-0.3791
	0.0000	-0.2678	-0.1966	
0.1565	0.0000	-0.3165	-0.4598	-1.1563
experiments of Nenner and Schulz[107]				
benzene	pyridine	pyrimidine	pyrazine	s-triazine
0.52	0.00	-0.62	-1.02	-1.07
	0.00	-0.43	-0.33	
0.27	0.00	-0.34	-0.48	-0.58

Table 2.10: Complex energies (eV) of the lowest three resonances of benzene, pyridine, pyrimidine, pyrazine, and s-triazine in the static-exchange approximation (caug-cc-pVDZ(cm+)) compared with the experimental results of Nenner and Schulz[107]. All values are relative to the three pyridine resonances.

Table 2.10 by showing the experimental and calculated resonances relative to the energies of the pyridine resonances. Note that all the qualitative trends from the experimental data are reproduced in the SE calculations.

Because of the relevance of these molecules to biomolecular processes, they have been the subject of a number of recent scattering calculations[111–118]. The results presented here agree qualitatively with most of these calculations. In particular,

present work				Mašín and Gorfinkiel[114]			
pyimidine		pyrazine		pyimidine		pyrazine	
pos.	width	pos.	width	pos.	width	pos.	width
2.3639	0.2860	2.1014	0.3754	0.554	0.016	0.14	0.015
2.7557	0.3362	2.8270	0.3322	1.068	0.015	1.12	0.03
8.9607	1.9280	8.8174	1.6011	5.328	0.574	5.19	0.527

Table 2.11: Comparison of positions and widths (eV) to the SEP results of Mašín and Gorfinkiel[114].

the SE results for pyrazine and pyrimidine are compared the R-matrix results of Mašín and Gorfinkiel[114] in Table 2.11. Because of the polarization effects included in the R-matrix expansion, the computed resonance positions are lower and the widths are significantly smaller than in the SE approximation. However, despite the predictable differences stemming from the use of different approximations, the trends agree qualitatively.

These molecules are by far the largest to have been investigated with complex basis functions, and even in the simplest approximation, the method can be used to obtain qualitatively correct results.

2.5.3 Computational requirements and timings

The method presented here differs from previous implementations in that the integrals are calculated in a direct manner and never explicitly stored which leads to a memory requirement of order N^2 and avoids storing integrals on disk. The actual computation is dominated by the Hamiltonian build which formally scales as N^4 if all ERIs are explicitly computed. In principle, integral screening techniques can be used to significantly reduce this scaling. However, the lack of an obvious Schwarz inequality for the complex ERIs limits available screening techniques to those based on overlaps of charge distributions and those based on the magnitude of density matrix elements. These methods are likely only significant in the limit of a very large molecule.

Timings in the caug-cc-pVDZ(cm+) basis are shown in Table 2.12. These timings represent the effort required to do the calculation at a single value of θ. Unlike in conventional complex scaling, all matrix elements must be recomputed for every value of θ. As expected, the scaling is roughly quartic. Symmetry is not used in the computation of the integrals, but the integral algorithms utilized in this implementation are more efficient for integrals involving fewer centers. Because the ERIs must

system	basis size	time (s)	time (relative)
N_2	105	4.2	1.0
CO_2	127	15.6	3.6
Benzene	251	233.6	55.6

Table 2.12: Timings in seconds and relative to N_2 for a single calculation in the the caug-cc-pVDZ(cm+) basis set.

be recomputed many times for these calculations and many more times in complex self-consistent field (SCF) calculations, it is worth further effort to reduce this scaling so that computations on truly large molecular systems are feasible.

2.6 Conclusions

In this study, an efficient and open-ended implementation of complex basis functions has been described, and the static-exchange approximation has been used to investigate the basis set requirements of the method. Some applications to larger molecules with multiple low energy shape resonances has been presented, and some general purpose complex basis sets for small molecules were introduced and used throughout.

Despite the limited utility of the static-exchange approximation, the results presented here set the stage for a general and efficient implementation of more sophisticated methods using complex basis functions. In particular, the complex SCF method is of considerable interest because the cost is just a multiple of the SE method and polarization effects are included.

Chapter 3

Non-Hermitian self-consistent field methods

3.1 Introduction

Metastable electronic states, or resonances, in molecules play an important role in a variety of chemical processes. They can be described by a Siegert energy:

$$E = \mathcal{E} - i\frac{\Gamma}{2} \tag{3.1}$$

where $\mathcal{E}$ is the position and Γ is the width of the resonance. Unfortunately, due to their continuum nature, these states have largely eluded large-scale, reliable computation. Many of the most promising candidates for reliable computation of Siegert energies are based on complex-coordinate methods[52, 59, 119].

Originally based on the mathematically rigorous theorems of Aguilar, Balsev, and Combes[41, 42], and Simon[43], these methods rely on the solution of a non-Hermitian effective Hamiltonian. This effective Hamiltonian is constructed so as to contain in its spectrum complex eigenvalues equal to the Siegert energies and corresponding to square integrable eigenfunctions. This process, which generally involves the scaling of some of the coordinates of the Hamiltonian by a complex number, is called complex-scaling. Unfortunately, non-analyticities arising from the Born-Oppenheimer approximation make the application to molecular systems difficult[44, 46, 85]. This problem can be overcome with the mathematically rigorous method of exterior complex scaling[44].

Though difficult to apply directly, the exterior complex-scaling transformation can be implicitly applied using complex basis functions[46, 56]. In this method,

complex Gaussian functions of the form

$$\begin{aligned} \phi_\theta(r) &= N(\theta)(x-A_x)^l(y-A_y)^m(z-A_z)^n \\ &\times \exp\left[-\alpha e^{-2i\theta}(\mathbf{r}-\mathbf{A})^2\right] \end{aligned} \tag{3.2}$$

are included in the basis set. The method of complex basis functions has been applied to a variety of diatomic molecules [46, 70, 71, 73–78] and has recently been applied to some larger, polyatomic molecules in the static exchange (SE) approximation[56]. In this study, we employ complex basis functions in computations on electronic shape resonances in molecules.

Complex coordinate methods, as they are usually used, reduce the full scattering problem to a variational search within a basis of square integrable functions. Unfortunately, in many electron systems one is almost always forced to make further approximations to make the many-body problem computationally feasible. In quantum chemistry, it is the self-consistent field (SCF) wavefuction that usually serves as a first approximation and as a starting point for more accurate methods. The SCF method was first introduced in the context of complex coordinate methods by McCurdy *et al.*[68] For metastable anions, these methods explicitly treat the polarization of the target molecule or atom due to the presence of an additional electron at a mean-field level. While these methods are usually called complex SCF or complex-scaled SCF, we will refer to them as non-Hermitian SCF (NH-SCF) methods so as to highlight the non-Hermitian nature of the problem and to avoid confusion with complex Hermitian SCF methods.

NH-SCF methods have been successfully applied in the context of straight complex-scaling to a variety of atomic shape resonances[40, 68, 72, 120–122]. NH-SCF methods employing complex basis functions have also been applied to shape resonances in a variety of diatomic molecules[70, 71, 73, 76]. Various types of non-Hermitian DFT methods have also been recently developed[123–126]. While SCF-type methods are not directly applicable to Feshbach resonances, non-Hermitian multiconfigurational self-consistent field (NH-MCSCF)[127, 128] or non-Hermitian configuration interaction (NH-CI)[129–131] approaches have been successfully applied to Feshbach resonances in atoms. For molecules, these multi-determinental methods have also been shown to provide a description of Feshbach resonances[74–78]. Recently, complex scaled coupled-cluster methods have also been been used for shape and Feshbach resonances in atoms[132, 133].

In this study, we discuss in detail the implementation and application of NH-SCF theory to molecular anionic shape resonances. After reviewing the non-Hermitian version of restricted open-shell Hartree-Fock (NH-ROHF), we introduce the spin-unrestricted variant (NH-UHF) and apply both to a variety of small diatomic and

polyatomic molecules. This is the first time that this method has been applied to polyatomic molecules. Additionally, we include a discussion of the calculation and interpretation of general molecular properties from a non-Hermitian wavefunction. A density based analysis and visualization of the electron attachment process is introduced and applied to the $^2B_1$ resonance in formaldehyde. Finally, we use NH-UHF to compute a complex potential energy surface for the carbon monoxide anion. Like its Hermitian counterpart, NH-UHF theory is found to be capable of describing full potential energy surfaces with qualitative accuracy.

3.2 Theory

The theoretical background of NH-SCF is described in detail in other works[68, 120]. Here we augment these discussions with a derivation in terms of the complex variational principle[82–84] which, in the context of complex basis functions, states that the Siegert energy of some trial, c-normalizable function $|\Psi)$,

$$E = \frac{(\Psi|H|\Psi)}{(\Psi|\Psi)}, \tag{3.3}$$

is stationary with respect to small variations about the true wavefunction. In the method of complex basis functions, the "true" wavefunction is the true exterior scaled wavefuction evaluated in a transformed variable as discussed in Ref. [56]. The brackets $(\ldots|\ldots)$ are used to denote the c-product[83], which means that the bra is not complex-conjugated. A complex NH-SCF energy is determined by requiring that the energy functional of equation 3.3 is made stationary to first order with respect to variations of a single Slater determinant trial wavefunction. This Slater determinant is constructed from molecular orbitals (MOs) that are constrained to be c-orthonormal. This gives rise to a Lagrangian

$$\mathcal{L} = (\Psi|H|\Psi) - \sum_{ij} \left[(\phi_i|\phi_j) - \delta_{ij}\right] \lambda_{ij} \tag{3.4}$$

where the many body state $|\Psi)$ is chosen to be a single Slater determinant of MOs $\phi_i(\mathbf{r})$, and the λ_{ij} are Lagrange multipliers. The MOs are c-orthonomal functions constructed from real and complex Gaussian basis functions as described in Ref [56]. As in the real case, the specification of any constraints on the spin part of the wavefunctions, followed by the extremization of $\mathcal{L}$, gives rise to the NH-SCF equations.

3.2.1 NH-ROHF and NH-UHF equations

The NH-ROHF equations are the same as in the real case[134]. Stationarity of the Lagrangian of Equation 3.4 gives rise to the NH-ROHF equations presented in Ref. [68]. For the Hermitian analog, see Ref. [135]. These equations are represented by a single Fock matrix of the form

$$\mathbf{F} = \begin{pmatrix} \mathbf{R}_{cc} & \mathbf{F}_{co} & \mathbf{F}_{cv} \\ \mathbf{F}_{oc} & \mathbf{R}_{oo} & \mathbf{F}_{ov} \\ \mathbf{F}_{vc} & \mathbf{F}_{vo} & \mathbf{R}_{vv} \end{pmatrix} \tag{3.5}$$

where the off-diagonal parts are

$$\begin{aligned} \mathbf{F}_{co} &= \mathbf{F}^{\beta} \\ \mathbf{F}_{cv} &= \mathbf{F}^{\alpha} + \mathbf{F}^{\beta} \\ \mathbf{F}_{ov} &= \mathbf{F}^{\alpha} \end{aligned} \tag{3.6}$$

in terms of the α and β Fock matrices from UHF theory. There is some ambiguity in the specification of the diagonal blocks of the Fock matrix (see Refs. [134, 136]) which can be exploited to improve convergence[135]. The diagonal terms are chosen to be:

$$\begin{aligned} \mathbf{R}_{cc} &= \mathbf{F}^{\alpha} + \mathbf{F}^{\beta} \\ \mathbf{R}_{oo} &= \mathbf{F}^{\beta} \\ \mathbf{R}_{vv} &= \mathbf{F}^{\alpha} + \mathbf{F}^{\beta}. \end{aligned} \tag{3.7}$$

This somewhat unconventional choice was found to have good convergence properties.

The NH-UHF equations are the same as in standard Hermitian UHF theory[137]. The α and β Fock matrices are given by

$$\begin{aligned} \mathbf{F}^{\alpha} &= \mathbf{h} + \mathbf{J}^{\alpha} + \mathbf{J}^{\beta} - \mathbf{K}^{\alpha} \\ \mathbf{F}^{\beta} &= \mathbf{h} + \mathbf{J}^{\alpha} + \mathbf{J}^{\beta} - \mathbf{K}^{\beta} \end{aligned} \tag{3.8}$$

where $\mathbf{J}^{\alpha}$ and $\mathbf{K}^{\alpha}$ are the Coulomb and exchange matrices generated from just the α electron density and those operators constructed from the β density are similarly defined. $\mathbf{h}$ is the basis set representation of the core Hamiltonian. These operators are distinguished from their Hermitian counterparts in that the matrix elements are computed with the c-norm.

The c-norm, while convenient, is somewhat restrictive in that it represents an analytic continuation of matrix elements of a real, symmetric Hamiltonian.[83] However, it has long been known that complex MO coefficients are sometimes necessary

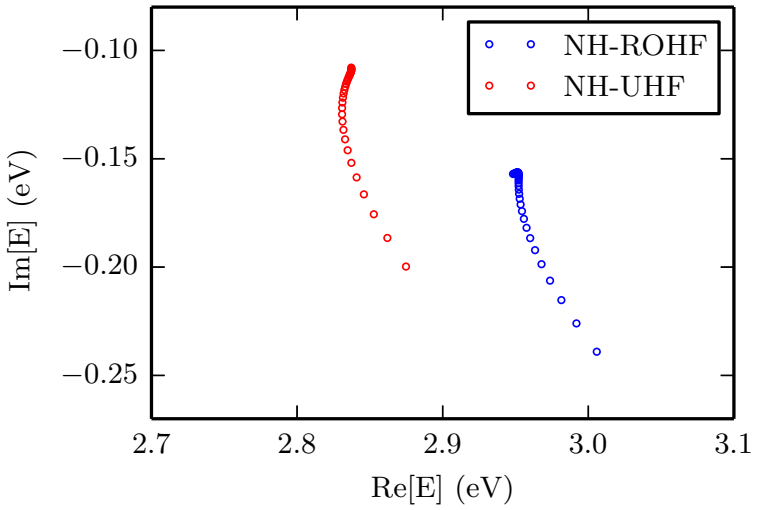

Figure 3.1: Representative θ-trajectories for N_2^- in the caug-cc-pVDZ(cm+) basis set. The complex basis function parameter, θ, is varied from $10^o \ldots 25^o$ in increments of 0.5^o. The approximate location of the stationary point is $(2.8, -0.1)$ for NH-UHF, while for NH-ROHF, it is $(2.9, -0.15)$.

to describe certain forms of symmetry breaking within the purely Hermitian formalism of traditional electronic structure theory[138, 139]. In these cases, the Fock matrix becomes complex Hermitian. In order to include in our description the degrees of freedom relevant to complex-Hermitian Hartree-Fock calculations, a more general bi-orthogonal space must be considered. While this would certainly be an interesting extension, it is not relevant to the examples presented in this study.

3.2.2 Practical considerations in the optimization of NH-SCF wavefunctions

The NH-SCF equations, like their Hermitian counterparts, will have continuum solutions. Special care must therefore be taken with the initial guess and the method of iteration so as to ensure convergence to the desired resonance state. It is important to emphasize that the desired solutions are not minima of Equation 3.3.

The natural starting point for an NH-SCF calculation is an SE result. Here, the procedure described in Ref. [56] was used to generate a guess density for the metastable anion. This is the same method employed in previous studies.[68, 70] In order to converge preferentially to a Siegert energy that is stationary but not in any

way a minimum, an overlap criterion similar to that of Gilbert *et al.*[140] was used to select the appropriate occupied space after each iteration.

In previous applications of NH-SCF, little is reported regarding convergence properties and simple iteration was generally found to yield convergent results. These studies differ from this work in that the basis sets were generally smaller and the complex functions were added only in a particular symmetry. We found that simple iteration only converged to the desired state in very few cases even when small basis sets were used. The direct inversion of the iterative subspace (DIIS) method of Pulay[26, 27] was found to be significantly more reliable.

The DIIS method, as it is usually applied to SCF convergence, computes an extrapolated Fock matrix as a linear combination of Fock matrices from previous iterations. The relative weights are determined by requiring that they minimize an error vector, which is also computed at each iteration, subject to a normalization constraint. In the standard SCF problem, this error vector (in this case a matrix) is usually taken to be

$$\mathbf{e} = \mathbf{SPF} - \mathbf{FPS} \tag{3.9}$$

where $\mathbf{S}$, $\mathbf{P}$ and $\mathbf{F}$ indicate the overlap, density, and Fock matrices respectively. The elements of this vector are elements of the orbital rotation gradient in the AO basis. In the non-Hermitian case, this method can be used with little modification because the (complex) orbital rotation gradient must still be zero at convergence which suggests that the error vector of equation 3.9 is still appropriate. In the non-Hermitian case the error vector is split into real and imaginary parts, and the real and imaginary parts of the extrapolated Fock matrix are found in the iterative subspace. In practice, an orthogonalized error vector is used to give a more balanced description of the error.

Unfortunately, the solution of the NH-SCF equations at a single value of θ will in general not yield a good approximation to the Siegert energy. In practice, the NH-SCF energy is computed at many values of θ and an analytic continuation scheme[56, 86] is used to compute the energy at the optimal value of θ. An example of these θ-trajectories is shown in Figure 3.1.

3.2.3 Properties of NH-SCF states

In the method of complex basis functions and in other complex-coordinate techniques, the wavefunction is not the true wavefunction of the system and is in fact not a physically realizable state of any kind. In this section, we briefly describe how properties of the resonance can be extracted from the non-Hermitian wavefunction in terms of the response of the complex Siegert energy.

Moiseyev *et al.* [83] showed that there exists an analog to the Hellmann-Feynman theorem in a c-normalizable space. It implies, in the context of complex basis functions, that given some Hamiltonian perturbed by some operator V with strength α,

$$H(\alpha) = H_0 + \alpha V, \tag{3.10}$$

the derivative of the energy with respect to α is

$$\frac{dE}{d\alpha} = (\Psi|V|\Psi) \tag{3.11}$$

given that $|\Psi)$ is variationally optimized and normalized, and that the complex basis functions are independent of V (i.e. no Pulay terms[141]). The c-expectation value will in general have both real and imaginary parts, but those parts are easily associated with the response of the position and width respectively:

$$\frac{d\mathcal{E}}{d\alpha} = \mathrm{Re}(\Psi|V|\Psi) \qquad \frac{d\Gamma}{d\alpha} = -2\mathrm{Im}(\Psi|V|\Psi). \tag{3.12}$$

Note that both these quantities are, at least in theory, observable.

For one-electron properties, the c-expectation value can be written as

$$(\Psi|V|\Psi) = \sum_{\mu\nu} V_{\mu\nu} P^{\nu\mu} \tag{3.13}$$

where μ and ν index AO basis functions and $\mathbf{V}$ and $\mathbf{P}$ are the AO matrix representations of operator V and the 1-particle density respectively. The c-normalization of the wave function implies that the 1-particle density matrix defined with the same complex inner product has a real part with a trace equal to the number of electrons and a traceless imaginary part.

The properties of the trace of the complex 1-particle density matrix are very similar to those of a real Hermitian density matrix. As such, it allows for similar kinds analysis. In particular, the complex difference density can be decomposed into complex attachment and detachment densities[142] that can be visualized to give a picture of both the electron-attached state and the polarization of the target. The difference density

$$\mathbf{\Delta} = \mathbf{P}^{\mathrm{res}} - \mathbf{P}^{\mathrm{tar}} \tag{3.14}$$

is defined as the difference between the complex electron density of the resonance and the real density of the target. This quantity can be uniquely decomposed by splitting its eigenvalues into those with positive real part and those with negative real part:

$$\mathbf{\Delta} = \mathbf{U}(\mathbf{a} - \mathbf{d})\mathbf{U}^{\mathrm{T}} = \mathbf{A} - \mathbf{D} \tag{3.15}$$

where **a** and **d** are diagonal matrices with positive real parts. **A** and **D** are termed the attachment and detachment densities respectively. These quantities describe the electron density and the hole density of the resonance relative to the target. Furthermore, the eigenvalues of these two matrices are related to the scattering process in that

$$\mathrm{Tr}(\mathbf{A}) - \mathrm{Tr}(\mathbf{D}) = \mathrm{Tr}(\mathbf{\Delta}) = n \tag{3.16}$$

where n is the number of electrons in the resonance state relative to the target; $n = 1$ for an anion resonance. Therefore, the two equivalent quantities

$$\mathrm{Tr}(\mathbf{A}) - n \quad \text{and} \quad \mathrm{Tr}(\mathbf{D}) \tag{3.17}$$

provide a measure of the magnitude of the polarization.

Two-electron properties can be expressed in terms of the 2-particle density matrix, but the only two-electron property relevant in this study is the square of the total spin which can be computed as[16]

$$\langle S^2 \rangle = \left(\frac{N_\alpha - N_\beta}{2} \right) \left(\frac{N_\alpha - N_\beta}{2} + 1 \right) + N_\beta - \sum_{ij}^{\mathrm{occ}} (i_\alpha | j_\beta)^2 \tag{3.18}$$

where N_α and N_β are the numbers of α and β electrons respectively. For spin-pure wavefunctions such as the NH-ROHF wavefunction, the expectation value of total spin squared is real and equal to $s(s+1)$ where s is the total spin quantum number. For NH-UHF wavefunctions, the expectation value can vary from the spin-pure value and can develop an imaginary part. As in the Hermitian case, the computation of the square of the total spin provides a measure of the spin contamination of the unrestricted wavefunction. In practice, the expectation value of S^2 is computed for each value of θ and the rational interpolation scheme described in Ref. [56] was used to compute the expectation value at the optimal value of θ.

3.3 Results

All computations reported in this study were performed with a modified version of the Q-Chem software package[88]. Matrix elements were computed by the methods described in Ref. [56], while the Armadillo C++ linear algebra library[89] was used for all matrix manipulations. All SCF calculations are converged to the extent that the maximum element of the (orthogonalized) DIIS error is less than 10^{-5}.

molecule	basis	SE[a]		NH-ROHF		NH-UHF		$\langle S^2 \rangle$	
		Re[E]	Im[E]	Re[E]	Im[E]	Re[E]	Im[E]	Re[$\langle S^2 \rangle$]	Im[$\langle S^2 \rangle$]
N_2	caug-cc-pVDZ(cm+)	3.9752	-0.6363	2.9517	-0.1566	2.8366	-0.1087	0.7580	-0.0044
	caug-cc-pVTZ(cm+)	3.8818	-0.6301	2.9621	-0.1613	2.8287	-0.1159	0.7594	-0.0049
	caug-cc-pVQZ(cm+)	3.8413	-0.6215	2.9525	-0.1547	2.8271	-0.1078	0.7590	-0.0041
CO	caug-cc-pVDZ(cm+)	3.4173	-0.9715	2.5253	-0.3463	2.4304	-0.2814	0.7568	-0.0015
	caug-cc-pVTZ(cm+)	3.3474	-0.9407	2.4124	-0.3185	2.4216	-0.2879	0.7570	-0.0020
	caug-cc-pVQZ(cm+)	3.3441	-0.9646	2.5423	-0.3534	2.4263	-0.3032	0.7574	-0.0020
CO_2	caug-cc-pVDZ(cm+)	5.5268	-0.2972	4.4207	-0.0175	4.0296	0.0302	0.7620	-0.0007
	caug-cc-pVTZ(cm+)	5.5035	-0.3435	4.4625	-0.0677	4.3096	-0.0516	0.7639	-0.0012
	caug-cc-pVQZ(cm+)	5.4733	-0.3500	4.4553	-0.0677	4.3111	-0.0559	0.7638	-0.0011
CH_2O	caug-cc-pVDZ(cm+)	2.6848	-0.8078	1.7544	-0.2245	1.6251	-0.1676	0.7613	-0.0064
	caug-cc-pVTZ(cm+)	2.6459	-0.7887	1.7861	-0.2012	1.6472	-0.1541	0.7624	-0.0063
	caug-cc-pVQZ(cm+)	2.5775	-0.8170	1.7467	-0.2007	1.6132	-0.1409	0.7623	-0.0065

Table 3.1: Positions and widths in eV of the lowest $^2\Pi_g$ resonance in N_2 and CO, the lowest $^2\Pi_u$ resonance in CO_2 and the lowest $^2B_1$ shape resonance in formaldehyde (CH_2O). Expected values of total spin-squared are reported for the NH-UHF calculations. The basis sets are described in detail in Ref. [56].

[a] Also reported in Ref. [56]

molecule	geometry
N_2	N≡N = 1.094Å
CO	C≡O = 1.128Å
CO_2	C=O = 1.16Å
CH_2O	C-H = 1.11Å, C=O = 1.205Å, H-C-H = 116.2°

Table 3.2: Geometries used throughout the present study.

3.3.1 Small molecules and comparison to static exchange

Table 3.1 shows the computed Siegert energies of low energy shape resonances in four different molecular systems and in three basis sets of increasing size. The geometries are reported in Table 3.2. The positions from NH-SCF calculations are reported relative to the total Hermitian RHF energy of the target in the same basis ($\theta = 0°$). The positions and widths are computed at the NH-UHF and NH-ROHF levels of theory and are compared to the SE results in the same basis sets. A recent summary of previous theoretical and experimental positions and widths for these resonances can be found in Ref. [79]. In general, the positions computed with NH-ROHF are $0.9-1$eV lower in energy than the corresponding SE result. The positions computed with NH-UHF are $1-1.1$eV lower in energy than the SE result making them on average about 0.1eV lower in energy than the corresponding NH-ROHF result. This is as expected; the extra polarization terms in the UHF wavefunction should lower the position relative to the energy of the neutral target.

The widths are not so predictable. We would expect the widths from NH-SCF calculations to be significantly smaller than for SE calculations due to the incorporation of polarization. This effect is indeed observed, but the magnitude of the difference is not as constant among different molecular systems. For similar reasons, the widths computed with NH-UHF would be expected to be lower than those computed with NH-ROHF, and this is generally the case.

The behavior of the Siegert energies as size of the basis is increased is also generally difficult to predict. However, despite a couple of exceptions, both the real and imaginary parts of the energy are relatively stable with respect to an increase in the size of the basis. The first exception is the Π_u resonance in CO_2 computed within the caug-cc-pVDZ(cm+) basis set. In this case, the positions are reasonable, but the computed widths are unreasonably small; the NH-UHF energy has a positive imaginary part. However, this case is a pathological one in that the basis set contains exactly one complex function of π_u symmetry. This grossly incomplete basis cannot be expected to yield an accurate width, and it is quite surprising that the SE

result is so reasonable. A more detailed discussion of basis set effects can be found in Ref. [56]. The other slight exception is the Π_g resonance in carbon monoxide as computed with NH-ROHF in the caug-cc-pVTZ(cm+) basis set. Both the position and width computed in this basis set differ from their values computed in the larger and smaller basis sets. The reason for this slight deviation is unknown.

We also report the expectation values of total spin-squared for the NH-UHF wavefunctions in Table 3.1. The real parts of the spin-squared values are comparable to what would be expected from a Hermitian calculation on a bound anion in that they are only slightly different from the pure doublet, while the imaginary parts are quite small. This suggests that for these cases, the unrestricted wavefunction is not significantly spin-contaminated.

Comparing to other theoretical and experimental results is difficult to do systematically because of the wide range of methods/basis sets and experimental conditions. However, the results presented here qualitatively reproduce the experimental numbers and agree with many other theoretical results (*cf.* Ref. [79]). Some selected literature values are shown in Table 3.3. In general, we can say that the positions are larger than those computed with correlated methods. The widths fall within the range of other theoretical results, but seem to be slightly smaller on average than widths computed at similar levels of theory.

3.3.2 Density based analysis of formaldehyde's B_1 resonance

In this section, the attachment and detachment densities of the $^2B_1$ resonance in formaldehyde are computed at the optimal value of θ in the caug-cc-pVTZ basis. Because the c-norm does not permit a rigorous notion of matrix positivity, there are in general no restrictions on the signs of the real and imaginary parts of these densities, though the real parts are generally observed to be mostly positive while imaginary parts are observed to be primarily negative.

The attachment and detachment densities, by definition, obey the relations of Equation 3.17. This is confirmed in Table 3.4 where the real and imaginary parts of the traces of the attachment and detachment densities are shown. Note that the attached electron has α spin in this case. These values provide an approximate, but quantitative, description of the polarization during the electron attachment process: approximately 0.32 α electrons and 0.39 β electrons are rearranged. The larger polarization of the β density is consistent with the nature of the exchange interaction.

The α and β attachment and detachment densities for formaldehyde's B_1 resonance are plotted in Figures 3.2 and 3.3 respectively. Note that it is the negative of

molecule	method	position	width
N_2	Stieltjes imaging[143]	2.23	0.40
	Schwinger variational + ADC(3) optical potential[144]	2.534	0.536
	NH-SCF with complex basis functions[70]	3.19	0.44
	3rd order decouplings of dilated electron propogator[145]	2.11	0.18
	EOM-EA-CCSD stabilization (aug-cc-pV5Z)[146]	2.49	0.248
	CAP EOM-EA-CCSD (1st order, aug-cc-pVQZ + 3s3p3d)[79]	2.478	0.286
	Experimental estimate[147]	2.32	0.41
CO	T-matrix (static-exchange)[148]	3.4	1.65
	2nd order electron propogator[149]	1.71	0.08
	3rd order decouplings of the electron propogator[145]	1.65	0.14
	CAP EOM-EA-CCSD (1st order, aug-cc-pV5Z + 3s3p3d)[79]	1.762	0.604
	Experimental estimate[150]	1.50	0.4
CO_2	Schwinger variational (static-exchange)[151]	5.39	0.64
	Schwinger variational (static-exchange + polarization)[152]	3.78	0.23
	CAP EOM-EA-CCSD (1st order, aug-cc-pVTZ + 3s3p3d)[79]	3.997	0.198
	Experiment[153]	3.14	0.20
CH_2O	Complex Kohn (static-exchange + polarization)[154]	1.0	$\sim$0.5
	2nd order decouplings of the dilated electron propogator (largest basis)[155]	0.887	0.076
	R-matrix (static-exchange + polarization)[156]	1.32	0.546
	CAP EOM-EA-CCSD (1st order, aug-cc-pVTZ + 3s3p3d)[79]	1.314	0.277
	Experiment[157]	$\sim$0.86	-

Table 3.3: Selected literature values (in eV) for the resonances studied here from experiment and various levels of theory.

	Attachment		Detachment	
	Re	Im	Re	Im
α	1.3233	-0.0391	0.3233	-0.0391
β	0.3905	-0.1140	0.3905	-0.1140

Table 3.4: Traces of attachment and detachment densities for the α and β difference densities corresponding to the B_1 resonance in formaldehyde. The densities were computed at the optimal value of θ in the caug-cc-pVTZ(cm+) basis set.

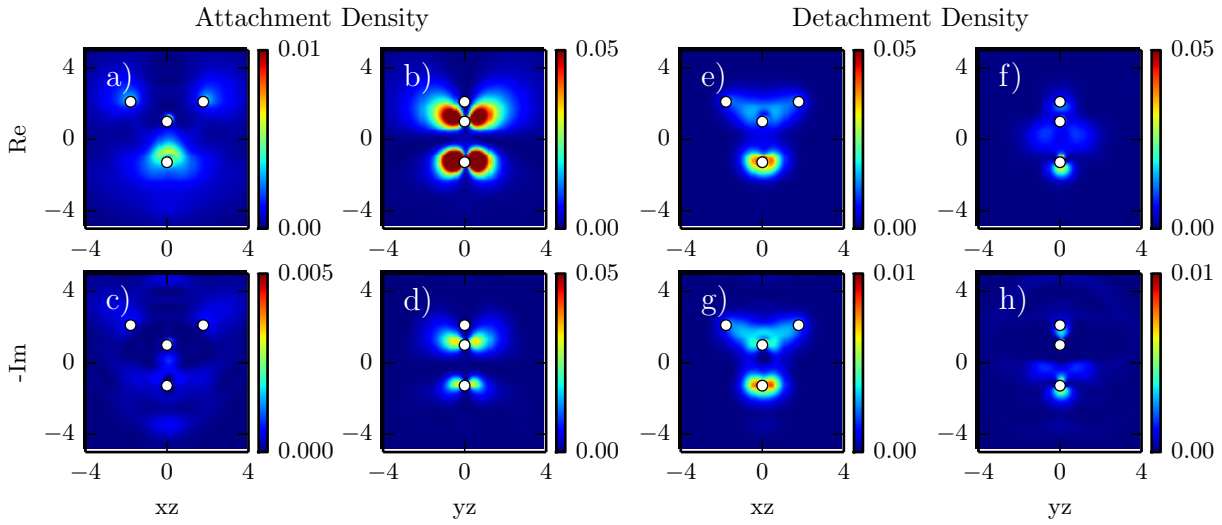

Figure 3.2: Real and imaginary parts of the α attachment and detachment densities for the $^2B_1$ resonance in formaldehyde are plotted in the xz and yz-planes. The top row shows the real part and the bottom row shows the negative of the imaginary part. The first four panels (a - d) show the attachment density while the second four (e - h) show the detachment density. Note the difference in scales. White dots are used to indicate the positions of the nuclear centers; the oxygen end of the molecule points in the negative z-direction. The axes are in atomic units (a_0). The real and imaginary parts of the attachment density, which correspond to the extra electron in the resonance state, are predominantly π^* in character. The detachment density, which corresponds to rearrangement, has largely σ character.

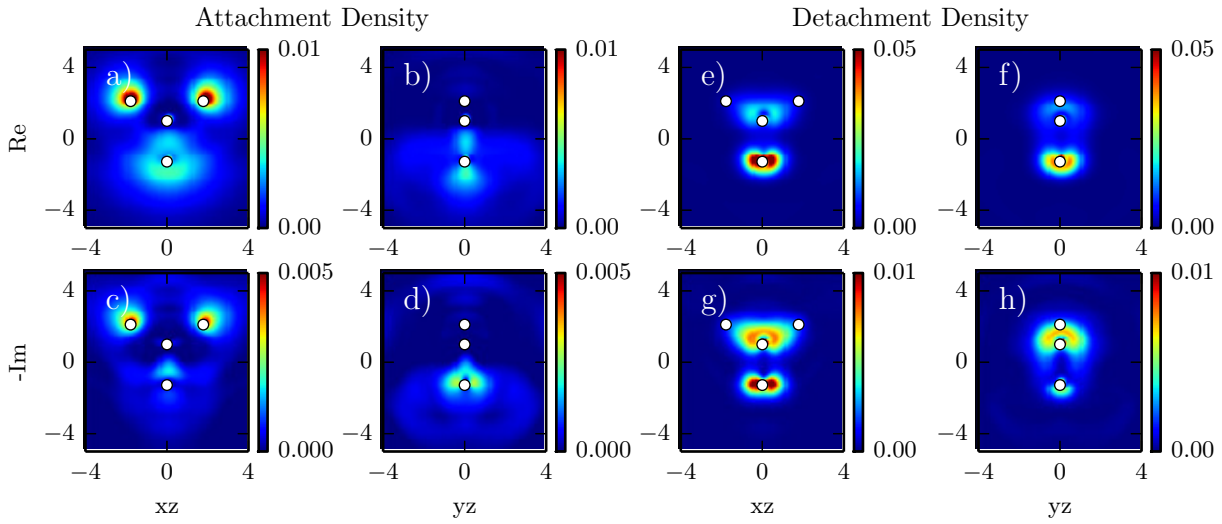

Figure 3.3: Real and imaginary parts of the β attachment and detachment densities for the $^2B_1$ resonance in formaldehyde are plotted in the xz and yz-planes. The top row shows the real part and the bottom row shows the negative of the imaginary part. The first four panels (a - d) show the attachment density while the second four (e - h) show the detachment density. Note the differences in scales. White dots are used to indicate the positions of the nuclear centers; the oxygen end of the molecule points in the negative z-direction. The axes are in atomic units (a_0). All changes in the β space are due to electron-rearrangement which is mostly of σ character.

the imaginary part that is plotted in the bottom rows of Figures 3.2 and 3.3 (c,d,g,h). The real part of the α attachment density has very little magnitude in the plane of the molecule and therefore resembles the density arising from attachment to a state with π character. The small σ character in the attachment density is likely the result of electron rearrangement.

Comparing the β attachment and detachment densities, it is clear that the rearrangement in the β space involves the movement of electron density from orbitals localized around the oxygen atom to the two hydrogen atoms. It is also interesting to note that the β attachment density is significantly delocalized in comparison with the detachment density.

reference	T_2 resonance		A_1 resonance		method
	Position	Width	Position	Width	
Huo[103]	6.6	4.1	11.7	22.8	Schwinger Variational(SE)
Modelli et al[104]	8.95	-	8.70	-	Multiple Scattering-Xα
Modelli et al[104]	8.58	-	8.98	-	Continuum Multiple Scattering-Xα
Winstead et al[105]	11.5	-	13.0	-	Schwinger Multichannel (SE)
Isaacson et al[158]	~ 9[1]	-	~ 9[1]	-	Complex Kohn
Curik et al[159]	$8 - 10$[1]	-	$8 - 10$[1]	-	Close-coupling (model potential)
Varella et al[102]	9.9	-	11.0	-	Schwinger Multichannel (SEP)
present work[2]	10.6301	2.0553	12.7184	2.0902	SE/caug-cc-pVDZ
present work[2]	11.0816	1.9737	12.0561	1.9617	SE/caug-cc-pVTZ
present work	8.6421	0.8530	9.7906	1.8189	NH-ROHF/caug-cc-pVDZ
present work	9.0738	0.7813	10.0711	1.1740	NH-ROHF/caug-cc-pVTZ
present work	8.5996	0.9139	9.5236	1.8346	NH-UHF/caug-cc-pVDZ
present work	8.8851	0.8191	9.9862	1.1490	NH-UHF/caug-cc-pVTZ

Table 3.5: Calculated positions and widths (eV) of low energy shape resonances in CF_4. Static-exchange plus polarization is abbreviated SEP.

[a] overlapping resonances not separately resolved
[b] Also reported in Ref. [56]

resonance	basis	$\langle S^2 \rangle$	
		$\mathrm{Re}[\langle S^2 \rangle]$	$\mathrm{Im}[\langle S^2 \rangle]$
A_1	caug-cc-pVDZ(cm+)	0.7542	-0.0032
	caug-cc-pVTZ(cm+)	0.7551	-0.0017
T_2	caug-cc-pVDZ(cm+)	0.7515	-0.0010
	caug-cc-pVTZ(cm+)	0.7588	-0.0018

Table 3.6: Spin-squared of the A_1 and T_2 shape resonances in CF_4 computed using NH-UHF.

3.3.3 A_1 and T_2 resonances in carbon tetrafluoride

Carbon tetrafluoride has been observed to have two low energy shape resonances of A_1 and T_2 symmetry. These two resonances have been the subject of some recent interest due to their role in dissociative electron attachment.[100, 101, 160] Computed positions and widths of these two shape resonances are shown in Table 3.5. The positions and widths computed at the SE, NH-ROHF, and NH-UHF levels of theory are shown along with literature values from various theoretical calculations. The spin-squared values for the UHF wavefunctions are shown in Table 3.6 and a summary of experimental results can be found in Refs. [99, 161].

This case is interesting in that the NH-ROHF and NH-UHF values agree quite closely. The spin squared values (shown in Table 3.6) show that there is very little spin contamination in the NH-UHF wavefunction, but the similarity is still quite striking when compared to similar calculations on small molecules. Furthermore, while the positions calculated with NH-UHF are smaller than those computed with NH-ROHF, the widths are slightly larger in several cases. This is contrary to the trends observed in other molecules, though it is in no way prohibited by the theory.

For these resonances in CF_4, like those of many polyatomic molecules, very few *ab initio* calculations have been performed. The results of the present study agree well with the previous theoretical results shown in Table 3.5 excluding the calculation of Huo[103]. Though Huo is the only author to report a width, all other studies report the computed cross-section which shows the widths of the two, not always resolveable, resonances to be on the order of 1eV which agrees well with the present study. The results presented here offer the most complete picture of these two resonances: the T_2 resonance clearly appears approximately 1eV lower energy and with a slightly narrower width, though both widths are on the order of 1eV. It is possible that this picture is significantly different when electron-correlation is explicitly included in the theory.

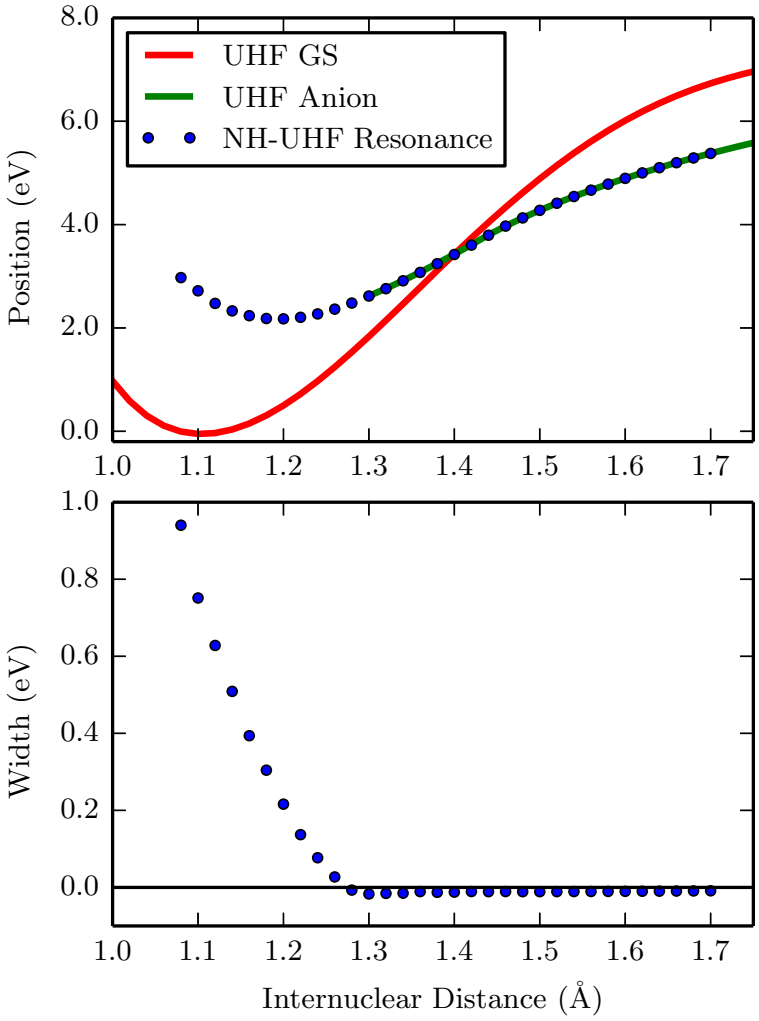

Figure 3.4: Carbon monoxide potential energy curves at the UHF/NH-UHF level of theory in the caug-cc-pVTZ(cm+) basis set.

3.3.4 Carbon monoxide potential energy curve

One of the great attractions of Hermitian UHF theory is that, in many situations, it provides a qualitatively correct description of dissociation processes. NH-UHF theory should be able to describe potential energy curves of resonances with the same qualitative accuracy.

As an example, we examine the potential energy curves of anionic and neutral carbon monoxide at the NH-UHF and UHF level of theory respectively. The an-

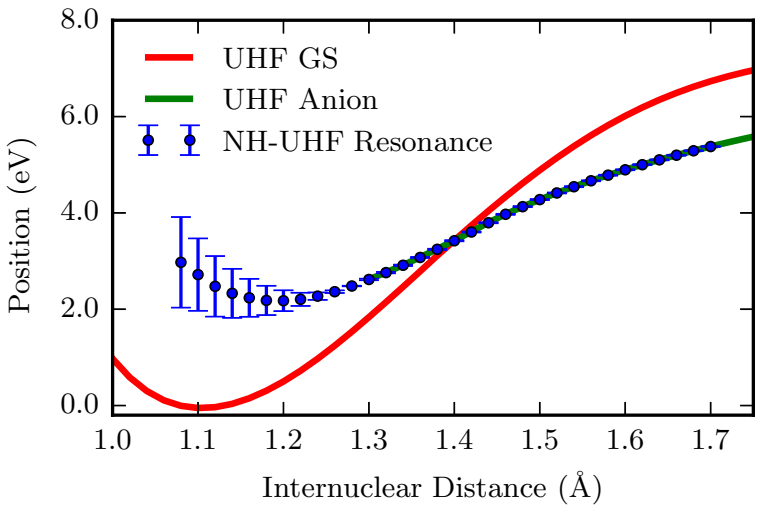

Figure 3.5: Carbon monoxide potential energy curves at the UHF/NH-UHF level of theory in the caug-cc-pVTZ(cm+) basis set. The width is represented as an uncertainty in the energy.

ion, metastable at the equilibrium geometry of the neutral, becomes bound as the molecule is stretched, eventually dissociating to oxygen neutral and carbon anion.

The potential energy curves at the UHF/NH-UHF level of theory are shown in Figure 3.4 and 3.5. The behavior is qualitatively what would be expected: the anion curve crosses that of the neutral and the width goes to zero. However, the point at which the width goes to zero occurs about 0.1Å before the curves cross. This is consistent with previous calculations[71, 73] and typical of cases where the same uncorrelated level of theory is used on the closed-shell neutral and open-shell anion. Higher levels of theory may be able to remove this discrepancy[162]. In the region where the anion is bound, the NH-UHF energy almost exactly reproduces the Hermitian UHF energy of the bound anion, but with a very small positive imaginary part. In the region where the anion is unbound and Hermitian UHF is not useful, NH-UHF provides a qualitatively correct complex potential. Such complex potential curves could be useful in calculations of vibrational structure in electron scattering experiments[38, 163, 164].

The real and imaginary parts of the expectation value of total spin squared are plotted in Figure 3.6. In this case, the Hermitian UHF solution was obtainable throughout the recoupling region. The expectation value of total spin-squared of the NH-UHF agrees remarkably well with that of the Hermitian UHF solution. This is not surprising, because the anion is bound for much of this region. It is, however,

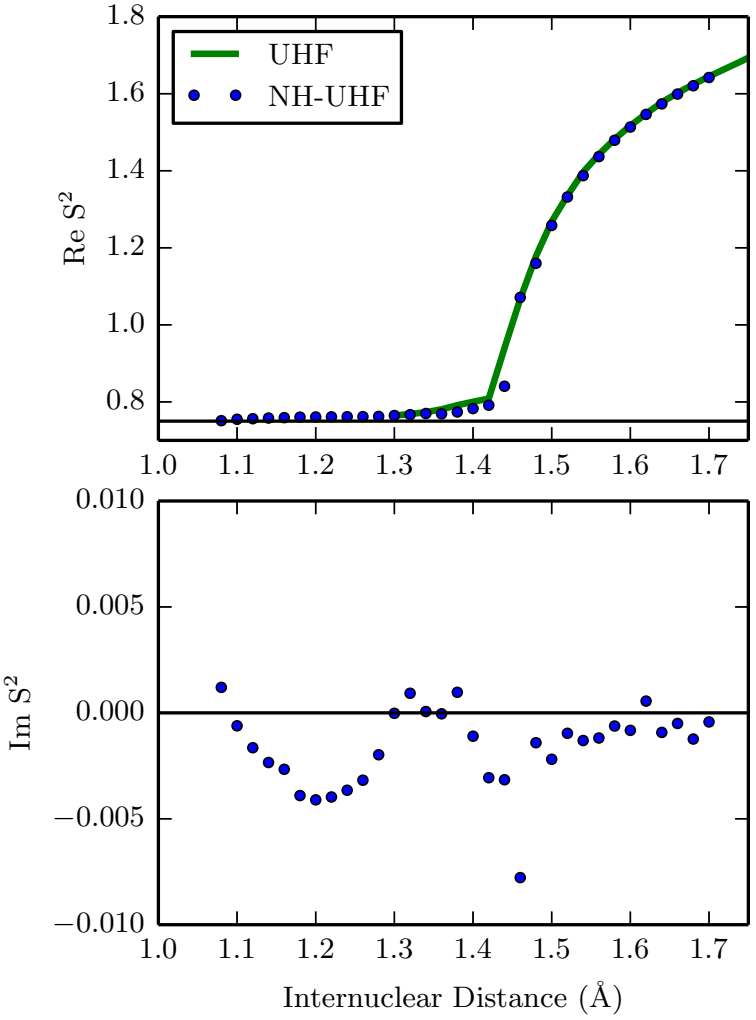

Figure 3.6: Total spin squared on the carbon monoxide PES in the caug-cc-pVTZ(cm+) basis set. The black line indicates a pure doublet.

worthy of note that the NH-UHF does essentially reproduce the Hermitian UHF solution in the region where the width is zero.

This potential energy curve was not easy to obtain. Only by reading in orbitals from previous calculations and taking small (0.02Å) steps in internuclear distance and similarly small (0.5°) steps in θ was convergence achieved at enough points so that the analytic continuation scheme could be confidently applied. Also, at some geometries multiple stationary points were observed, and great care had to be taken to make sure that we followed a single stationary solution.

3.4 Conclusions

In this study complex basis functions were employed in the implementation of the NH-ROHF method, and the novel NH-UHF method. These methods were described in detail and applied to a variety of small diatomic and polyatomic molecules including carbon tetrafluoride. The computation and interpretation of molecular properties from non-Hermitian wavefunctions was discussed and a density-based analysis was applied to the $^2B_1$ resonance in formaldehyde. This analysis of the complex analogs of the attachment and detachment densities allows for an intuitive discussion of target polarization during the process of resonant electron attachment. The NH-UHF method was also utilized in the computation of a NH-UHF potential energy surface for the metastable carbon monoxide anion. These promising results make it worth investigating the possibility of using an NH-SCF reference for highly accurate correlated calculations on small molecules.

However, it is also important to be aware that there are significant challenges in extending NH-SCF methods to larger systems than reported here. First, NH-SCF with complex basis functions often suffers from slow convergence. Second, there are serious numerical problems associated with linear dependence in very large basis sets, associated for instance with diffuse complex Gaussians on multiple atomic centers. Third, the occasional appearance of multiple stationary points can make the identification of the Siegert energy ambiguous, though we have not yet seen a case where the difference is significant. Finally, the θ-trajectories are a significant burden relative to conventional SCF. More effort is necessary to remedy these problems so that the method can be applied confidently to large molecules.

molecule	basis	SE		NH-ROHF		NH-UHF	
		$\|s\|$	phase[s]	$\|s\|$	phase[s]	$\|s\|$	phase[s]
N_2	caug-cc-pVDZ(cm+)	1.0989	20.864	1.0187	13.746	1.0338	10.930
	caug-cc-pVTZ(cm+)	0.9604	23.427	0.9787	9.7308	0.9620	8.8183
	caug-cc-pVQZ(cm+)	1.1052	21.120	1.0005	9.0439	0.9989	12.264
CO	caug-cc-pVDZ(cm+)	0.9638	25.628	0.9310	19.862	0.9544	14.889
	caug-cc-pVTZ(cm+)	1.0264	23.195	0.9935	25.186	0.9518	11.023
	caug-cc-pVQZ(cm+)	1.0167	27.888	0.9855	17.874	1.0126	17.255
CO_2	caug-cc-pVDZ(cm+)	0.9067	10.560	1.0010	14.383	1.0043	17.380
	caug-cc-pVTZ(cm+)	1.0687	19.233	1.0654	14.960	1.0720	15.507
	caug-cc-pVQZ(cm+)	1.0025	20.992	0.9208	25.423	1.0284	14.639
CH_2O	caug-cc-pVDZ(cm+)	1.0359	23.459	0.9934	19.944	0.9938	19.765
	caug-cc-pVTZ(cm+)	0.9742	18.154	1.0790	4.799	1.0626	17.062
	caug-cc-pVQZ(cm+)	1.0880	26.177	1.0021	22.736	1.0227	24.807
$CF_4(T_2)$	caug-cc-pVDZ(cm+)	0.94872	24.188	1.0838	6.0529	1.0299	15.164
	caug-cc-pVTZ(cm+)	1.0060	16.176	0.9877	10.535	1.0247	15.479
$CF_4(A_1)$	caug-cc-pVDZ(cm+)	1.0010	14.521	1.0916	11.890	1.1124	18.417
	caug-cc-pVTZ(cm+)	0.9807	19.842	1.0154	15.300	1.0120	15.265

Table 3.7: Optimal values of θ for all single point energy calculations. θ is reported in polar form with the phase in degrees.

3.5 Appendix: Optimal theta values

Optimal values of the scaling factor for all single point energy calculations are provided in Table 3.7. The optimal values for the carbon monoxide PES are shown in Table 3.8. Note that the scaling factor is defined as

$$s \equiv e^{i\theta}.$$

R(Å)	$\|s\|$	phase[s]
1.08	0.9277	11.639
1.10	1.0998	15.963
1.12	0.9498	11.797
1.14	0.9849	10.117
1.16	1.0154	8.9519
1.18	0.9346	11.334
1.20	0.9495	10.702
1.22	0.9204	11.089
1.24	0.9598	10.566
1.26	0.9655	10.324
1.28	0.9738	9.4073
1.30	1.0000	9.9328
1.32	0.9808	10.255
1.34	0.9981	9.9255
1.36	1.0000	4.0001
1.38	0.9822	9.2917
1.40	1.0051	9.1503
1.42	0.9710	8.7806
1.44	1.0036	9.2459
1.46	0.9799	8.9373
1.48	0.9950	8.8133
1.50	0.9972	8.9010
1.52	0.9981	8.9202
1.54	1.0010	8.9371
1.56	1.0011	8.9626
1.58	1.0009	8.9886
1.60	1.0016	9.0031
1.62	1.0016	9.0394
1.64	0.9983	9.0643
1.66	0.9958	9.0609
1.68	0.9946	9.1075
1.70	0.9907	8.9882

Table 3.8: Optimal values of θ for all points on the carbon monoxide PES. θ is reported in polar form with the phase in degrees.

Chapter 4

Electron correlation with complex basis functions

4.1 Introduction

Metastable electronic states, or resonances, have long been recognized as important intermediate states in a variety of chemical applications[2]. Such states can decay and are therefore characterized by a finite lifetime, $\tau = \hbar/\Gamma$. Despite their importance, simple, black-box, methods for the computation of electronic resonances have been elusive. The difficulty is a result of the complexity of the quantum many-body problem with the additional difficulty of scattering boundary conditions.

Complex coordinate methods offer an attractive solution to the scattering problem: the resonance parameters are found as a complex eigenvalue of an appropriately constructed non-Hermitian Hamiltonian[52, 59, 119]. The eigenvalue is discrete and the corresponding eigenfunction is square-integrable[41–43]. The problem can then be solved by the finite-basis methods of quantum chemistry.

For the molecular, Born-Oppenheimer problem, the method of exterior complex scaling[44] is a rigorously justifiable means of obtaining an appropriate non-Hermitian Hamiltonian. Unfortunately the method is difficult to apply, and in practice one is forced to use a more approximate method. One such method is the method of complex basis functions (CBFs) in which the transformation is applied to the basis set itself[46]. The result is that standard electronic structure methods can be used but in a basis set including Gaussians with complex exponents. The method is related to the analytic continuation of matrix elements[45] and is a complex-variational[84, 87] approximation to the exterior-scaled wavefunction[56]. The method of complex basis functions has been most extensively applied to molecular shape-resonances at

the Hatree-Fock level of theory. There have been various applications to diatomic molecules[70, 71, 73, 76], and a recent application to some polyatomic molecules[57].

Since molecular resonances are ultimately a many-body problem, accurate computation necessitates taking account of electron correlation effects. Feshbach resonances in particular have lifetimes that are entirely determined by electron correlation. Complex coordinate methods must therefore include electron correlation if they are to achieve quantitative accuracy. While correlated calculations on atomic resonances are fairly routine[128, 165–167], correlated calculations on molecular resonances are not as commonplace. Applications to polyatomic molecules are particularly rare, though calculations on formaldehyde, acetylene, carbon dioxide, ethylene, and 1,3-butadiene have been performed at correlated levels of theory[79, 155, 168, 169]. In past complex basis function calculations, correlation has been taken into account by means of various types of configuration interaction[74–76, 170], but these studies have been limited to atoms and diatomic molecules.

In the present study, we discuss the application of correlated electronic structure methods to molecular resonances using the method of complex basis functions. Møller-Plesset perturbation theory at second order[19] (MP2) and coupled-cluster singles and doubles[171] (CCSD) are both size-consistent, correlated methods with computational scaling with the system size of N^5 and N^6 respectively. Specifically, we evaluate the ΔMP2 and equation of motion, electron affinity CCSD[172] (EOM-EA-CCSD) methods for accurate computation of resonance parameters. Furthermore, we explore the possibility of using EOM-EA-CCSD to obtain accurate complex potential energy surfaces, and to compute positions and widths of Feshbach resonances.

4.2 Theory

4.2.1 Complex basis functions

To compute the complex Seigert energy associated with a narrow resonance, we employ the method of complex basis functions for all calculations. This method is described in detail in the literature[46, 56, 57]. Diffuse Gaussian basis functions of the form

$$\begin{aligned} \phi_\theta(\mathbf{r}) &= N(\theta)(x-A_x)^l(y-A_y)^m(z-A_z)^n \\ &\times \exp\left[-\alpha e^{-2i\theta}(\mathbf{r}-\mathbf{A})^2\right] \end{aligned} \tag{4.1}$$

are included in the basis set. These basis functions provide a reasonable basis for representing the exterior-scaled resonance wavefunction in a c-normalized space. The c-product, in which the bra-side is not complex conjugated, will be denoted using

curved brakets $(\ldots|\ldots)$. The application of the complex variational principle[84, 87] allows for derivations of electronic structure methods in this space of c-normalized states.

4.2.2 The non-Hermitian SCF reference

As in traditional electronic structure theory, the starting point for the correlated calculations is a self-consistent field (SCF) reference. The theories considered here are based upon a single, c-normalized, determinant. The methods described in Ref. [57] can be used to obtain the single determinant reference from a non-Hermitian SCF (NH-SCF) calculation. For the NH-MP2 methods considered here, the reference is a single determinant from a non-Hermitian unrestricted Hartree-Fock or non-Hermitian restricted open-shell Hatree-Fock calculation on the anion. For EOM-EA-CCSD, the reference can come from a NH-SCF calculation on the neutral molecule.

4.2.3 Non-Hermitian MP2

The application of many-body perturbation theory through second order to the problem of electron correlation is well established in quantum chemistry. The derivation of the analogous non-Hermitian method (NH-MP2) exactly parallels that of the Hermitian case. The MP2 correction to the energy in terms of canonical spin-orbitals is given by

$$E^{(2)} = -\frac{1}{4}\sum_{ijab} t_{ij}^{ab}(ij||ab) \tag{4.2}$$

where

$$t_{ij}^{ab} \equiv \frac{(ab||ij)}{\epsilon_a + \epsilon_b - \epsilon_i - \epsilon_j}. \tag{4.3}$$

Here and elsewhere we use $(ab||ij)$ to indicate the antisymmetrized electron repulsion integral in 12-12 (or "physicist's") notation. The curved bracket is used to indicate the use of the c-product. This equation assumes that the spin-orbital Fock matrix is diagonal where the occupied and virtual eigenvalues are given by ϵ_i and ϵ_a respectively. For an RHF or a UHF reference, the spin-orbital Fock matrix is diagonal and Equation 4.2 is used to compute the MP2 correction to the energy.

In the case of an ROHF reference, the spin orbital Fock matrix is not diagonal. We therefore apply the restricted Moller-Plesset perturbation theory of Knowles *et al.*[173] This non-Hermitian restricted MP2 (NH-RMP2) yields an energy expression in the pseudo-canonical basis that takes explicit account of non-zero off-diagonal

matrix elements of the Fock matrix (f):

$$E^{(2)} = -\frac{(f_i^a)^2}{\epsilon_a - \epsilon_i} - \frac{1}{4}\sum_{ijab} t_{ij}^{ab}(ij||ab). \tag{4.4}$$

In the Δ-MP2 method, the excitation/attachment energy is found as the difference between the MP2 energies of the excited/electron-attached state and the ground state.

4.2.4 Complex coupled cluster methods

The theory behind the coupled cluster method has been described in detail (See recent reviews of CC[174] and EOM-CC[175] theory). Here we review only those points relevant to our complex implementation. From the reference NH-SCF wavefunction, the coupled-cluster equations are solved to determine the T-amplitudes:

$$(\Phi_\mu|e^{-T}He^{T}|\Phi_0) = (\Phi_\mu|\bar{H}|\Phi_0) = 0. \tag{4.5}$$

Again we have used curved brackets to indicate the c-product. $|\Phi_0)$ is the reference wavefunction, and $|\Phi_\mu)$ is an excited determinant relative to the reference. For CCSD, μ runs over all single and double excitations, and the equations are used to determine T truncated to include only the singles and doubles part[171].

The equation of motion (EOM) formalism can then be used to compute electron affinities (EA) or excitation energies (EE)[21, 172]. In this method, one ultimately diagonalizes $\bar{H}$ in the basis of excited determinants:

$$(\bar{H} - E_{\mathrm{CCSD}})R|\Phi_0) = \omega R|\Phi_0). \tag{4.6}$$

R is an excitation operator,

$$R^{\mathrm{EA}} = \sum_a r^a a^\dagger + \frac{1}{2}\sum_{ia,b} r_i^{ab} a^\dagger i b^\dagger \tag{4.7}$$

$$R^{\mathrm{EE}} = \sum_{ia} r_i^a a^\dagger i + \frac{1}{4}\sum_{ia,jb} r_{ij}^{ab} a^\dagger i b^\dagger j, \tag{4.8}$$

where the r-amplitudes are determined from the eigenvalue problem. Note that in a c-normalizable space, the creation and annihilation operators are related by the transpose and not the adjoint[127]. However, we still use †-notation to indicate creation operators to avoid confusion. The complex CCSD and EOM-CCSD methods

have already been described in conjunction with complex scaling[132] and complex absorbing potentials[79, 132, 133, 162, 169].

The biorthogonal version of Davidson's iterative diagonalization method[28] is used to solve the large eigenvalue problem. For temporary anion shape-resonances, the orbital of the neutral molecule associated with the resonance is easily identified from its behavior as we vary θ. This orbital is used to construct a simple Koopman's type guess that is input to the Davidson procedure.

4.2.5 θ-trajectories and the computation of the Siegert energy

Despite the θ-independent properties of the exact theory, it has long been recognized that in a finite basis set, the results will depend heavily on the value of θ. We therefore search for solutions that satisfy

$$\frac{dE}{d\theta} = 0. \tag{4.9}$$

This is equivalent to treating θ as a variational parameter. The stationary point is found by computing the energy for many values of θ. This "θ-trajectory" is then used as input into the analytic continuation procedure described in Ref. [56]. This is a reproducible method to compute Seigert energies from θ-trajectories. However, within this method, there are still three different ways that the stationary point may be computed in practice.

For the moment, we ignore the complication that there are in general multiple points where the energy is stationary with respect to variations in θ and define a functional $\mathcal{S}[f(\theta)]$ that returns the value of the function at the point that it is stationary:

$$S[f(\theta)] = f(\theta_0) \quad \text{s.t.} \quad \left.\frac{df}{d\theta}\right|_{\theta=\theta_0} = 0. \tag{4.10}$$

Using this notation, we can describe three methods, all equivalent in the complete basis set limit, for finding the Siegert energy of temporary anions as a complex attachment energy:

1. $E_{\text{res}} = S\left[E^{\text{anion}}(\theta)\right] - E^{\text{neutral}}(0)$
2. $E_{\text{res}} = S\left[E^{\text{anion}}(\theta)\right] - S\left[E^{\text{neutral}}(\theta)\right]$
3. $E_{\text{res}} = S\left[E^{\text{anion}}(\theta) - E^{\text{neutral}}(\theta)\right]$.

In general, these methods will yield different results in a finite basis. In Ref. [57], method 1 was used to determine the stationary point for NH-SCF calculations. While these three methods yield very similar results in the case of NH-SCF, we will see that this is not the case in correlated calculations. Because the stationary point in a calculation on a neutral molecule is usually very nearly on the real axis, method 2 will in practice yield very similar results to method 1 and we will be primarily concerned with the differences between methods 1 or 2 and method 3. In Sections 4.3.1 and 4.3.2 we will find that method 3 is the most reliable.

4.3 Results

All methods are implemented in a development version of the QChem 4.4 package[88]. Libtensor[30] is used for all tensor manipulations, and the complex EOM-CC code presented in Refs. [79, 132, 162] is reused. The basis sets are the same as those presented in Ref. [56]. They are constructed from Dunning's augmented correlation-consistent basis sets (aug-cc-pVXZ)[97, 98], but with added diffuse functions on the center of mass. The basis sets including core-valence polarization functions are constructed in precisely the same manner, but from the corresponding cc-pCVXZ basis[176].

4.3.1 Benchmark calculations on N_2^-

The $^2\Pi_g$ shape resonance in e^--N_2 scattering is nearly unique in that there is a experimentally derived estimate of the position and width of the *pure electronic* resonance[147]. We will refer to this position of 2.32 eV and width of 0.41 eV as the accepted values. The resonance parameters computed in different basis sets at different levels of theory are shown in Table 4.1. Here the stationary point is computed using method 1 of Section 4.2.5.

Note that while the NH-SCF results are unchanged by the inclusion of core-valence polarization functions, the results of the correlated calculations change significantly when core-valence polarization functions are included. Furthermore, while there is evidence of convergence with respect to basis set size, it is clear that even in the caug-cc-pCVQZ(cm+) basis set, the results are not entirely converged with respect to basis set size. This is in contrast to the NH-SCF results which are largely converged in the smallest caug-cc-pVDZ(cm+) basis set.

In Table 4.2 we show results from the same set of calculations, but compute the stationary point using method 3 of Section 4.2.5. While the method used for finding the stationary point makes little difference in the case of NH-SCF calculations, there

	caug-cc-pVDZ(cm+)		caug-cc-pVTZ(cm+)		caug-cc-pVQZ(cm+)	
	Re[E]	Im[E]	Re[E]	Im[E]	Re[E]	Im[E]
NH-ROHF	2.9517	-0.1566	2.9704	-0.1692	2.9525	-0.1547
NH-UHF	2.8366	-0.1087	2.8330	-0.1167	2.8271	-0.1078
NH-RMP2	2.6899	-0.2009	2.5203	-0.0500	2.4245	-0.1828
NH-UMP2	2.8226	-0.1661	2.5733	-0.2475	2.5532	-0.1916
EOM-EA-CCSD	2.7616	-0.1961	2.5418	-0.0223	2.5178	-0.1332
	caug-cc-pCVDZ(cm+)		caug-cc-pCVTZ(cm+)		caug-cc-pCVQZ(cm+)	
	Re[E]	Im[E]	Re[E]	Im[E]	Re[E]	Im[E]
NH-ROHF	2.9472	-0.1565	2.9709	-0.1657	2.9523	-0.1544
NH-UHF	2.8328	-0.1087	2.8380	-0.1152	2.8159	-0.1239
NH-RMP2	2.6922	-0.1995	2.5082	-0.1856	2.4493	-0.3030
NH-UMP2	2.8273	-0.1622	2.6701	-0.2633	2.6193	-0.2805
EOM-EA-CCSD	2.7571	-0.1931	2.5300	-0.1873	2.4591[1]	-0.2069[1]

Table 4.1: Computed Seigert energies for the lowest $^2\Pi_g$ shape resonance of N_2^-. The energies are computed as a stationary point using method 1 of Section 4.2.5. We attribute the significant differences between the energies in valence polarized and core-valence polarized basis sets to use of method 1. Method 3 (see Table 4.2) provides more consistent results.

[a]The EOM results in the largest basis are based on only 5 θ-points and are therefore more uncertain.

	caug-cc-pVDZ(cm+)		caug-cc-pVTZ(cm+)		caug-cc-pVQZ(cm+)	
	Re[E]	Im[E]	Re[E]	Im[E]	Re[E]	Im[E]
NH-ROHF[1]	2.9531	-0.1593	2.9513	-0.1551	2.9529	-0.1511
NH-UHF[1]	2.8346	-0.1178	2.8261	-0.1067	2.8267	-0.1040
NH-RMP2	2.6726	-0.3624	2.5054	-0.2841	2.4719	-0.3121
NH-UMP2	2.8042	-0.3198	2.6612	-0.2885	2.6066	-0.2888
EOM-EA-CCSD	2.6974	-0.3137	2.5653	-0.2770	2.5205	-0.2759
	caug-cc-pCVDZ(cm+)		caug-cc-pCVTZ(cm+)		caug-cc-pCVQZ(cm+)	
	Re[E]	Im[E]	Re[E]	Im[E]	Re[E]	Im[E]
NH-ROHF	2.9493	-0.1602	2.9711	-0.1432	2.9530	-0.1517
NH-UHF	2.8289	-0.1164	2.8338	-0.1167	2.8145	-0.1221
NH-RMP2	2.6687	-0.3647	2.5017	-0.2860	2.4957	-0.3269
NH-UMP2	2.7950	-0.3217	2.6452	-0.3091	2.6175	-0.3150
EOM-EA-CCSD	2.6844	-0.3166	2.5342	-0.2584	2.5360[2]	-0.2604[2]

Table 4.2: Computed Seigert energies for the lowest $^2\Pi_g$ shape resonance of N_2^-. The energies are computed as a stationary point using method 3 of Section 4.2.5.

[a] These results were also reported in Ref. [57]

[b] The EOM results in largest basis are based on only 5 θ-points and are therefore more uncertain.

are significant differences in the correlated calculations. In particular, the widths tend to be larger when computed using method 3. Only in the largest basis (caug-cc-pCVQZ(cm+)) do the two methods provide similar results. In all other cases, method 3 is clearly superior: the results are much less sensitive to the inclusion of core-valence polarization functions and the basis set effects are less pronounced. For this reason, we advocate the use of this method for all complex-basis function calculations.

This is, to our knowledge, the first explicit application of a complex-coordinate based MP2 theory to molecular resonances, and we note that while the MP2 methods are unable to fully reproduce the EOM-EA-CCSD results, they represent a significant improvement relative to the NH-SCF results. In general, the effect of correlation is to lower the position but increase the width relative to NH-SCF methods. This is consistent with previous observations of similar behavior in CAP calculations[177].

Some selected literature results are shown in Table 4.3. We note that at the highest level of theory (EOM-EA-CCSD), our results do not reproduce the accepted value, even in the largest basis set (caug-cc-pCVQZ(cm+)). We still overestimate both the position and width by approximately 0.15-0.2 eV. This is not surprising considering that the results are not entirely converged with respect to basis set size or level of correlation. Based on the effect of changing the basis set size, we estimate the effect of basis set incompleteness to be less than 0.05eV in the caug-cc-pCVQZ(cm+) basis. The correlation energy due to full inclusion of triple and higher excitations is more difficult to quantify. Our method can be viewed as an analytic continuation of the Gaussian-exponent stabilization method of Ref. [146]. For this reason, we would expect agreement at a given level of theory and basis set. The agreement with other theoretical results is reasonable considering the basis/method-dependence of most of these methods. Also, the width is highly dependent on the bond length as will be shown in Figure 4.1. This means that even small geometrical discrepancies can lead to significant differences in the computed width.

4.3.2 Shape resonances in small molecules

Seigert energies for several well-known low-energy shape resonances in the caug-cc-pVTZ(cm+) and caug-cc-pCVTZ(cm+) basis sets are shown in Table 4.4.

These values are computed using method 3 of Section 4.2.5. Method 1, which we do not recommend, yields results that are considerably less consistent and more dependent on the basis set. These results are given in the Appendix (Table 4.7), and we do not refer to them further.

Again we note that the results obtained with method 3 show little sensitivity to the inclusion of core-valence polarization functions. We make no attempt to fully

method	position	width
Stieltjes imaging[143]	2.23	0.40
Schwinger variational + ADC(3) optical potential[144]	2.53	0.54
3rd order decouplings of dilated electron propagator[145]	2.11	0.18
Multi-partitioning perturbation theory stabilization[178]	2.36	0.43
Analytic continuation in the coupling constant CCSD[55]	2.56	0.55
CAP EOM-EA-CCSD (11s,8p,3d)[168]	2.44	0.39
EOM-EA-CCSD stabilization (aug-cc-pV5Z)[146]	2.49	0.50
CAP EOM-EA-CCSD (1st order, aug-cc-pVQZ + 3s3p3d)[79]	2.48	0.29
Analytic continuation in the coupling constant CCSD(T)[58][1]	2.46	0.49
Experimental estimate (accepted value)[147]	2.32	0.41
This work (EOM-EA-CCSD)	2.54	0.52

Table 4.3: Selected literature values (in eV) for the $^2\Pi_g$ shape resonance in electron-N_2 scattering from experiment and various *correlated* levels of theory. The EOM-EA-CCSD results from the caug-cc-pCVQZ(cm+) are given as the results of "This work."

[a]The results using the attenuated Coulomb potential with $\omega = 0.01$ in the t-aug-cc-pVQZ basis set are given here.

caug-cc-pVTZ(cm+)	CO^-		CO_2^-		CH_2O^-	
	Re[E]	Im[E]	Re[E]	Im[E]	Re[E]	Im[E]
NH-ROHF	2.5367	-0.3576	4.4648	-0.0780	1.7769	-0.2003
NH-UHF	2.4194	-0.2964	4.3063	-0.0619	1.6399	-0.1411
NH-RMP2	2.1193	-0.5200	4.1018	-0.1832	1.0120	-0.3011
NH-UMP2	2.1968	-0.4826	4.1829	-0.1555	1.0986	-0.2859
EOM-EA-CCSD	2.0395	-0.4974	4.0193	-0.1422	1.1810	-0.2788
caug-cc-pCVTZ(cm+)	CO^-		CO_2^-		CH_2O^-	
	Re[E]	Im[E]	Re[E]	Im[E]	Re[E]	Im[E]
NH-ROHF	2.5405	-0.3542	4.4654	-0.0801	1.7696	-0.2113
NH-UHF	2.4241	-0.3004	4.3114	-0.0634	1.6313	-0.1478
NH-RMP2	2.1149	-0.5026	4.0919	-0.1871	1.0066	-0.2997
NH-UMP2	2.1892	-0.4784	4.1734	-0.1576	1.0934	-0.2836
EOM-EA-CCSD	2.0434	-0.5164	3.9951	-0.1432	1.1632	-0.2837

Table 4.4: Computed Seigert energies for low energy shape resonances in some molecules in caug-cc-pVTZ(cm+) and caug-cc-pCVTZ(cm+). The energies are computed as a the stationary point using method 3 of Section 4.2.5.

explore the basis-set convergence, but these numbers are very unlikely to be fully converged in the triple-zeta basis sets. The true values of the pure electronic Seigert energies are not known in these cases. From the basis set convergence of N_2^- and the level of correlation, we are likely overestimating positions by 0.1-0.3 eV and width by 0.05-0.2eV. As in the case of N_2^-, the NH-MP2 results are improved significantly over the NH-SCF results.

We show some selected literature values which include electron correlation effects in Table 4.5. Note that the experimental results listed in Table 4.5 cannot be directly compared with theory because they have not been corrected to extract the location of the pure electronic resonance. As with N_2, our results for the position of these resonances agree fairly well with other theory. Our estimates for the widths are a bit high compared with other theoretical results, but not unreasonably so. Comparing complex basis functions to CAPs at the EOM-EA-CCSD level of theory, we find that the positions agree quite well, but widths computed with complex basis functions are consistently larger than those computed with CAPs.

molecule	method	position	width
CO	2nd order electron propagator[149]	1.71	0.08
	3rd order decouplings of the electron propagator[145]	1.65	0.14
	Multi-partitioning perturbation theory stabilization[178]	2.02	0.35
	CAP EOM-EA-CCSD (largest basis)[168]	2.07	0.42
	CAP EOM-EA-CCSD (1st order, aug-cc-pV5Z + 3s3p3d)[79]	1.76	0.60
	Experiment[150]	1.50	0.40
	This work (EOM-EA-CCSD)	2.04	1.03
CO_2	CAP EOM-EA-CCSD(aug-cc-pVTZ-f+ 1s3p)[169]	4.20	0.22
	CAP EOM-EA-CCSD (1st order, aug-cc-pVTZ + 3s3p3d)[79]	4.00	0.20
	Analytic continuation in the coupling constant SAC-CI[179]	4.18	0.24
	CAP SAC-CI (cc-pVDZ + (2s5p2d))[179]	4.21	0.20
	Experiment[153]	3.14	0.20
	This work (EOM-EA-CCSD)	4.00	0.29
CH_2O	2nd order decouplings of the dilated electron propagator (largest basis)[155]	0.89	0.076
	CAP SAC-CI (cc-pVQZ + diffuse)[180]	1.09	0.42
	CAP EOM-EA-CCSD (1st order, aug-cc-pVTZ + 3s3p3d)[79]	1.31	0.28
	Experiment[157]	$\sim$0.67	-
	This work (EOM-EA-CCSD)	1.16	0.57

Table 4.5: Selected literature values (in eV) for the resonances studied here from experiment and various levels of theory. The experimental values are uncorrected and therefore do *not* represent the properties of the pure electronic resonance. The results from EOM-EA-CCSD in the caug-cc-pCVTZ(cm+) basis are also given labelled as "This work."

4.3.3 Complex potential energy curves

An important challenge for electronic resonance methods is the computation of smooth, consistent potential energy surfaces. By "consistent," we mean that the imaginary part of the resonance goes to zero at the same point that the state crosses the ground state of the target. A potential energy curve for N_2^- at the EOM-EA-CCSD level of theory is shown in Figure 4.1 and 4.2. We used a spin-restricted, NH-RHF determinant as the reference wavefunction. This choice of reference prevents us from obtaining a qualitatively correct potential energy surface at significantly stretched geometries, but we can still observe the behavior of the resonance as it crosses the ground state of the neutral. The two curves are not completely consistent: the width of the temporary anion goes to zero a bit before the two curves cross. However, this discrepancy (~ 0.05Å) is fairly small considering that the width depends only weakly on internuclear distance near the crossing region. This means that a very small absolute error in the width can lead to much larger errors in apparent point where it goes to zero. Similar curves are provided in Ref. [162] at the CAP-EOM-EA-CCSD level of theory in a very similar basis set. The positions agree very well (see the upper panel of Figure 2 of Ref. [162]) with our results. The widths (see the lower panel of Figure 2 of Ref. [162]) agree qualitatively, but disagree in the point where they go to zero. There is agreement that the position goes to zero at 1.40Å, but we find the width goes to zero closer to 1.35Å whereas it goes to zero around 1.45Å in Ref. [162].

Nitrogen is a difficult case for potential energy curves because it is a triple bonded system and because its dissociation products are bound by very little. For simpler, single-bonded cases, a qualitatively correct potential energy curve can be obtained from EOM-EA on top of a triplet reference. We demonstrate this process for H_2 in Figure 4.3. H_2 has two temporary anions of Σ symmetry that are anti-symmetric (u) and symmetric (g) with respect to inversion. The $^2\Sigma_u$ state is the lowest energy resonance and has been studied extensively[45, 71, 181, 182]. This resonance is quite broad near equilibrium and we were unable to easily distinguish it from the continuum in this region. However, as the bond is stretched, it becomes bound near 1.60Å. There is also a $^2\Sigma_g$ state[182–184] which is not easily discernible in our calculations until around 2.6Å where it is briefly a Feshbach resonance: its position is above the singlet ground state but below the triplet parent state. Near 2.7Å this state becomes bound. The results for the crossing points agree to within 0.1Å with the calculations of Bardsley and Cohen[183]. Both these states can be obtained by adding an electron to the triplet configuration. Even though both singlet and triplet states are treated exactly at the CCSD level of theory, the triplet reference is preferable because it can be reached from either anion state by a single excitation. In this way,

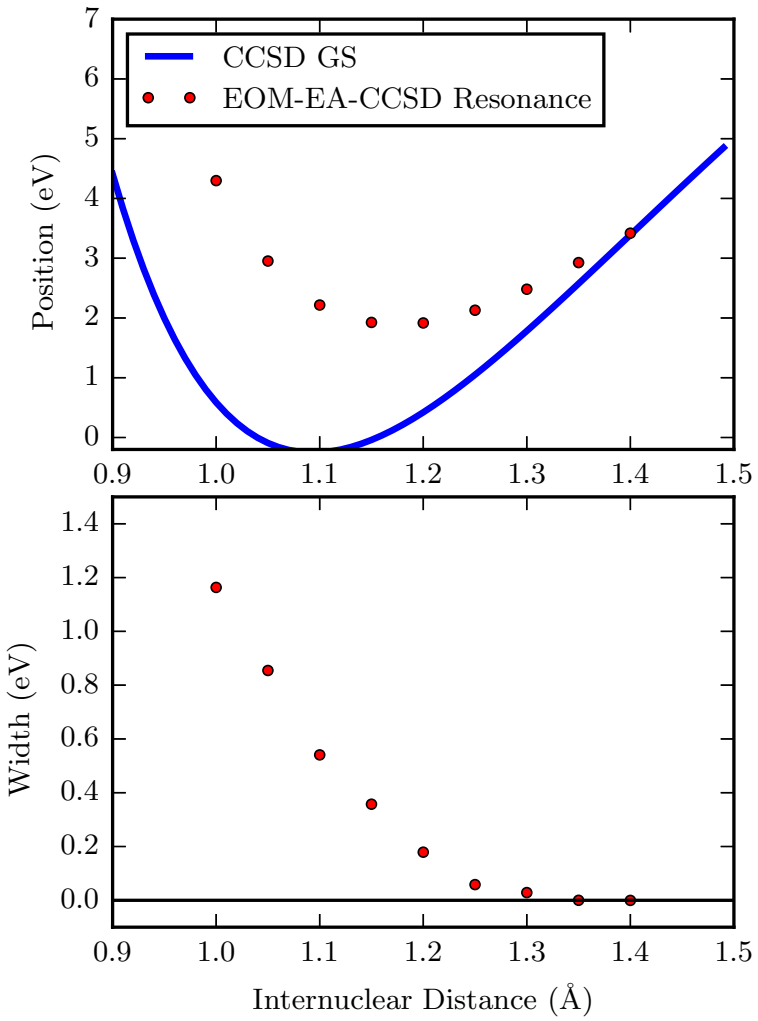

Figure 4.1: Potential energy curve of N_2 neutral and anion. The neutral is computed at the complex RCCSD level of theory, and the complex excitation energy of the anion is computed at the complex restricted EOM-EA-CCSD level of theory. The basis set is caug-cc-pCVTZ(cm+).

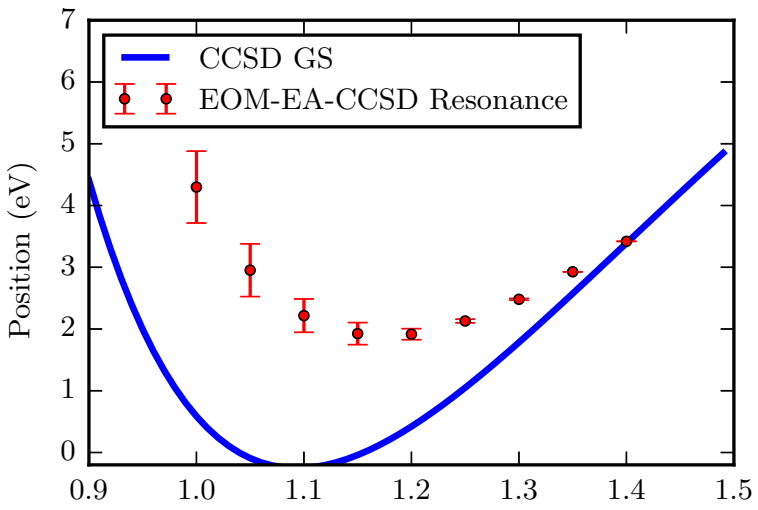

Figure 4.2: Potential energy curve of N_2 neutral and anion. The neutral is computed at the complex RCCSD level of theory, and the complex excitation energy of the anion is computed at the complex restricted EOM-EA-CCSD level of theory. The basis set is caug-cc-pCVTZ(cm+). The width is shown as an uncertainty in the position of the resonance.

we are able to treat both states consistently throughout the full potential energy surface in the spirit of spin-flip methods[185]. The point where the lowest energy resonance crosses the ground state of the neutral to become bound differs from the point where the width goes to zero. This is not necessarily surprising considering that the basis is relatively small and that the singlet CCSD neutral and EOM-EA anion (from the triplet reference) are *not* eigenfunctions of the same effective Hamiltonian.

4.3.4 The $1s2s^2$ Feshbach resonance in e-helium scattering

One of the simplest and most well-studied Feshbach resonances is the $1s2s^2$ Feshbach resonance in e-helium scattering. See Ref. [186] for a recent review and Ref. [187] for a fairly complete table of experimental and theoretical results. Selected theoretical and experimental results (largely reproduced from Ref. [187]) are given in Table 4.6 along with the results of this study.

EOM-EA-CCSD was used to compute the the complex energy relative to a triplet He reference. The energy relative to the singlet ground state is reported in Table 4.6, for two different basis sets. The basis sets were chosen to be small enough that full diagonalization of $\bar{H}$ is feasible while still including functions necessary to

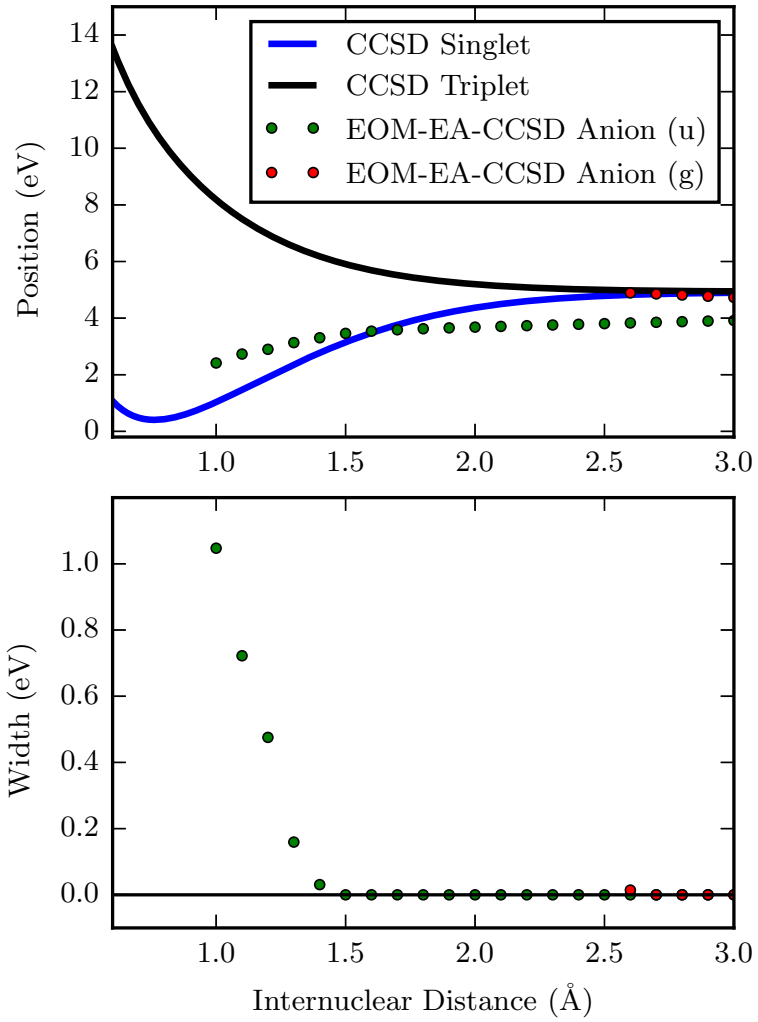

Figure 4.3: Potential energy curve of H_2 neutral and anion. The neutral curves are computed at the CCSD level of theory, and the complex excitation energy of the anion is computed at the complex EOM-EA-CCSD level of theory relative to the triplet reference. The basis set is caug-cc-pVDZ(cm+). For H_2, CCSD reproduces full-CI.

Experiment		
Reference	position (eV)	width (meV)
Brunt *et al*[188]	19.366(5)	9.(1)
Kennerly *et al*[189]	19.36(2)	11.0(5)
Buckman *et al*[190]	19.367(5)	-
Dube *et al*[191]	-	10.3(3)
Gopalan *et al*[187]	19.365(1)	11.2(5)
Theory		
Reference	position (eV)	width (meV)
Junker[165]	19.387	11.72
Bylicki[192]	19.367	8.6
Gil *et al*[193]	19.357	14
Gopalan *et al*[187]	19.366	10.7
Results of the present study		
Basis	position (eV)	width (meV)
basis 1	19.28200	7.02475
basis 2	19.33005	6.88694

Table 4.6: Results from the literature and from this study for the $1s2s^2$ Feshbach resonance in e-helium scattering. Note the high precision to which the resonance parameters are known both theoretically and experimentally. The basis sets used for these computations are described in the text of Section 4.3.4

describe the principal contribution to the correlation energy. The first basis set is caug-cc-pVTZ(cm+) but with no d-functions. The second basis set is the caug-cc-pVTZ(cm+) basis set including valence and augmenting d-functions but without the additional diffuse d-functions. The agreement with precise theoretical and experimental results is good: the width is underestimated by a large relative amount that is nonetheless very small in absolute terms. We cannot expect to be able to reproduce the accuracy of atomic calculations employing numerical basis sets, but the modest agreement in fairly small Gaussian basis sets is encouraging.

Despite this encouraging result, it can be difficult to converge iterative diagonalization algorithms to the high lying roots that are associated with Feshbach resonances. More development is necessary to make this approach applicable in general to molecular Feshbach resonances. However, this study shows that the EOM-CCSD method is, as we might expect, capable of qualitative, and maybe even quantitative, calculations on Feshbach resonances.

4.4 Conclusions

We have presented an efficient implementation of correlated electronic structure methods utilizing complex basis functions for the computation of positions and widths of molecular resonances. Benchmark calculations on temporary anions of small molecules indicate that analytic continuation of the complex excitation energy (method 3 of Section 4.2.5) is the preferred method for extracting resonance parameters from θ-trajectories. Our results for the positions of these resonances agree well with the literature values, while our results for the widths are larger than those of most other correlated methods. However, because of the very large number of diffuse basis functions included in our basis sets, we believe our results to be among the most accurate available. The consistent accuracy of the NH-MP2 results should be viewed as one of the primary successes of this project. While EOM-EA-CCSD is more accurate, its computational cost makes NH-MP2 a more attractive candidate for larger systems.

We have also explored the ability of EOM-EA-CCSD to accurately describe complex potential energy surfaces and the essential physics of Feshbach resonances. The results are very encouraging overall, but currently, the computational cost and extreme basis-set requirements of the EOM-EA-CCSD method make it impractical for all but the smallest polyatomic molecules. Feshbach resonances bring additional difficulty in the convergence of the iterative diagonalization method. Further work is needed to improve the efficiency and general convergence properties of the iterative diagonalization step.

Δ-NH-MP2 is cheaper and has the advantage that it does not require solution of a large NH eigenvalue problem. However, it does require the convergence of NH-SCF calculations which can be difficult and it will break down when bonds are stretched. Further work is needed in the form of:

1. Better NH-SCF optimization algorithms for more consistent convergence
2. EOM-EA-MP2 for Feshbach resonances
3. Orbital optimized MP2 methods for an improved description of open-shell resonances

4.5 Appendix: Additional results

See Table 4.7 for additional results mentioned in the text.

caug-cc-pVTZ(cm+)	CO^-		CO_2^-		CH_2O^-	
	Re[E]	Im[E]	Re[E]	Im[E]	Re[E]	Im[E]
NH-ROHF	2.5242	-0.3485	4.4625	-0.0677	1.7861	-0.2012
NH-UHF	2.4020	-0.2914	4.3096	-0.0516	1.6472	-0.1541
NH-RMP2	1.9277	-0.5528	4.2200	0.1516	1.1039	-0.1326
NH-UMP2	1.9968	-0.4565	4.2916	0.1967	1.1965	-0.1204
EOM-EA-CCSD	2.1717	0.0569	4.1477	0.1960	1.3333	-0.2025
caug-cc-pCVTZ(cm+)	CO^-		CO_2^-		CH_2O^-	
	Re[E]	Im[E]	Re[E]	Im[E]	Re[E]	Im[E]
NH-ROHF	2.5192	-0.3450	4.4599	-0.0795	1.7970	-0.1712
NH-UHF	2.4045	-0.2934	4.3140	-0.0569	1.6735	-0.1589
NH-RMP2	2.0872	-0.4445	4.0971	-0.0727	1.0269	-0.1852
NH-UMP2	2.1716	-0.4042	4.1792	-0.0481	1.0968	-0.2151
EOM-EA-CCSD	1.9148	-0.2368	3.9970	-0.0426	1.1876	-0.1808

Table 4.7: Computed Seigert energies for low energy shape resonances in some molecules in caug-cc-pVTZ(cm+) and caug-cc-pCVTZ(cm+). The energies are computed as a the stationary point using method 1 of Section 4.2.5.

Chapter 5

Stabilizing potentials for analytic continuation methods

5.1 Introduction

Anions that lie energetically above the associated neutral molecule can decay by autodetachment and are therefore characterized by a finite lifetime. Such temporary anions are resonances in the scattering sense and are specified by their energy above that of the neutral molecule, or position,(E_{r}) and their inverse lifetime or width (Γ)[8, 194, 195]. These parameters can be specified by a complex Siegert energy

$$E = E_{\mathrm{r}} - i\frac{\Gamma}{2} \tag{5.1}$$

which specifies the location of the S-matrix pole that is associated with the resonance[8, 52].

Despite their importance in a variety of chemical processes, reliable computation of resonance positions and widths is still far from routine. The primary difficulty arises from the need to consider the electronic continuum. There exists a variety of methods for computing resonance parameters, though none have been sufficiently developed so as to provide a reliable algorithm that can be generally applied even to the low-lying resonances of small molecules. Scattering methods[32–34, 196–198] treat the continuum with explicit use of scattering boundary conditions in order to compute observables like the cross-section. Stabilization methods[35, 36] and associated analytic continuation methods[37–39], use continuum eigenvalues from bound state calculations to extract resonance parameters. Complex coordinate methods[46, 49, 52, 56, 59, 65, 199] compute the Siegert energy as an eigenvalue of a transformed,

non-Hermitian, Hamiltonian operator. Bound state extrapolation[200, 201] or analytic continuation[53, 55] methods rely on the analytic continuation of bound-state energies to find resonance parameters. The focus of this study is this final class of methods; in particular, we focus on the method of analytic continuation in the coupling constant (ACCC) for shape resonances in molecules.

The ACCC method was first proposed within the nuclear physics community[53, 54]. A potential is added to the Hamiltonian to make the resonance state bound and then the bound state energies are analytically continued, as a function of the potential coupling, to determine the Seigert energy at zero coupling. Nestmann *et al.*[200, 201] independently proposed an extrapolation method for molecular resonances based on scaled nuclear charges. Recently, these two methods have been combined and applied to molecular shape resonances[55, 179, 202–204]. In most of these studies, a Coulomb potential is used to bind the resonance as in the method of scaled nuclear charges. The exception is the manifestly short-range Voronoi potential suggested by Sommerfeld *et al.*[179] Sommerfeld and coworkers noted that the long-range Coulomb potential is not formally applicable and obtained much more consistent results with their Voronoi potential. Despite this fact, methods employing a Coulomb potential have had moderate success with shape resonances in polyatomic molecules. However, these methods suffer from two well-understood afflictions. The first is associated with the difficulty in representing the analytic structure of the resonance trajectory which, for short-range potentials, has a square root branch point in the complex momentum plane[8, 195]. The second is that the analytic continuation itself can easily become numerically unstable[205, 206].

Horáček and coworkers have made a recent attempt to ameliorate these issues[203, 204]. Their method, which they have termed regularized analytic continuation (RAC), relies on the inverse variant of the ACCC method (IACCC) and therefore avoids many of the difficulties associated with the analytic structure of the resonance in the complex-momentum plane. Furthermore, they have incorporated the known features of the analytic structure of the problem into low order Padé approximants which are well-behaved numerically. Unfortunately, the functional form of the RAC Padé approximants is formally appropriate only for short-range potentials and not for the Coulomb potentials with which it has been applied.

In this study we evaluate the RAC method of Horáček and coworkers and compare their low order, type III Padé approximants with a high-order, type II Padé approximant for the analytic continuation of the inverse problem. Both functional forms are used along with three classes of potential: a Coulomb potential that is consistent with previous work, a Gaussian potential, and an attenuated Coulomb potential. The Gaussian and attenuated Coulomb potentials are short-range and therefore compliant with the formal requirements of the ACCC method. These methods are applied

to two problems where the answer is largely known: a model diatomic potential which is numerically solvable, and the $^2\Pi_g$ shape resonance in $e-N_2^-$ scattering.

5.2 Theory

The methods discussed in this paper are based on the IACCC method. In the ACCC method, the Hamiltonian is modified by the introduction of an attractive potential and expressed as a function of a coupling constant λ:

$$H(\lambda) = H + \lambda U. \tag{5.2}$$

The energy of the desired state is then evaluated at several values of λ that are large enough that the desired state is bound. In other words, the energy of the anion relative to the neutral molecule, E, is negative. Introducing a momentum-like variable, κ, such that $E \equiv -\kappa^2$ we construct an analytic continuation $\kappa(\lambda)$. Finally, κ is evaluated at $\lambda = 0$ to obtain the complex Siegert energy associated with the resonance.

Unfortunately, even in the case where U is short-range (falling off at large distances faster than $1/r^2$), the analytic structure of the momentum is such that it has a square root branch point which must be properly represented as a function of λ. A simpler and numerically better behaved method is the analytic continuation of the inverse problem (IACCC).[203, 207] In this method the procedure is the same except that starting from a set of computed values of κ for corresponding values of λ, we construct $\lambda(\kappa)$ and find its zeros to determine the Siegert energy.

$\lambda(\kappa)$ is constructed using a Padé approximant[206]. The method of determining the fit from the input points is important to the results, and finite order Padé approximants are in usually constructed in one of three ways. Type I Padé approximants are determined by matching the coefficients of a power series about a single point. This method is not applicable to the IACCC method as applied here. Type II Padé approximants are required to interpolate some set of input points. Type III Padé approximants are determined by minimizing the χ^2 error in the fit.

5.2.1 The type III (RAC) method

The regularized analytic continuation (RAC) method of Horáček and coworkers specifically relies on low order, type III Padé approximants to accomplish the analytic continuation of $\lambda(\kappa)$. The low order Padé approximants recommended in Ref. [203]

have functional forms given by

$$\lambda^{[2/1]}(\kappa) = \lambda_0 \frac{\kappa^2 + 2\alpha^2\kappa + \alpha^4 + \beta^2}{\alpha^4 + \beta^2 + 2\alpha^2\kappa} \tag{5.3}$$

$$\lambda^{[3/1]}(\kappa) = \lambda_0 \frac{(\kappa^2 + 2\alpha^2\kappa + \alpha^4 + \beta^2)(1 + \delta^2\kappa)}{\alpha^4 + \beta^2 + \kappa[2\alpha^2 + \delta^2(\alpha^4 + \beta^2)]} \tag{5.4}$$

$$\lambda^{[4/2]}(\kappa) = \lambda_0 \frac{(\kappa^2 + 2\alpha^2\kappa + \alpha^4 + \beta^2)(\kappa^2 + 2\gamma^2\kappa + \gamma^4 + \delta^2)}{(\alpha^4 + \beta^2)(\gamma^4 + \delta^2)(1 + \mu^2\kappa)(1 + \mu^2\epsilon^2\kappa)} \tag{5.5}$$

where

$$\mu^2 = \frac{2}{\epsilon^2 + 1}\left[\frac{\alpha^2}{\alpha^4 + \beta^2} + \frac{\gamma^2}{\gamma^4 + \delta^2}\right]. \tag{5.6}$$

These functional forms are specifically constructed to conform to the known analytic structure of $\lambda(\kappa)$ in that the square root branch cut requires that $\lambda(\kappa) \sim \lambda_0 + b\kappa^2$ as $\kappa \to 0$. In Ref. [204] a slightly different [4/2] Padé approximant is suggested, but we will not investigate this alternate functional form in this study. The optimal least-squares fit is obtained by solving the non-linear optimization problem. In the present study, this problem is solved using Newton's method with analytic first derivatives and finite difference second derivatives. The expressions for the first derivatives of these expressions are given in Appendix 5.6.1.

5.2.2 The type II method

We have also investigated the use of high order Padé approximations for analytic continuation of $\lambda(\kappa)$. While the use of high order Padé approximants for analytic continuation has known numerical problems[205], we are unaware of applications of this particular method to the inverse problem.

We use the continued fraction representation given by Schlessinger:[86]

$$\lambda(\kappa) = \frac{\lambda(\kappa_1)}{1+}\frac{a_1(\kappa - \kappa_1)}{1+}\cdots\frac{a_n(\kappa - \kappa_n)}{1}. \tag{5.7}$$

For n input points, this yields a $[N/M]$ Padé approximant where $N + M = n$ and

$$M = \begin{cases} N & , n \text{ even} \\ N - 1 & , n \text{ odd} \end{cases}. \tag{5.8}$$

This is sometimes called a type II, or Thiele-type, Padé approximant. This representation has the advantages that it exactly interpolates all of the input points and does not require the solution a non-linear least squares problem. However, due to the more complicated form, the zeroes must be found numerically. We use Newton's method to solve the root search problem.

5.2.3 The added attractive potential

The precise form of the attractive potential U is flexible, though it must be short range: it must decay faster than r^{-2} at large distances if the analytic structure of $\kappa(\lambda)$ is to be a square root branch point at the critical value of λ where the resonance becomes bound. Despite this restriction, many other authors have advocated using a Coulomb potential. This functional form has the advantage that it requires little to no modification of existing quantum chemistry software, but it is not short-range. The given justification is that in a finite basis, the low-energy part of the spectrum can be effectively ignored so that the long-range part of the Coulomb potential is not important. While it may be effective in practice, this argument lacks formal justification. We will therefore consider two types of added potentials.

First, we consider a Coulomb potential of the form:

$$U_C(\mathbf{r}) = -\lambda \sum_A \frac{Z_A}{|\mathbf{r} - \mathbf{R}_A|}. \tag{5.9}$$

This differs slightly from the potential used in Ref. [203] but is identical to the potential used in other studies[179, 200, 201].

Second we consider an attractive Gaussian potential of the form

$$U_G(\mathbf{r}) = -\lambda \sum_A Z_A e^{-\alpha(\mathbf{r}-\mathbf{R}_A)^2}. \tag{5.10}$$

This potential is chosen to transform as the totally symmetric representation of the molecular point group. The proportionality to the nuclear charges is chosen in analogy with U_C to provide a potential which will affect molecular many-electron states in a balanced way. Note that α is a free parameter that can be chosen arbitrarily in theory, though it will turn out to be important in practice. The appropriate integrals required for matrix elements of such a potential are 3-center overlap integrals and are easily computed by a variety of methods. We briefly describe the computation of such integrals in Appendix 5.6.2.

Finally, we consider an attenuated-Coulomb potential of the form:

$$U_{AC}(\mathbf{r}) = -\lambda \sum_A \frac{Z_A \mathrm{erfc}\left(\omega|\mathbf{r} - \mathbf{R}_A|\right)}{|\mathbf{r} - \mathbf{R}_A|}. \tag{5.11}$$

Unlike the Coulomb potential, this potential is short-range. In contrast to the, also short-range, Voronoi potential of Sommerfeld and Ehara,[179] the molecular integrals over this potential are similar to those required for certain attenuated electronic structure methods and are therefore available in many quantum chemistry programs[208, 209]. ω is likewise a free parameter.

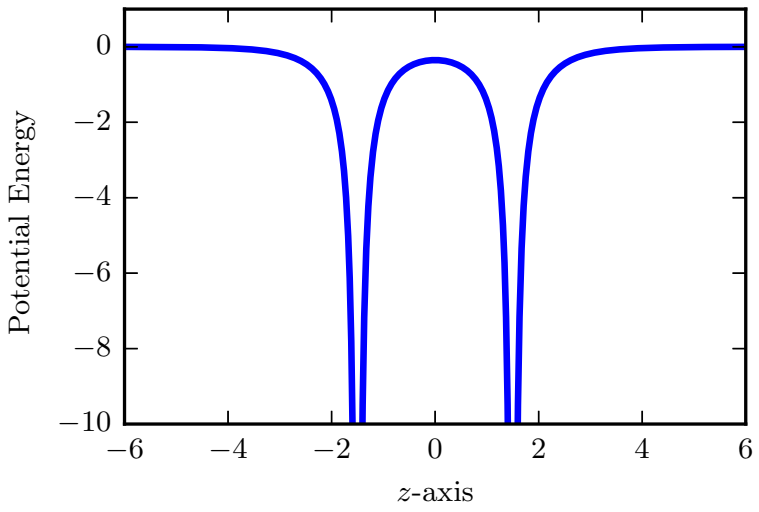

Figure 5.1: The model potential given in Equation 5.12 is plotted along the line defined by the two nuclei. We take this line to be the z-axis.

5.3 Results for a model potential

In order to test these methods on a problem where the answer is known to high numerical accuracy, we can construct a model 1-electron potential that approximates an effective diatomic molecular potential from electron-molecule scattering. We will use **A** and **B** to denote the centers of the two "nuclei." The model potential is of the form

$$V(\mathbf{r}) = -e^{-1.5r_A}\left(\frac{1}{r_A}+1\right) - e^{-1.5r_B}\left(\frac{1}{r_B}+1\right) \tag{5.12}$$

where

$$r_A = |\mathbf{r}-\mathbf{A}| \qquad r_B = |\mathbf{r}-\mathbf{B}|. \tag{5.13}$$

A plot of this potential along the line defined by the positions of the two nuclei is shown in Figure 5.1. There is, to our knowledge, no analytical solution to this problem, but the problem has cylindrical symmetry and may be solved numerically in prolate-spheroidal coordinates using grid methods. This potential supports a bound σ_g-like state ($m = 0$, symmetric under inversion), and a σ_u-like state ($m = 0$, anti-symmetric under inversion) which is a bound state at large (> 4) internuclear distances and a resonance at short internuclear distances. For the purpose of this investigation, we want the second state to be a resonance, so we set the "internuclear" distance to $|\mathbf{A}-\mathbf{B}| = 3$.

5.3.1 Numerical details

In order to perform the analytic continuation methods described in the introduction we add either a Coulomb potential of the form

$$U_C(\mathbf{r}) = -\lambda \left(\frac{1}{r_A} + \frac{1}{r_B} \right), \tag{5.14}$$

a Gaussian potential of the form

$$U_G(\mathbf{r}) = -\lambda \left(e^{-\alpha r_A^2} + e^{-\alpha r_B^2} \right), \tag{5.15}$$

or a screened Coulomb potential of the form

$$U_{GC}(\mathbf{r}) = -\lambda e^{-\alpha (r_A + r_B)^2} \left(\frac{1}{r_A} + \frac{1}{r_B} \right). \tag{5.16}$$

The Gaussian-attenuated Coulomb potential is similar to the erfc-attenuated Coulomb potential that we have used for molecular calculations. All three have cylindrical symmetry and are easily representable in prolate spheroidal coordinates.

Schrödinger's equation was solved in prolate-spheroidal discrete variable representation (DVR) basis for $m = 0$. The DVR method is described in detail in Refs. [210–212]. We used 15 points in the η variable and 200 points on the interval (0, 100) in ξ. All eigenvalues used for analytic continuation were converged to better than 10 significant figures and 10 significant figures were used in all analytic continuations.

The resonance energy was computed by complex scaling the ξ variable as described in Ref. [210]. At this internuclear distance ($R_{AB} = 3$), the resonance has a position of 0.02555645961 and a width of 0.02354423918 in units natural to the problem. These values are similar to those of the σ_u-shape resonance in e^--H_2 scattering, in atomic units, at a slightly stretched geometry.

5.3.2 Evaluation of analytic continuation methods

The analytic continuations were each accomplished from 15 bound state energies bound by 0.01-0.3 units of energy. This is roughly based on the recommendations given in Ref. [203]. The resonance position and width were computed with type II ([8/7] in this case), type III [2/1], and type III [4/2] methods. The three classes of stabilizing potentials are Coulomb potentials (Equation 5.14), Gaussian potentials (Equation 5.15), and Gaussian-attenuated Coulomb potentials (Equation 5.16). We furthermore tested Gaussian potentials with three different exponents,

$\alpha = 0.01, 0.1, 1.0$, and Gaussian-attenuated Coulomb potentials with exponents of $\alpha = 0.005, 0.025, 0.25$.

The results are shown in Table 5.1 along with percent error relative to the numerically exact answer. For this model system, the type II method almost universally outperforms the type III methods by a significant margin. In particular, the widths computed by the type III methods are significantly smaller than the true widths. The type II method is significantly more accurate, but still has relative errors on the order of a couple of percent in some cases which, while small compared to those of the type III methods, are large compared with the accuracy of the input values. We attribute the large errors in the type III methods to be due to insufficient flexibility in the functional form used to fit $\lambda(\kappa)$. On the other hand, the errors in the type II method could be partially due to the inherent numerical instability of extrapolation using high order Padé approximations. This is supported by the fact that the error in the type II calculations is of indeterminate sign. For the type III calculations, the width is always underestimated which suggests some systematic error. We shall see that in real molecular calculations, where the width is often significantly smaller than the position, the type III method may not so drastically underestimate the width.

The type III [4/2] Padé approximant improves very slightly over the results obtained with a [2/1] Padé approximant, but at the cost of a much more difficult non-linear optimization.

Across all analytic continuation schemes the Gaussian-attenuated Coulomb potential produces the most accurate results. The results with the Gaussian-attenuated Coulomb potentials are slightly better than those obtained with a Coulomb potential and significantly better than those obtained with the various Gaussian potentials. Note that the Gausian-attenuated Coulomb potential with the smallest attenuation parameter produces the best results across all methods. This is not surprising, since the theory should be ideal for short-range potentials. However, it is surprising that the that long-range Coulomb potential produces such accurate results compared with the short-range Gaussian-potentials.

Since the attenuated Coulomb potential must ultimately reproduce the results of the Coulomb potential as $\alpha \to 0$, we expect the optimal value of α to be small enough that the potential is minimally distorted in the valence region, but large enough that the potential is still effectively short-range. This "optimal α" will depend on the basis set. For this model problem, our basis extends to $\xi = 100$, and the results in Table 5.1 (c) indicate that the optimal α is less than or equal to $\alpha = 0.005$.

		Type II		Type III [2/1]		Type III [4/2]	
		Position	Width	Position	Width	Position	Width
	Coulomb	0.025644	0.023308	0.027575	0.009680	0.023961	0.012078
	Gaussian ($\alpha = 0.01$)	0.025839	0.022663	0.027013	0.001845	0.023024	0.004761
	Gaussian ($\alpha = 0.1$)	0.025681	0.024694	0.026386	0.003606	0.018890	0.017603
(a)	Gaussian ($\alpha = 1.0$)	0.024454	0.021806	0.026375	0.002578	0.021244	0.006470
	Gauss. Coul. ($\alpha = 0.005$)	0.025561	0.023651	0.030915	0.016863	0.027157	0.019401
	Gauss. Coul. ($\alpha = 0.025$)	0.025448	0.023504	0.028691	0.010971	0.025458	0.013786
	Gauss. Coul. ($\alpha = 0.25$)	0.025731	0.023798	0.027957	0.009963	0.024448	0.012618
	Coulomb	0.343	-1.005	7.898	-58.884	-6.244	-48.699
	Gaussian ($\alpha = 0.01$)	1.106	-3.745	5.701	-92.165	-9.908	-79.778
	Gaussian ($\alpha = 0.1$)	0.487	4.883	3.245	-84.685	-26.086	-25.233
(b)	Gaussian ($\alpha = 1.0$)	-4.314	-7.383	3.204	-89.049	-16.873	-72.520
	Gauss. Coul. ($\alpha = 0.005$)	0.017	0.453	20.968	-28.376	6.263	-17.599
	Gauss. Coul. ($\alpha = 0.025$)	-0.426	-0.171	12.267	-53.403	-0.384	-41.445
	Gauss. Coul. ($\alpha = 0.25$)	0.682	1.077	9.394	-57.683	-4.337	-46.408
	Coulomb	0.523		25.659		21.149	
	Gaussian ($\alpha = 0.01$)	1.861		38.906		34.569	
	Gaussian ($\alpha = 0.1$)	2.090		35.553		25.939	
(c)	Gaussian ($\alpha = 1.0$)	4.989		37.370		33.992	
	Gauss. Coul. ($\alpha = 0.005$)	0.190		22.442		9.304	
	Gauss. Coul. ($\alpha = 0.025$)	0.393		24.967		17.343	
	Gauss. Coul. ($\alpha = 0.25$)	0.766		25.597		19.812	

Table 5.1: Positions and widths, percent relative error (signed) in positions and widths, and percent relative error of the complex resonance energy are shown in panels a, b, and c respectively. All values are computed for the model problem using the specified stabilizing potential with the given analytic continuation method. Compare with the numerically exact value– Position: 0.02555645961, Width: 0.02354423918.

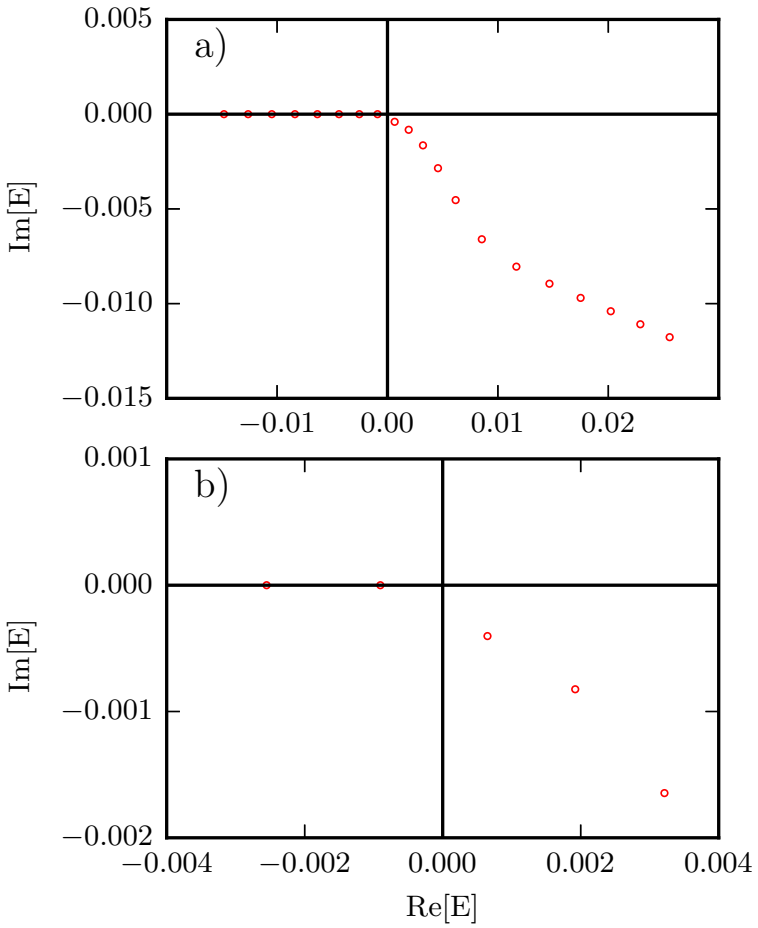

Figure 5.2: The behavior of the resonance under the influence of an attractive Gaussian ($\alpha = 0.1$) potential is shown in (a) with a detailed view near the origin in (b). The coupling constant is increased in the range $\lambda = 0.00, \ldots, 0.038$. At $\lambda = 0$ the resonance is at the lower right of (a). As the potential increases, the resonance's position and width decrease until it becomes bound when passing through $E = 0$.

5.3.3 Analytic structure of the resonance trajectory

In order to further evaluate the analytic continuation methods described in this study, we investigate the behavior of the resonance pole under the influence of an added Gaussian, Coulomb, or Gaussian-attenuated Coulomb potential. The trajectory of the resonance as it becomes bound under the influence of a Gaussian potential ($\alpha = 0.1$) is shown in Figure 5.2. This behavior is well-understood[8], and it is

therefore somewhat surprising that the type III method is not successful with this potential since it precisely encodes the correct analytic structure. However, though the type III methods have the correct form of $\lambda(\kappa)$ near $\kappa = 0$, it is possible that the small number of free parameters are not sufficient to adequately model the function away from $\kappa = 0$. Note that in Figure 5.2, the behavior of the resonance far away from $\kappa = 0$ is complicated and likely not well modeled by the simple functional forms used in the type III method.

The trajectory of the resonance as it becomes bound under the influence of a Coulomb potential is shown in Figure 5.3. Note that the resonance crosses $E = 0$ with a finite, negative imaginary part. This behavior, which plays a role in theories of dissociative recombination, [213] has been known for quite some time, [214–216] and it was also recognized in Ref. [217], where it was further shown that the pole corresponding to the resonance is not analytically connected to that of the bound state. It is evident from Figure 5.3 and from Ref. [217] that the analytic structure that is built into the RAC class of type III approximations is not correct for a Coulomb potential: the resonance does not even pass through the point $E = -\kappa^2 = 0$ in the energy plane.

However, in contrast to the case of a Gaussian potential, the behavior of the resonance far from $\kappa = 0$ is quite simple: the large linear region in energy space gives rise to a large square-root region in momentum space. In this sense, the Coulomb potential appears to be ideal for the type III methods except for near $\kappa = 0$.

The trajectory of the resonance as it becomes bound under the influence of the Gaussian-attenuated Coulomb potential ($\alpha = 0.025$) is shown in Figure 5.4. The Gaussian-attenuated coulomb potential is short-range, and, as with the Gaussian potential, this fact is reflected in the behavior at the origin. However, the behavior away from the origin is more similar to that of the Coulomb potential: there is a large linear region in energy space. The Gaussian-attenuated Coulomb potential retains the desirable features of the Coulomb potential while still being short-range.

5.4 Results for the N_2^- shape resonance

All calculations were performed on N_2^- at its equilibrium geometry (N≡N = 1.094Å). A slightly modified version of the Q-Chem 4 quantum chemistry package[88] was used for all computations. This problem has been very thoroughly studied, and some selected literature values are shown in Table 5.2. The experimental estimate given in Ref. [147] is nearly unique in the electron-molecule scattering literature in that it is an estimate of the position and width of the pure *electronic* resonance and therefore directly comparable to the results of our computations. We will refer to

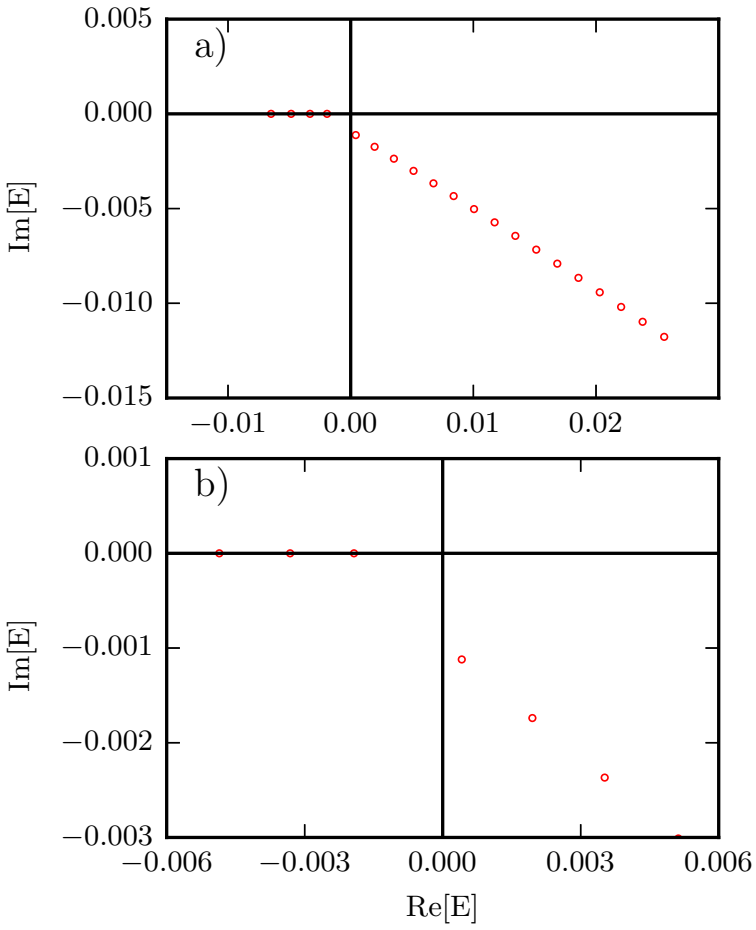

Figure 5.3: The behavior of the resonance under the influence of an attractive Coulomb potential is shown in (a) with a detailed view near the origin in (b). The coupling constant is increased in the range $\lambda = 0.00, \ldots, 0.038$. At $\lambda = 0$ the resonance is at the lower right of (a). As the potential increases, the resonance's position and width decrease, but it does not pass through $E = 0$. The point $\lambda = 0.032$ is omitted because the limits of complex scaling prevent us from easily distinguishing the resonance.

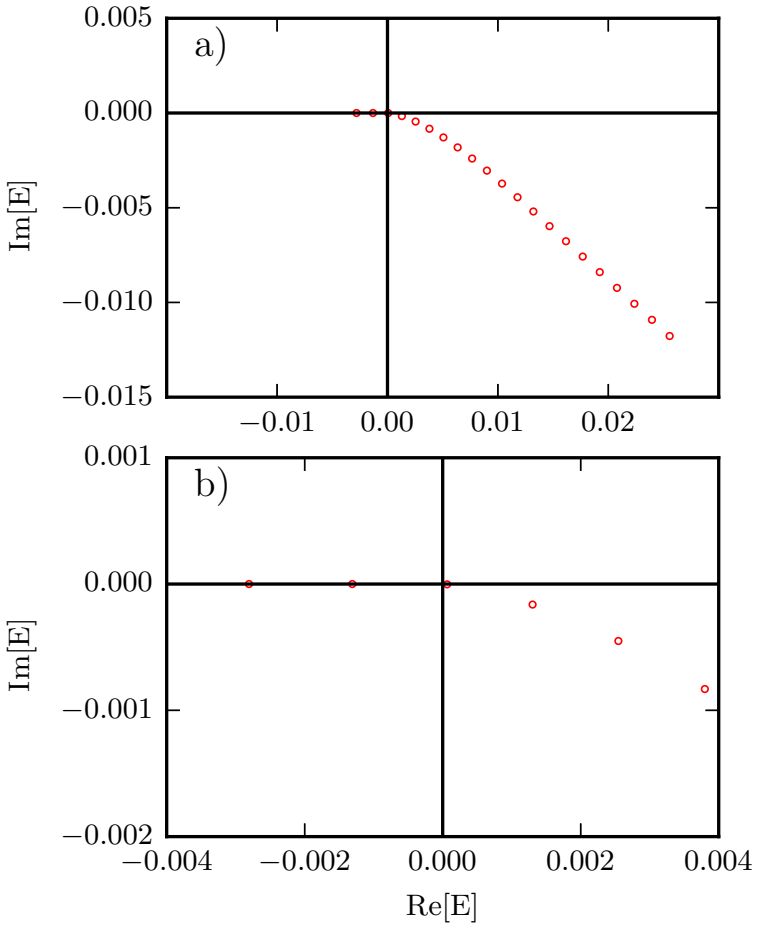

Figure 5.4: The behavior of the resonance under the influence of an attractive Gaussian-attenuated Coulomb potential is shown in (a) with a detailed view near the origin in (b). The coupling constant is increased in the range $\lambda = 0.00, \ldots, 0.040$. At $\lambda = 0$ the resonance is at the lower right of (a). As the potential increases, the resonance's position and width decrease. The complex energy passes through the origin at approximately $\lambda \approx 0.036$.

method	position	width
Stieltjes imaging[143]	2.23	0.40
Schwinger variational + ADC(3) optical potential[144]	2.534	0.536
3rd order decouplings of dilated electron propogator[145]	2.11	0.18
EOM-EA-CCSD stabilization (aug-cc-pV5Z)[146]	2.49	0.5
CAP EOM-EA-CCSD (1st order, aug-cc-pVQZ + 3s3p3d)[79]	2.478	0.286
NH-ROHF with complex basis functions[57]	2.95	0.31
NH-UHF with complex basis functions[57]	2.83	0.22
Experimental estimate[147]	2.32	0.41

Table 5.2: Selected literature values (in eV) for the resonances studied here from experiment and various levels of theory. The experimental estimate given in the final line is an estimate of the purely electronic resonance parameters that has been extracted from experiment.

this experimentally derived estimate (E_r = 2.32 eV, Γ = 0.41 eV) as the accepted value.

We compare results at the ΔSCF and ΔCCSD(T) levels of theory. Further results at intermediate levels of theory (ΔMP2, ΔCCSD) are shown in the supporting material and in selected cases. We use the correlation-consistent basis sets of Dunning and coworkers.[97, 98] The double and triple augmenting functions were obtained by even-tempered extrapolation. For a given basis and angular momentum, the even-tempered factor was taken to be the ratio between the exponents of the most diffuse valence basis function and the augmenting function as specified in the appropriate aug-cc-pVXZ basis set.

In all cases a minimum of 20 (maximum of 23) different coupling strengths corresponding to electron affinities in the range 0 - 20 eV were used in the analytic continuation. This corresponds to type II Padé approximants with a minimum order of [10/10] and maximum order of [12/11].

5.4.1 Evaluation of the type III-Coulomb method

The results of the type III method using an attractive Coulomb potential for the N_2^- shape resonance are shown in Table 5.3. We will focus on the [2/1] Padé approximant. However, for completeness, we show some results obtained with a [4/2] Padé approximant.

The [2/1] Padé approximation proved to be simple to implement and we found the least squares problem to be easily solved. Furthermore, the method appears to

method	basis	Position	Width
ΔSCF [2/1]	aug-cc-pVDZ	2.74110	0.70651
	d-aug-cc-pVDZ	2.73775	0.70488
	t-aug-cc-pVDZ	2.73815	0.70516
	aug-cc-pVTZ	2.76426	0.62306
	d-aug-cc-pVTZ	2.76112	0.62566
	t-aug-cc-pVTZ	2.76130	0.62669
	aug-cc-pVQZ	2.76009	0.62897
	d-aug-cc-pVQZ	2.75868	0.62994
	t-aug-cc-pVQZ	2.75874	0.63018
ΔCCSD(T) [2/1]	aug-cc-pVDZ	2.55676	0.76962
	d-aug-cc-pVDZ	2.49716	0.77837
	t-aug-cc-pVDZ	2.51582	0.77359
	aug-cc-pVTZ	2.41758	0.61607
	d-aug-cc-pVTZ	2.37994	0.62489
	t-aug-cc-pVTZ	2.37848	0.62606
	aug-cc-pVQZ	2.35872	0.60604
	d-aug-cc-pVQZ	2.33451	0.61071
	t-aug-cc-pVQZ	2.33383	0.61100
ΔCCSD(T) [4/2]	t-aug-cc-pVQZ	2.3658	0.5531

Table 5.3: Positions and widths (in eV) of the $^2\Pi_g$, N_2^- shape resonance computed using the type III-Coulomb method. Note the favorable convergence with respect to basis set size.

be numerically stable and the computed resonance parameters converge well with respect to basis set size. Comparing with the literature values in Table 5.2 we see that positions computed with the type III-Coulomb method agree modestly with the large spread of different theoretical values. But more importantly, the computed position seems to converge well to the experimental estimate of the position in a large basis set at the ΔCCSD(T) level of theory. However, the width computed with the type III-Coulomb method is consistently too large, and does not converge to the correct limit with increasing basis set size and level of theory. The performance of the type III method on this particular problem is better than might be expected from the application to the model potential. This may be because, unlike in the case of the model potential, the width is almost an order of magnitude smaller than the position. This could reduce the error due to behavior of the resonance near $\kappa = 0$.

The use of a [4/2] Padé approximant (also see supplementary material: Table

II) does not significantly change the computed positions and widths. However, we found the least squares problem to be significantly more difficult to solve and in some cases complicated by multiple solutions. It is possible that the [4/2] Padé approximant suggested in Ref. [204] will give better results. We also used a [3/1] Padé approximate, but, in comparison with the [2/1] Padé approximant, we found the differences in both the practical aspects and the results to be insignificant.

5.4.2 Evaluation of the type II-Coulomb method

The results for the type II-Coulomb method are shown in Table 5.4. As expected, the width appears to be slightly more accurate than that computed with the type III-Coulomb method, but it is more difficult to converge the results with respect to the basis set size. The type II method proved to be simple to use, and in no case did we observe severe numerical problems.

Furthermore, we note that at the ΔSCF level of theory, the results agree well with the complex basis function results of Ref. [57] computed at the same level of theory (see the "NH-UHF" row of Table 5.2). This agreement between different methods at the same approximate level of theory is encouraging. The fact that the CCSD(T) results do not reproduce the accepted value in the largest basis set is not surprising, because even in this basis, the numbers do not appear to be converged with respect to basis set size. It is also possible that the results are not fully converged with these treatments of correlation.

5.4.3 Evaluation of the type III-Gaussian method

The type III method with an added Gaussian potential is found to be critically dependent upon the form of the added Gaussian potential. Some results for three different Gaussian exponents are shown in Table 5.5. Note that despite the apparently good basis set convergence for a given value of α, the resonance parameters are very dependent on the exponent of the Gaussian potential. This suggests that the functional form used for the analytic continuation is not sufficiently flexible to accurately model $\lambda(\kappa)$ for all values of α. This is consistent with the performance of the type III methods on the model potential.

Using a higher level of theory and a higher order Padé approximant improves the agreement between the $\alpha = 0.01$ and $\alpha = 0.1$ cases, but does little to improve the $\alpha = 1$ case. This further suggests that the [2/1] Padé approximant is not sufficiently flexible to accurately describe the complex energy as a function of the coupling constant. Also, as noted in the previous section, the [4/2] Padé approximation is in practical terms much inferior to the simpler [2/1] and [3/1] approximations. The

method	basis	Position	Width
ΔSCF	aug-cc-pVDZ	2.8326	-0.0029
	d-aug-cc-pVDZ	2.8096	0.2590
	t-aug-cc-pVDZ	2.8462	0.1863
	aug-cc-pVTZ	2.8003	0.0051
	d-aug-cc-pVTZ	2.8324	0.1629
	t-aug-cc-pVTZ	2.7967	0.1955
	aug-cc-pVQZ	2.8124	0.1138
	d-aug-cc-pVQZ	2.8175	0.2344
	t-aug-cc-pVQZ	2.8206	0.2071
ΔCCSD(T)	aug-cc-pVDZ	2.5401	0.0322
	d-aug-cc-pVDZ	2.7727	0.0372
	t-aug-cc-pVDZ	2.6694	0.6235
	aug-cc-pVTZ	2.3678	0.3940
	d-aug-cc-pVTZ	2.4952	0.5432
	t-aug-cc-pVTZ	2.4940	0.4426
	aug-cc-pVQZ	2.3284	0.4049
	d-aug-cc-pVQZ	2.4343	0.5048
	t-aug-cc-pVQZ	2.4564	0.4563

Table 5.4: Positions and widths (in eV) of the $^2\Pi_g$, N_2^- shape resonance computed using the type II-Coulomb method. Note that the method does not have the stability of the type III-Coulomb method, but it does provide a more accurate value for the width.

non-linear, least-square optimization is much more difficult to solve and, unlike in the [2/1] case, there can be several nearby minima.

Both the failure of the type III-Gaussian method, and the moderate success of the type III-Coulomb method can be explained by the model potential calculations shown in Figures 5.2 and 5.3. These trajectories suggest that the Gaussian potential gives rise to an analytic form that is more complicated than that of the Coulomb potential and is therefore more difficult to reproduce with the simple Padé approximants used in the type III method.

5.4.4 Evaluation of the type II-Gaussian method

The type II-Gaussian method uses a functional form that is significantly more flexible than the low order Padé approximations used in the type III family of meth-

method	basis	$\alpha = 0.01$		$\alpha = 0.1$		$\alpha = 1.00$	
		Position	Width	Position	Width	Position	Width
ΔSCF [2/1]	aug-cc-pVDZ	2.8433	0.0513	2.9523	0.4598	2.5565	2.9050
	d-aug-cc-pVDZ	2.8029	0.0784	2.9448	0.4599	2.6556	2.9297
	t-aug-cc-pVDZ	2.8006	0.0802	2.9449	0.4604	2.5456	2.8870
	aug-cc-pVTZ	2.8215	0.0590	2.9291	0.4606	2.6216	2.7584
	d-aug-cc-pVTZ	2.7972	0.0757	2.9264	0.4662	2.7144	2.7894
	t-aug-cc-pVTZ	2.7970	0.0766	2.9265	0.4679	2.6209	2.7557
	aug-cc-pVQZ	2.6237	0.0608	2.9250	0.4686	2.6996	2.7860
	d-aug-cc-pVQZ	2.7977	0.0761	2.9248	0.4701	2.6024	2.7506
	t-aug-cc-pVQZ	2.7976	0.0761	2.9251	0.4705	2.5600	2.7328
ΔCCSD(T) [2/1]	t-aug-cc-pVQZ	2.2089	0.1707	2.5551	0.5163	2.4757	2.9159
ΔCCSD(T), [4/2]	t-aug-cc-pVQZ	2.4018	0.6343	2.5317	0.5752	2.5608	2.4871

Table 5.5: Positions and widths (in eV) of the $^2\Pi_g$, N_2^- shape resonance computed using the type III-Gaussian method at the ΔSCF and ΔCCSD(T) levels of theory. Note the strong dependence on the exponent of the added Gaussian potential (α).

ods which should, to some extent, remedy the problem discussed in the previous section. The results for different basis sets at the ΔSCF and ΔCCSD(T) levels of theory are shown in Table 5.6. Overall, the results are much more consistent as the exponent of the added Gaussian potential is varied. That being said, the numbers are not as stable with respect to basis set size as in the type III method, and there is still an undesirable α-dependence.

For the CCSD(T) results, there is again fairly good agreement when the exponent of the added Gaussian potential is changed over 2 orders of magnitude. There is still disagreement for $\alpha = 1$, but such a narrow Gaussian affects the core orbitals so disproportionately relative to the diffuse orbitals, that a basis set with core-valence polarization functions and/or a higher-level treatment of electron correlation may be necessary to achieve solid agreement in this case.

5.4.5 Evaluation of the type III-attenuated Coulomb method

The results of the type III-attenuated Coulomb method applied to the $^2\Pi_g$ shape resonance in N_2 are shown in Table 5.7 at the ΔSCF and ΔCCSD(T) levels of theory. For a small attenuation parameter, there is negligible difference between these results and the results obtained with the Coulomb potential. Despite apparent basis-set convergence, the numbers have an ω-dependence that is nonetheless not as severe as the α-dependence in the case of the Gaussian potential. More distressing is that the widths do not appear to converge to the accepted value of the width. However the position of the resonance seems to be computed accurately and has very little ω-dependence at the CCSD(T) level of theory.

For completeness, the results in the largest basis set using a [4/2] Padé approximant are given in the supplementary material (Table VII). Only for $\omega = 0.1$ was the [4/2] fit different than the [2/1] at the ΔSCF level of theory. Despite this very slight improvement in the ω-dependence, the results are not significantly different, and again fitting the the [4/2] Padé approximant proved to be a more difficult optimization problem.

Some results for different treatments of correlation in the largest basis set are shown in Table 5.8. As we might expect, MP2 theory recovers a significant, but still incomplete, portion of the correlation contribution. The effect of the triples correction is negligible in this case. The width does not change significantly as the treatment or correlation is changed, and it does not converge to the accepted value.

method	basis	$\alpha = 0.01$		$\alpha = 0.1$		$\alpha = 1.00$	
		Position	Width	Position	Width	Position	Width
ΔSCF	aug-cc-pVDZ	2.8423	-0.0008	2.8394	0.0415	2.8129	0.4298
	d-aug-cc-pVDZ	2.8875	0.0871	2.8515	0.1599	2.8006	0.4190
	t-aug-cc-pVDZ	2.8327	0.2327	2.8491	0.1721	2.8307	0.2376
	aug-cc-pVTZ	2.8064	0.0015	2.7958	0.0671	2.8533	0.3916
	d-aug-cc-pVTZ	2.8512	0.1279	2.8377	0.1553	2.8081	0.4032
	t-aug-cc-pVTZ	2.8358	0.2158	2.8415	0.1673	2.7915	0.3429
	aug-cc-pVQZ	2.5834	0.0034	2.8039	0.1559	2.7885	0.3914
	d-aug-cc-pVQZ	2.8326	0.2005	2.8380	0.1742	2.8452	0.4210
	t-aug-cc-pVQZ	2.8299	0.2154	2.8412	0.1718	2.7963	0.4007
ΔCCSD(T)	t-aug-cc-pVQZ	2.4419	0.5908	2.4820	0.5360	2.4510	0.7185

Table 5.6: Positions and widths (in eV) of the $^2\Pi_g$, N_2^- shape resonance computed using the type II-Gaussian method. Note that there is significantly reduced dependence on the exponent of the added Gaussian potential (α).

method	basis	$\omega = 0.001$		$\omega = 0.01$		$\omega = 0.1$	
		Position	Width	Position	Width	Position	Width
ΔSCF [2/1]	aug-cc-pVDZ	2.74217	0.70854	2.75251	0.72708	2.68530	1.05547
	d-aug-cc-pVDZ	2.73879	0.70692	2.74905	0.72543	2.75149	1.02148
	t-aug-cc-pVDZ	2.73920	0.70719	2.74781	0.72579	2.75192	1.02192
	aug-cc-pVTZ	2.76522	0.62485	2.77457	0.64119	2.72995	0.93501
	d-aug-cc-pVTZ	2.76209	0.62746	2.77149	0.64389	2.73919	0.92092
	t-aug-cc-pVTZ	2.76227	0.62849	2.77171	0.64494	2.73911	0.92266
	aug-cc-pVQZ	2.76087	0.63085	2.77034	0.64736	2.72381	0.94495
	d-aug-cc-pVQZ	2.75966	0.63175	2.76914	0.64830	2.73459	0.92812
	t-aug-cc-pVQZ	2.75972	0.63200	2.76921	0.64855	2.73479	0.92839
ΔCCSD(T) [2/1]	aug-cc-pVDZ	2.55822	0.77198	2.57251	0.79356	2.56588	1.14238
	d-aug-cc-pVDZ	2.49861	0.78082	2.50061	0.80643	2.54943	1.13871
	t-aug-cc-pVDZ	2.51745	0.77596	2.49981	0.80661	2.54894	1.13888
	aug-cc-pVTZ	2.41852	0.61804	2.42736	0.63629	2.47546	0.89812
	d-aug-cc-pVTZ	2.38092	0.62691	2.38958	0.64573	2.45552	0.90377
	t-aug-cc-pVTZ	2.37963	0.62805	2.38836	0.64690	2.45512	0.90525
	aug-cc-pVQZ	2.35958	0.60802	2.36776	0.62623	2.37978	0.89098
	d-aug-cc-pVQZ	2.33540	0.61272	2.34348	0.63124	2.37299	0.89164
	t-aug-cc-pVQZ	2.33466	0.61301	2.34256	0.63159	2.39789	0.88717

Table 5.7: Positions and widths (in eV) of the $^2\Pi_g$, N_2^- shape resonance computed using the type III-attenuated Coulomb method with a [2/1] Padé approximant at various levels of theory. Note the dependence on the attenuation parameter (ω).

	Position	Width
ΔSCF	2.76921	0.64855
ΔMP2	2.54952	0.68410
ΔCCSD	2.34915	0.61525
ΔCCSD(T)	2.34256	0.63159

Table 5.8: Positions and widths (in eV) of the $^2\Pi_g$, N_2^- shape resonance computed using the type III-attenuated Coulomb method using a [2/1] Padé approximant at various levels of theory. The basis set is the t-aug-cc-pVQZ basis set and $\omega = 0.01$.

5.4.6 Evaluation of the type II-attenuated Coulomb method

The type II-attenuated Coulomb method performs well when applied to the $^2\Pi_g$, N_2^- shape-resonance. The results at the ΔSCF and ΔCCSD(T) levels of theory are shown in Table 5.9. Despite slow convergence with respect to the diffuse part of the basis set, the type II-attenuated Coulomb method has negligible ω-dependence. In the largest basis, the results do not quite converge to the accepted value, but it is apparent the the numbers are not entirely converged with respect to the basis set. At the ΔSCF level of theory, the results agree remarkably well with the complex basis function, non-Hermitian UHF results of Ref. [57]. Finally, notice that the dependence on ω is small compared to probable error due to the incomplete basis and incomplete description of electron correlation. The primary drawback of this method that it requires a large, diffuse basis set to achieve consistent results.

Results for different treatments of electron correlation are shown in Table 5.10. Both the position and the width are significantly affected by the level of correlation in a manner which is consistent with other methods. The results at the CCSD level of theory agree fairly well with the EOM-EA-CCSD stabilization results presented in Ref. [146]. The small differences are easily attributed to the slightly different level of theory and the different basis set.

5.5 Conclusions and future work

The performance of two different analytic continuation schemes for 3 classes of stabilizing potentials has been critically evaluated. Results for a model problem suggest that the accuracy of the type III methods is limited by the simple functional form. Furthermore, the results for both analytic continuation schemes depend on the functional form of the stabilizing potential. While the Gaussian potential is

	basis	$\omega = 0.001$		$\omega = 0.01$		$\omega = 0.1$	
		Position	Width	Position	Width	Position	Width
SCF	aug-cc-pVDZ	2.83173	-0.00320	2.83333	0.00155	2.82576	0.01793
	d-aug-cc-pVDZ	2.84264	0.16154	2.84648	0.16814	2.84740	0.16000
	t-aug-cc-pVDZ	2.85043	0.17558	2.84711	0.17931	2.84503	0.18047
	aug-cc-pVTZ	2.79090	0.00204	2.74397	0.10855	2.77907	0.07895
	d-aug-cc-pVTZ	2.83293	0.16192	2.83551	0.15931	2.83411	0.16129
	t-aug-cc-pVTZ	2.79914	0.20080	2.79953	0.17272	2.83240	0.18002
	aug-cc-pVQZ	2.78391	0.22003	2.81807	0.06469	2.77191	0.20154
	d-aug-cc-pVQZ	2.83282	0.18578	2.82263	0.10278	2.83902	0.17423
	t-aug-cc-pVQZ	2.80872	0.20374	2.81202	0.19265	2.83933	0.17521
CCSD(T)	aug-cc-pVDZ	2.72974	0.04936	2.61625	0.01137	2.69380	-0.12249
	d-aug-cc-pVDZ	2.58293	0.58125	2.51936	0.53558	2.68915	0.60403
	t-aug-cc-pVDZ	2.60820	0.54588	2.70268	0.51919	2.66480	0.57979
	aug-cc-pVTZ	2.55929	0.28910	2.38274	-0.16756	2.27533	-0.24968
	d-aug-cc-pVTZ	2.38438	0.02248	2.58832	0.28094	2.50422	0.48415
	t-aug-cc-pVTZ	2.52261	0.52226	2.57618	0.53210	2.50365	0.49965
	aug-cc-pVQZ	2.30677	0.35992	2.45588	0.43936	2.37634	0.49320
	d-aug-cc-pVQZ	2.48175	0.47893	2.48287	0.29264	2.45698	0.46146
	t-aug-cc-pVQZ	2.47390	0.48362	2.46018	0.48523	2.45495	0.46199

Table 5.9: Positions and widths (in eV) of the $^2\Pi_g$, N_2^- shape resonance computed using the type II-attenuated Coulomb method at various levels of theory.

method	Position	Width
ΔSCF	2.81202	0.19265
ΔMP2	2.58212	0.47505
ΔCCSD	2.47772	0.41312
ΔCCSD(T)	2.46018	0.48523

Table 5.10: Positions and widths (in eV) of the $^2\Pi_g$, N_2^- shape resonance computed using the type II-attenuated Coulomb method at various levels of theory. The basis set is the t-aug-cc-pVQZ basis set and $\omega = 0.01$.

short-range, better results are obtained with the Coulomb potential. An attenuated Coulomb potential retains the best features of the Coulomb potential without the long range tail. It is with the attenuated Coulomb potential that the best results are obtained.

The performance of the type III method on the $^2\Pi_g$ state of N_2^- is surprisingly good. There is systematic error in the width, but the position agrees well with the accepted value. The type III-Gaussian method does not perform well; this is probably due to a lack of flexibility in the functional form used in the analytic continuation. We do not recommend the use of a Gaussian potential. The type III-attenuated Coulomb method is somewhat sensitive to the attenuation parameter, ω, but retains many of the nice features of the type III-Coulomb method while being formally justifiable. We recommend an ω-value lying in the range that we have investigated (0.001-0.1). This broad range of ω, corresponding to characteristic lengths in the range 10 to 1000 Bohr, is likely appropriate for most low energy shape resonances which share physical characteristics with the N_2^- shape resonance.

The type II method performs decently well for all three potentials, though both the accuracy and basis-set convergence properties are best when combined with the attenuated Coulomb potential. Despite slow basis set convergence and some sensitivity to the precision of the inputs, in no case did we observe multiple nearby solutions or other pathological numerical problems. Furthermore, analytic continuation with type II Padé approximants provided more accurate widths, significantly less ω-dependence, and agreed better with other theoretical methods. We therefore suggest that the use of such high order Padè approximants in the analytic continuation of the inverse problem should not be discounted, especially if high precision input data is available. The type III-Coulomb or type III-attenuated Coulomb method may be used in cases where precise computations in large basis sets are not feasible, but with the caveat that there will likely be systematic error in the computed widths.

To summarize, for the IACCC method:

- We suggest an attenuated Coulomb potential as a formally justifiable, simple to implement alternative to a Coulomb potential.
- The type II method is most accurate and should be used if high precision calculations in large basis sets are feasible.
- The type III method can be used in cases where the use of large basis sets is not feasible, but there will likely be systematic error in the computed widths.

5.6 Appendix

5.6.1 Derivatives of RAC Padé approximants

In order to solve the non-linear least-squares problem by minimizing

$$\chi^2 = \frac{1}{N}\sum_{i=1}^{N}\left|\tilde{\lambda}(\kappa_i) - \lambda_i\right| \tag{5.17}$$

where $\tilde{\lambda}(\kappa)$ is one of either $\lambda^{[2/1]}(\kappa;\alpha,\beta,\lambda_0)$, $\lambda^{[3/1]}(\kappa;\alpha,\beta,\delta,\lambda_0)$, or $\lambda^{[4/2]}(\kappa;\alpha,\beta,\gamma,\delta,\epsilon,\lambda_0)$. The non-linear optimization can be easily accomplished using a some variant of Newton's method with analytic derivatives of χ^2 from which finite difference second derivatives can be computed. Specifically, we require derivatives with respect to the fitting parameters α, β, etc. Since all of these Padé approximants have the form

$$\lambda^{[N/M]} = \lambda_0 g^{[N/M]}, \tag{5.18}$$

the derivative of χ^2 with respect to λ_0 is trivial, and we further require only the derivatives of $g^{[M/N]}$ with respect to the remaining parameters.

For the [2/1] Padé approximant, we get

$$\frac{\partial g^{[2/1]}}{\partial\alpha} = \frac{4\alpha\kappa + 4\alpha^3}{\alpha^4+\beta^2+2\alpha^2\kappa} - \frac{\kappa^2+2\alpha^2\kappa+\alpha^4+\beta^2}{(\alpha^4+\beta^2+2\alpha^2\kappa)^2}(4\alpha\kappa+4\alpha^3) \tag{5.19}$$

$$\frac{\partial g^{[2/1]}}{\partial\beta} = \frac{2\beta}{\alpha^4+\beta^2+2\alpha^2\kappa} - \frac{\kappa^2+2\alpha^2\kappa+\alpha^4+\beta^2}{(\alpha^4+\beta^2+2\alpha^2\kappa)^2}(2\beta) \tag{5.20}$$

For the [3/1] Padé approximant, we get

$$\frac{\partial g^{[3/1]}}{\partial \alpha} = \frac{(4\alpha\kappa + 4\alpha^3)(1+\delta^2\kappa)}{\alpha^4+\beta^2+\kappa[2\alpha^2+\delta^2(\alpha^4+\beta^2)]} \tag{5.21}$$

$$- \frac{(\kappa^2+2\alpha^2\kappa+\alpha^4+\beta^2)(1+\delta^2\kappa)}{\{\alpha^4+\beta^2+\kappa[2\alpha^2+\delta^2(\alpha^4+\beta^2)]\}^2}(4\alpha^3+4\alpha\kappa+4\delta^2\alpha^3\kappa) \tag{5.22}$$

$$\frac{\partial g^{[3/1]}}{\partial \beta} = \frac{2\beta(1+\delta^2\kappa)}{\alpha^4+\beta^2+\kappa[2\alpha^2+\delta^2(\alpha^4+\beta^2)]} \tag{5.23}$$

$$- \frac{(\kappa^2+2\alpha^2\kappa+\alpha^4+\beta^2)(1+\delta^2\kappa)}{\{\alpha^4+\beta^2+\kappa[2\alpha^2+\delta^2(\alpha^4+\beta^2)]\}^2}(2\beta+2\delta^2\beta\kappa) \tag{5.24}$$

$$\frac{\partial g^{[3/1]}}{\partial \delta} = \frac{(\kappa^2+2\alpha^2\kappa+\alpha^4+\beta^2)2\delta\kappa}{\alpha^4+\beta^2+\kappa[2\alpha^2+\delta^2(\alpha^4+\beta^2)]} \tag{5.25}$$

$$- \frac{(\kappa^2+2\alpha^2\kappa+\alpha^4+\beta^2)(1+\delta^2\kappa)}{\{\alpha^4+\beta^2+\kappa[2\alpha^2+\delta^2(\alpha^4+\beta^2)]\}^2}2\delta(\alpha^4+\beta^2)\kappa \tag{5.26}$$

For the [4/2] Padé approximate, we define the numerator and denominator as

$$N \equiv (\kappa^2+2\alpha^2\kappa+\alpha^4+\beta^2)(\kappa^2+2\gamma^2\kappa+\gamma^4+\delta^2) \tag{5.27}$$

$$D \equiv (\alpha^4+\beta^2)(\gamma^4+\delta^2)(1+\mu^2\kappa)(1+\mu^2\epsilon^2\kappa), \tag{5.28}$$

as well as the derivatives of μ^2:

$$\mu^2_\alpha \equiv \frac{\partial \mu^2}{\partial \alpha} = \frac{2}{\epsilon^2+1}\left[\frac{2\alpha}{\alpha^4+\beta^2} - \frac{4\alpha^5}{(\alpha^4+\beta^2)^2}\right] \tag{5.29}$$

$$\mu^2_\beta \equiv \frac{\partial \mu^2}{\partial \beta} = -\frac{4\alpha^2\beta}{(\epsilon^2+1)(\alpha^4+\beta^2)} \tag{5.30}$$

$$\mu^2_\gamma \equiv \frac{\partial \mu^2}{\partial \gamma} = \frac{2}{\epsilon^2+1}\left[\frac{2\gamma}{\gamma^4+\delta^2} - \frac{4\gamma^5}{(\gamma^4+\delta^2)^2}\right] \tag{5.31}$$

$$\mu^2_\delta \equiv \frac{\partial \mu^2}{\partial \delta} = -\frac{4\gamma^2\delta}{(\epsilon^2+1)(\gamma^4+\delta^2)} \tag{5.32}$$

$$\mu^2_\epsilon \equiv \frac{\partial \mu^2}{\partial \epsilon} = -\frac{4\epsilon}{(\epsilon^2+1)^2}\left[\frac{\alpha^2}{\alpha^4+\beta^2} + \frac{\gamma^2}{\gamma^4+\delta^2}\right]. \tag{5.33}$$

In terms of these quantities, the derivatives are given by

$$\frac{\partial g^{[4/2]}}{\partial \alpha} = \frac{4(\alpha\kappa+\alpha^3)(\kappa^2+2\gamma^2\kappa+\gamma^4+\delta^2)}{D} - \frac{4N\alpha^3}{(\alpha^4+\beta^2)D} \tag{5.34}$$

$$- \frac{N\mu_\alpha^2\kappa}{(1+\mu^2\kappa)D} - \frac{N\epsilon^2\mu_\alpha^2\kappa}{(1+\mu^2\epsilon^2\kappa)D} \tag{5.35}$$

$$\frac{\partial g^{[4/2]}}{\partial \beta} = \frac{(2\beta)(\kappa^2+2\gamma^2\kappa+\gamma^4+\delta^2)}{D} - \frac{2N\beta}{(\alpha^4+\beta^2)D} \tag{5.36}$$

$$- \frac{N\mu_\beta^2\kappa}{(1+\mu^2\kappa)D} - \frac{N\epsilon^2\mu_\beta^2\kappa}{(1+\mu^2\epsilon^2\kappa)D} \tag{5.37}$$

$$\frac{\partial g^{[4/2]}}{\partial \gamma} = \frac{(\kappa^2+2\alpha^2\kappa+\alpha^4+\beta^2)4(\gamma\kappa+\gamma^3)}{D} - \frac{4N\gamma^3}{(\gamma^4+\delta^2)D} \tag{5.38}$$

$$- \frac{N\mu_\gamma^2\kappa}{(1+\mu^2\kappa)D} - \frac{N\epsilon^2\mu_\gamma^2\kappa}{(1+\mu^2\epsilon^2\kappa)D} \tag{5.39}$$

$$\frac{\partial g^{[4/2]}}{\partial \delta} = \frac{(\kappa^2+2\alpha^2\kappa+\alpha^4+\beta^2)(2\delta)}{D} - \frac{2N\delta}{(\gamma^4+\delta^2)D} \tag{5.40}$$

$$- \frac{N\mu_\delta^2\kappa}{(1+\mu^2\kappa)D} - \frac{N\epsilon^2\mu_\delta^2\kappa}{(1+\mu^2\epsilon^2\kappa)D} \tag{5.41}$$

$$\frac{\partial g^{[4/2]}}{\partial \epsilon} = -N\left[\frac{\mu_\epsilon^2\kappa}{(1+\mu^2\kappa)D} + \frac{\mu_{\epsilon^2}\epsilon^2\kappa+2\epsilon\mu^2\kappa}{(1+\mu^2\epsilon^2\kappa)D}\right] \tag{5.42}$$

5.6.2 Molecular Gaussian attraction integrals

The analytic continuation methods involving an added Gaussian potential require integrals of the form

$$\langle\phi_\mu|U_G|\phi_\nu\rangle = -\sum_{k=1}^{P} A_k V_{\mu\nu}^{(k)} \tag{5.43}$$

where

$$V_{\mu\nu}^{(k)} \equiv \int d^3\mathbf{r}\phi_\mu(\mathbf{r})e^{-\alpha(\mathbf{r}-\mathbf{C}_k)^2}\phi_\nu(\mathbf{r}). \tag{5.44}$$

The sum over k is over added Gaussian potentials centered at $\mathbf{C}_k$ and ϕ_μ, ϕ_ν are primitive Gaussian type orbitals. In order to derive an explicit formula for these integrals, we first use Gaussian product theorem (GPT) twice to combine the three Gaussian factors into a single Gaussian:

$$N_\mu N_\nu G_{AB} G_{PC} P(x,y,z)\exp\left[-\eta(\mathbf{r}-\mathbf{Q})\right]. \tag{5.45}$$

The polynomial, $P(x, y, z)$ is just a product of polynomial factors from the two basis functions, N_μ and N_ν are normalization factors, and the other quantities are given by

$$\begin{aligned} G_{\mathbf{PC}} &= \exp\left[-\frac{\gamma\alpha}{\gamma+\alpha}(\mathbf{P}-\mathbf{C})^2\right] \\ \eta &= \gamma+\alpha \\ \mathbf{Q} &= \frac{\gamma\mathbf{P}+\alpha\mathbf{C}}{\gamma+\alpha} \end{aligned} \tag{5.46}$$

where $\mathbf{P}$ and γ are the GPT center and exponent associated with the product of basis functions. The explicit formula is now easily derived in analogy to the case of simple overlap integrals given in Reference [90]. This allows for direct reuse of the explicit formulas that are used to compute overlaps, the only difference is that $\mathbf{P} \to \mathbf{Q}$ and $\gamma \to \eta$. We compute the integrals using this method. However it is also possible to compute the integrals using a special case of the recurrence relation for 3-center overlaps given by Obara and Saika:[93]

$$\begin{aligned} (\mathbf{a}+\mathbf{1}_i|\mathbf{0}|\mathbf{b}) &= \frac{a_i}{2\eta}(\mathbf{a}-\mathbf{1}_i|\mathbf{0}|\mathbf{b}) + \frac{b_i}{2\eta}(\mathbf{a}|\mathbf{0}|\mathbf{b}-\mathbf{1}_i) \\ &+ (Q_i - A_i)(\mathbf{a}|\mathbf{0}|\mathbf{b}). \end{aligned} \tag{5.47}$$

The extension of either method to contracted Gaussian basis functions is trivial.

5.7 Supplementary material

Supplementary material to accompany: "Stabilizing potentials in bound state analytic continuation methods for electronic resonances in polyatomic molecules" by Alec F. White, Martin Head-Gordon, and C. William McCurdy. This supplement includes the complete set of results discussed in the aforementioned manuscript.

5.7.1 The Type III-Coulomb method

- See Table 5.11 for the results using the Type III-Coulomb method with a [2/1] Padé approximant.
- See Table 5.12 for the results using the Type III-Coulomb method with a [4/2] Padé approximant.

5.7.2 The Type II-Coulomb method

- See Table 5.13 for the results using the Type II-Coulomb method.

5.7.3 The Type III-Gaussian method

- See Table 5.14 for the results using the Type III-Gaussian method.

5.7.4 The Type II-Gaussian method

- See Table 5.15 for the results using the Type II-Gaussian method.

5.7.5 The Type III-attenuated Coulomb method

- See Table 5.16 for the results using the Type III-attenuated Coulomb method with [2/1] Padé approximant.
- See Table 5.17 for the results using the Type III-attenuated Coulomb method with [4/1] Padé approximant.

5.7.6 The Type II-attenuated Coulomb method

- See Table 5.18 for the results using the Type II-attenuated Coulomb method.

method	basis	Position	Width
ΔSCF	aug-cc-pVDZ	2.74110	0.70651
	d-aug-cc-pVDZ	2.73775	0.70488
	t-aug-cc-pVDZ	2.73815	0.70516
	aug-cc-pVTZ	2.76426	0.62306
	d-aug-cc-pVTZ	2.76112	0.62566
	t-aug-cc-pVTZ	2.76130	0.62669
	aug-cc-pVQZ	2.76009	0.62897
	d-aug-cc-pVQZ	2.75868	0.62994
	t-aug-cc-pVQZ	2.75874	0.63018
ΔMP2	aug-cc-pVDZ	2.74227	0.84903
	d-aug-cc-pVDZ	2.73641	0.84616
	t-aug-cc-pVDZ	2.73630	0.84638
	aug-cc-pVTZ	2.63010	0.66458
	d-aug-cc-pVTZ	2.61303	0.66998
	t-aug-cc-pVTZ	2.59806	0.67592
	aug-cc-pVQZ	2.56596	0.65534
	d-aug-cc-pVQZ	2.55392	0.65757
	t-aug-cc-pVQZ	2.55429	0.65746
ΔCCSD	aug-cc-pVDZ	2.54866	0.75106
	d-aug-cc-pVDZ	2.48654	0.76109
	t-aug-cc-pVDZ	2.46934	0.76534
	aug-cc-pVTZ	2.41731	0.60046
	d-aug-cc-pVTZ	2.38406	0.60869
	t-aug-cc-pVTZ	2.38236	0.60999
	aug-cc-pVQZ	2.36226	0.59093
	d-aug-cc-pVQZ	2.34158	0.59505
	t-aug-cc-pVQZ	2.34106	0.59532
ΔCCSD(T)	aug-cc-pVDZ	2.55676	0.76962
	d-aug-cc-pVDZ	2.49716	0.77837
	t-aug-cc-pVDZ	2.51582	0.77359
	aug-cc-pVTZ	2.41758	0.61607
	d-aug-cc-pVTZ	2.37994	0.62489
	t-aug-cc-pVTZ	2.37848	0.62606
	aug-cc-pVQZ	2.35872	0.60604
	d-aug-cc-pVQZ	2.33451	0.61071
	t-aug-cc-pVQZ	2.33383	0.61100

Table 5.11: Positions and widths (in eV) of the $^2\Pi_g$, N_2^- shape resonance computed using the Type III-Coulomb method with a [2/1] Padé approximant. Note the favorable convergence with respect to basis set size.

	basis	Position	Width
ΔCCSD(T)	aug-cc-pVDZ	2.5919	0.6923
	d-aug-cc-pVDZ	2.5365	0.6971
	t-aug-cc-pVDZ	2.5535	0.6940
	aug-cc-pVTZ	2.4464	0.5598
	d-aug-cc-pVTZ	2.4070	0.5741
	t-aug-cc-pVTZ	2.4034	0.5794
	aug-cc-pVQZ	2.3892	0.5497
	d-aug-cc-pVQZ	2.3666	0.5528
	t-aug-cc-pVQZ	2.3658	0.5531

Table 5.12: Positions and widths (in eV) of the $^2\Pi_g$, N_2^- shape resonance computed using the Type III-Coulomb method with a [4/2] Padé approximant at the ΔCCSD level of theory. Note the small differences in comparison with the analogous calculations in Table 5.11

method	basis	Position	Width
ΔSCF	aug-cc-pVDZ	2.8326	-0.0029
	d-aug-cc-pVDZ	2.8096	0.2590
	t-aug-cc-pVDZ	2.8462	0.1863
	aug-cc-pVTZ	2.8003	0.0051
	d-aug-cc-pVTZ	2.8324	0.1629
	t-aug-cc-pVTZ	2.7967	0.1955
	aug-cc-pVQZ	2.8124	0.1138
	d-aug-cc-pVQZ	2.8175	0.2344
	t-aug-cc-pVQZ	2.8206	0.2071
ΔMP2	aug-cc-pVDZ	2.5058	0.1907
	d-aug-cc-pVDZ	2.7916	0.4777
	t-aug-cc-pVDZ	2.8025	0.5145
	aug-cc-pVTZ	2.5271	-0.3799
	d-aug-cc-pVTZ	2.6269	0.4719
	t-aug-cc-pVTZ	2.6268	0.4871
	aug-cc-pVQZ	2.5085	0.1227
	d-aug-cc-pVQZ	2.5774	0.4802
	t-aug-cc-pVQZ	2.5843	0.4571
ΔCCSD	aug-cc-pVDZ	2.6180	0.3299
	d-aug-cc-pVDZ	2.5228	0.4706
	t-aug-cc-pVDZ	2.7251	0.5156
	aug-cc-pVTZ	2.3695	0.3384
	d-aug-cc-pVTZ	2.5666	0.2585
	t-aug-cc-pVTZ	2.5133	0.4438
	aug-cc-pVQZ	2.3317	0.3533
	d-aug-cc-pVQZ	2.4523	0.4773
	t-aug-cc-pVQZ	2.4706	0.4205
ΔCCSD(T)	aug-cc-pVDZ	2.5401	0.0322
	d-aug-cc-pVDZ	2.7727	0.0372
	t-aug-cc-pVDZ	2.6694	0.6235
	aug-cc-pVTZ	2.3678	0.3940
	d-aug-cc-pVTZ	2.4952	0.5432
	t-aug-cc-pVTZ	2.4940	0.4426
	aug-cc-pVQZ	2.3284	0.4049
	d-aug-cc-pVQZ	2.4343	0.5048
	t-aug-cc-pVQZ	2.4564	0.4563

Table 5.13: Positions and widths (in eV) of the $^2\Pi_g$, N_2^- shape resonance computed using the Type II-Coulomb method. Note that the method does not have the stability of the Type III-Coulomb method, but it does provide a more accurate value for the width.

		$\alpha = 0.01$		$\alpha = 0.1$		$\alpha = 1.00$	
method	basis	Position	Width	Position	Width	Position	Width
	aug-cc-pVDZ	2.8433	0.0513	2.9523	0.4598	2.5565	2.9050
	d-aug-cc-pVDZ	2.8029	0.0784	2.9448	0.4599	2.6556	2.9297
	t-aug-cc-pVDZ	2.8006	0.0802	2.9449	0.4604	2.5456	2.8870
	aug-cc-pVTZ	2.8215	0.0590	2.9291	0.4606	2.6216	2.7584
ΔSCF [2/1]	d-aug-cc-pVTZ	2.7972	0.0757	2.9264	0.4662	2.7144	2.7894
	t-aug-cc-pVTZ	2.7970	0.0766	2.9265	0.4679	2.6209	2.7557
	aug-cc-pVQZ	2.6237	0.0608	2.9250	0.4686	2.6996	2.7860
	d-aug-cc-pVQZ	2.7977	0.0761	2.9248	0.4701	2.6024	2.7506
	t-aug-cc-pVQZ	2.7976	0.0761	2.9251	0.4705	2.5600	2.7328
ΔCCSD(T), [2/1]	t-aug-cc-pVQZ	2.2089	0.1707	2.5551	0.5163	2.4757	2.9159
ΔSCF [4/2]	t-aug-cc-pVQZ	2.7846	0.1592	2.9310	0.4467	2.7023	2.3768
ΔCCSD(T), [4/2]	t-aug-cc-pVQZ	2.4018	0.6343	2.5317	0.5752	2.5608	2.4871

Table 5.14: Positions and widths (in eV) of the $^2\Pi_g$, N_2^- shape resonance computed using the Type III-Gaussian method at the Δ-SCF level of theory. Note the strong dependence on the exponent of the added Gaussian potential (α).

		$\alpha = 0.01$		$\alpha = 0.1$		$\alpha = 1.00$	
method	basis	Position	Width	Position	Width	Position	Width
ΔSCF	aug-cc-pVDZ	2.8423	-0.0008	2.8394	0.0415	2.8129	0.4298
	d-aug-cc-pVDZ	2.8875	0.0871	2.8515	0.1599	2.8006	0.4190
	t-aug-cc-pVDZ	2.8327	0.2327	2.8491	0.1721	2.8307	0.2376
	aug-cc-pVTZ	2.8064	0.0015	2.7958	0.0671	2.8533	0.3916
	d-aug-cc-pVTZ	2.8512	0.1279	2.8377	0.1553	2.8081	0.4032
	t-aug-cc-pVTZ	2.8358	0.2158	2.8415	0.1673	2.7915	0.3429
	aug-cc-pVQZ	2.5834	0.0034	2.8039	0.1559	2.7885	0.3914
	d-aug-cc-pVQZ	2.8326	0.2005	2.8380	0.1742	2.8452	0.4210
	t-aug-cc-pVQZ	2.8299	0.2154	2.8412	0.1718	2.7963	0.4007
ΔCCSD(T)	t-aug-cc-pVQZ	2.4419	0.5908	2.4820	0.5360	2.4510	0.7185

Table 5.15: Positions and widths (in eV) of the $^2\Pi_g$, N_2^- shape resonance computed using the Type II-Gaussian method at the ΔSCF level of theory. Note that there is significantly reduced dependence on the exponent of the added Gaussian potential (α).

	basis	$\omega = 0.001$		$\omega = 0.01$		$\omega = 0.1$	
		Position	Width	Position	Width	Position	Width
SCF	aug-cc-pVDZ	2.74217	0.70854	2.75251	0.72708	2.68530	1.05547
	d-aug-cc-pVDZ	2.73879	0.70692	2.74905	0.72543	2.75149	1.02148
	t-aug-cc-pVDZ	2.73920	0.70719	2.74781	0.72579	2.75192	1.02192
	aug-cc-pVTZ	2.76522	0.62485	2.77457	0.64119	2.72995	0.93501
	d-aug-cc-pVTZ	2.76209	0.62746	2.77149	0.64389	2.73919	0.92092
	t-aug-cc-pVTZ	2.76227	0.62849	2.77171	0.64494	2.73911	0.92266
	aug-cc-pVQZ	2.76087	0.63085	2.77034	0.64736	2.72381	0.94495
	d-aug-cc-pVQZ	2.75966	0.63175	2.76914	0.64830	2.73459	0.92812
	t-aug-cc-pVQZ	2.75972	0.63200	2.76921	0.64855	2.73479	0.92839
MP2	aug-cc-pVDZ	2.74374	0.85167	2.75787	0.87582	2.76442	1.25953
	d-aug-cc-pVDZ	2.73785	0.84880	2.75179	0.87294	2.76349	1.25344
	t-aug-cc-pVDZ	2.73774	0.84902	2.75168	0.87317	2.76372	1.25363
	aug-cc-pVTZ	2.61073	0.67357	2.62010	0.69347	2.68056	0.97534
	d-aug-cc-pVTZ	2.61435	0.67202	2.60835	0.69722	2.67307	0.97909
	t-aug-cc-pVTZ	2.61452	0.67297	2.60845	0.69822	2.67313	0.98072
	aug-cc-pVQZ	2.54912	0.66307	2.55790	0.68291	2.61251	0.96208
	d-aug-cc-pVQZ	2.54104	0.66402	2.54979	0.68394	2.60741	0.96223
	t-aug-cc-pVQZ	2.55488	0.65977	2.54952	0.68410	2.60641	0.96315
CCSD	aug-cc-pVDZ	2.55002	0.75336	2.56318	0.77454	2.54911	1.11532
	d-aug-cc-pVDZ	2.48791	0.76348	2.49285	0.78761	2.53384	1.11226
	t-aug-cc-pVDZ	2.47073	0.76776	2.49180	0.78796	2.53354	1.11251
	aug-cc-pVTZ	2.41819	0.60237	2.42644	0.62009	2.46461	0.87591
	d-aug-cc-pVTZ	2.38497	0.61064	2.39308	0.62886	2.44771	0.88117
	t-aug-cc-pVTZ	2.38343	0.61192	2.39160	0.63018	2.44744	0.88267
	aug-cc-pVQZ	2.36306	0.59285	2.37073	0.61049	2.37322	0.86910
	d-aug-cc-pVQZ	2.34241	0.59699	2.35000	0.61489	2.36771	0.86971
	t-aug-cc-pVQZ	2.34171	0.59729	2.34915	0.61525	2.39292	0.86534
CCSD(T)	aug-cc-pVDZ	2.55822	0.77198	2.57251	0.79356	2.56588	1.14238
	d-aug-cc-pVDZ	2.49861	0.78082	2.50061	0.80643	2.54943	1.13871
	t-aug-cc-pVDZ	2.51745	0.77596	2.49981	0.80661	2.54894	1.13888
	aug-cc-pVTZ	2.41852	0.61804	2.42736	0.63629	2.47546	0.89812
	d-aug-cc-pVTZ	2.38092	0.62691	2.38958	0.64573	2.45552	0.90377
	t-aug-cc-pVTZ	2.37963	0.62805	2.38836	0.64690	2.45512	0.90525
	aug-cc-pVQZ	2.35958	0.60802	2.36776	0.62623	2.37978	0.89098
	d-aug-cc-pVQZ	2.33540	0.61272	2.34348	0.63124	2.37299	0.89164
	t-aug-cc-pVQZ	2.33466	0.61301	2.34256	0.63159	2.39789	0.88717

Table 5.16: Positions and widths (in eV) of the $^2\Pi_g$, N_2^- shape resonance computed using the Type III-attenuated Coulomb method using a [2/1] Padé approximant at various levels of theory. Note the dependence on the attenuation parameter (ω).

method	$\omega = 0.001$		$\omega = 0.01$		$\omega = 0.1$	
	Position	Width	Position	Width	Position	Width
SCF	2.75972	0.63200	2.76921	0.64855	2.78722	0.82602
MP2	2.55488	0.65977	2.54952	0.68410	2.60641	0.96315
CCSD	2.34171	0.59729	2.34915	0.61525	2.39292	0.86534
CCSD(T)	2.33466	0.61301	2.34256	0.63158	2.39789	0.88717

Table 5.17: Positions and widths (in eV) of the $^2\Pi_g$, N_2^- shape resonance computed using the Type III-attenuated Coulomb method using a [4/2] Padé approximant at various levels of theory. The basis set is t-aug-cc-pVQZ.

	basis	$\omega = 0.001$		$\omega = 0.01$		$\omega = 0.1$	
		Position	Width	Position	Width	Position	Width
SCF	aug-cc-pVDZ	2.83173	-0.00320	2.83333	0.00155	2.82576	0.01793
	d-aug-cc-pVDZ	2.84264	0.16154	2.84648	0.16814	2.84740	0.16000
	t-aug-cc-pVDZ	2.85043	0.17558	2.84711	0.17931	2.84503	0.18047
	aug-cc-pVTZ	2.79090	0.00204	2.74397	0.10855	2.77907	0.07895
	d-aug-cc-pVTZ	2.83293	0.16192	2.83551	0.15931	2.83411	0.16129
	t-aug-cc-pVTZ	2.79914	0.20080	2.79953	0.17272	2.83240	0.18002
	aug-cc-pVQZ	2.78391	0.22003	2.81807	0.06469	2.77191	0.20154
	d-aug-cc-pVQZ	2.83282	0.18578	2.82263	0.10278	2.83902	0.17423
	t-aug-cc-pVQZ	2.80872	0.20374	2.81202	0.19265	2.83933	0.17521
MP2	aug-cc-pVDZ	2.72208	0.10005	2.76340	0.03997	2.80038	1.86645
	d-aug-cc-pVDZ	2.79832	0.46639	2.78683	0.47052	2.78802	0.48432
	t-aug-cc-pVDZ	2.80063	0.52466	2.79462	0.51529	2.80264	0.47192
	aug-cc-pVTZ	2.48001	0.31983	2.51110	0.11634	2.56937	0.48062
	d-aug-cc-pVTZ	2.62834	0.47483	2.61889	0.46801	2.64243	0.42030
	t-aug-cc-pVTZ	2.62737	0.48742	2.63073	0.46836	2.63600	0.45675
	aug-cc-pVQZ	2.66374	0.63313	2.60000	0.55719	2.56286	0.47250
	d-aug-cc-pVQZ	2.58564	0.47698	2.58334	0.47452	2.61899	0.43433
	t-aug-cc-pVQZ	2.57487	0.47333	2.58212	0.47505	2.60651	0.45710
CCSD	aug-cc-pVDZ	2.57055	0.02392	2.56503	0.00359	2.60025	0.04038
	d-aug-cc-pVDZ	2.73816	0.66168	2.56172	0.50997	2.70311	0.63669
	t-aug-cc-pVDZ	2.70858	0.46955	2.69172	0.46732	2.67951	0.54334
	aug-cc-pVTZ	2.44712	0.27579	2.37959	0.33977	2.39581	0.42919
	d-aug-cc-pVTZ	2.50792	0.01880	2.52948	0.41762	2.52205	0.47867
	t-aug-cc-pVTZ	2.52638	0.42976	2.52075	0.44425	2.51313	0.45117
	aug-cc-pVQZ	2.34967	0.38529	2.36206	0.37646	2.38293	0.43632
	d-aug-cc-pVQZ	2.46865	0.47828	2.50812	0.38895	2.47236	0.37347
	t-aug-cc-pVQZ	2.47671	0.39002	2.47772	0.41312	2.47069	0.42980
CCSD(T)	aug-cc-pVDZ	2.72974	0.04936	2.61625	0.01137	2.69380	-0.12249
	d-aug-cc-pVDZ	2.58293	0.58125	2.51936	0.53558	2.68915	0.60403
	t-aug-cc-pVDZ	2.60820	0.54588	2.70268	0.51919	2.66480	0.57979
	aug-cc-pVTZ	2.55929	0.28910	2.38274	-0.16756	2.27533	-0.24968
	d-aug-cc-pVTZ	2.38438	0.02248	2.58832	0.28094	2.50422	0.48415
	t-aug-cc-pVTZ	2.52261	0.52226	2.57618	0.53210	2.50365	0.49965
	aug-cc-pVQZ	2.30677	0.35992	2.45588	0.43936	2.37634	0.49320
	d-aug-cc-pVQZ	2.48175	0.47893	2.48287	0.29264	2.45698	0.46146
	t-aug-cc-pVQZ	2.47390	0.48362	2.46018	0.48523	2.45495	0.46199

Table 5.18: Positions and widths (in eV) of the $^2\Pi_g$, N_2^- shape resonance computed using the Type II-attenuated Coulomb method at various levels of theory.

Chapter 6

Concluding remarks

The goal of the work presented here is the development of *ab initio* electronic structure methods for molecular resonances. Towards this end, we have pursued two extensions of bound state electronic structure theory that should be capable in principle of nearly black-box computation of resonance positions and lifetimes.

First, we implemented the numerical routines required for efficient computation of molecular integrals over Gaussian basis functions with complex exponents. This is the first step in an open-ended implementation of the method of complex basis functions, which fits naturally into the hierarchy of standard molecular electronic structure methods. Specifically, we implemented static exchange, non-Hermitian SCF, non-Hermitian MP2, and complex EOM-CCSD. Within the static exchange approximation, we investigated the basis set dependence of the method and designed a simple hierarchy of complex basis sets. Using these basis sets, we computed positions and widths of low energy shape resonances in carbon tetrafluoride, benzene, pyridine, pyrimidine, pyrazine, and s-triazine. Orbital relaxation can be taken into account with non-Hermitian restricted, unrestricted, or restricted open-shell self-consistent field methods. We utilized these methods for benchmark calculations on shape resonances in small molecules. Using non-Hermitian unrestricted Hartree-Fock, we were able to compute a qualitatively correct complex potential energy curve for the carbon monoxide anion. We also discussed the general computation of molecular properties within a non-Hermitian formalism. This discussion led to the development of a density-based analysis which was applied to a shape resonance in electron-formaldehyde scattering. Despite these successes, the NH-SCF methods are plagued by convergence problems that severely limit their applicability to larger molecules. We explicitly included electron correlation within the method of complex basis functions via non-Hermitian MP2 or complex EOM-CCSD. These methods proved to be computationally very expensive in practice, and our study was

largely limited to high-quality benchmark calculations on shape resonances in small molecules. However, we were able to compute the position and width of the $1s2s^2$ Feshbach resonance in electron-helium scattering which suggests that the method can be used for Feshbach resonances.

Second, we have looked into the computational feasibility of using analytic continuation in the coupling constant (ACCC), specifically the inverse variant (IACCC), to compute positions and widths of shape resonances. We considered two types of Padé approximants and 3 classes of stabilizing potentials: Coulomb potentials, Gaussian potentials, and attenuated Coulomb potentials. These methods were applied to a model potential where the exact answer can be computed numerically and to the $^2\Pi_g$ shape resonance of N_2^-. In these two benchmark cases, the attenuated Coulomb potential proved to be the most effective. In general, methods based on analytic continuation in the coupling constant have the potential to be very useful for the computation of positions and widths of low-energy shape resonances in medium sized molecules.

These two methods are largely complementary in their strengths and weaknesses. With our implementation, complex basis functions can now be applied at many different levels of theory. Our results suggest that the method is very general and can achieve high accuracy for many different types of resonances. Unfortunately, the method is still expensive and is not black-box. More development is necessary to make the method practical for the non-expert. In contrast, the method of inverse analytic continuation in the coupling constant requires little code development and should be fairly practical even for non-experts. Unfortunately, the method is applicable to a relatively limited class of problems; it is particularly useful when one is interested in the lowest energy shape resonance. Even though these methods are each limited in their own way, the combination of both should allow us to confidently treat chemical reactions proceeding through metastable intermediates in small to medium-sized molecules.

Despite the progress that we have made, there are still many topics that remain largely unexplored. The method of complex basis functions in particular would benefit from more work to accelerate the SCF convergence, explore the effect of triple excitations in coupled cluster methods, and develop a practical Kohn-Sham DFT scheme for resonances. Finally, the field will benefit from high quality benchmark calculations so that different treatments of the continuum problem can be meaningfully compared.

Bibliography

(1) Schulz, G. Measurement of Atomic and Molecular Excitation by a Trapped-Electron Method. *Physical Review* **1958**, *1179*, 150–154.

(2) Schulz, G. Resonances in Electron Impact on Diatomic Molecules. *Rev. Mod. Phys.* **1973**, *45*, 423–486.

(3) Winstead, C.; Mckoy, V., *Electron-Molecule Collisions in Low-Temperature Plasmas. The Role of Theory*; C; Elsevier Masson SAS: 2000; Vol. 43, pp 111–145.

(4) Geppert, W.; Larsson, M. Dissociative recombination in the interstellar medium and planetary ionospheres. *Molecular Physics* **2008**, *106*, 2199–2226.

(5) Boudaïffa, B.; Cloutier, P.; Hunting, D; Huels, M. A.; Sanche, L. Resonant Formation of DNA Strand Breaks by Low-Energy (3 to 20 eV) Electrons. *Science* **2000**, *287*, 1658–1660.

(6) Corkum, P. B. Attosecond science. *Nature Physics* **2007**, *3*, 381387.

(7) Sansone, G et al. Electron localization following attosecond molecular photoionization. *Nature* **2010**, *465*, 763–766.

(8) Taylor, J., *Scattering Theory*; John Wiley & Sons, Inc.: New York, 1972.

(9) Newton, R. G., *Scattering Theory of Waves and Particles*, 2nd ed.; Springer Science+Business Media, LLC: New York, 1966.

(10) Nesbet, R. K. Interpretation of low-energy electron-HCl scattering phenomena. *Journal of Physics B: Atomic and Molecular Physics* **1977**, *10*, 739–743.

(11) Smith, F. T. Lifetime matrix in collision theory. *Physical Review* **1960**, *118*, 349–356.

(12) Burke, P. G., *R-Matrix Theory of Atomic Collisions: Application to Atomic, Molecular, and Optical Processes*; Springer: Heidelberg, 2011.

(13) Hazi, A. U. Behavior of the eigenphase sum near a resonance. *Physical Review A* **1979**, *19*, 920–922.

(14) O'Malley, T. Theory of Dissociative Attachment. *Physical Review* **1966**, *150*, 14–29.

(15) Brian, J. The dissociative recombination of molecular ions. *Physics Reports* **1990**, *186*, 215–248.

(16) Szabo, A.; Ostlund, N., *Modern Quantum Chemistry*; McGraw-Hill: New York, 1982.

(17) Helgaker, T.; Jørgensen, P.; Olsen, J., *Molecular Electronic Structure Theory*; John Wiley & Sons, Inc.: Chichester, West Sussex, England, 2000.

(18) Parr, R. G.; Yang, W., *Density-Functional Theory of Atoms and Molecules*; Oxford University Press: New York, 1989.

(19) Møller, C.; Plesset, M. S. Note on an approximation treatment for many-electron systems. *Phys. Rev.* **1934**, *46*, 618–622.

(20) Sekino, H.; Bartlett, R. J. A linear response, coupled-cluster theory for excitation energy. *Int. J. Quant. Chem.* **1984**, *26*, 255–265.

(21) Stanton, J. F.; Bartlett, R. J. The equation of motion coupled-cluster method. A systematic biorthogonal approach to molecular excitation energies, transition probabilities, and excited state properties. *J. Chem. Phys.* **1993**, *98*, 7029.

(22) Roos, B. The Complete Active Space Self-Consistent Field Method and its Applications in Electronic Structure Calculations. *Advances in Chemical Physics: Ab Initio Methods in Quantum Chemistry Part 2,* **1987**, *69*, 399–445.

(23) Gill, P. M. W. Molecular integrals over Gaussian basis functions. *Adv. Quantum Chem.* **1994**, *25*, 141–205.

(24) Whitten, J. L. Coulombic potential energy integrals and approximations. *J. Chem. Phys.* **1973**, *58*, 4496.

(25) Douady, J.; Ellinger, Y.; Subra, R.; Levy, B. Exponential transformation of molecular orbitals: A quadratically convergent SCF procedure. I. General formulation and application to closed-shell ground states. *The Journal of Chemical Physics* **1980**, *72*, 1452.

(26) Pulay, P. Convergence acceleration of iterative sequences. The case of SCF iteration. *Chem. Phys. Lett.* **1980**, *73*, 393–398.

(27) Pulay, P Improved SCF convergence acceleration. *J. Comput. Chem.* **1982**, *3*, 556–560.

(28) Davidson, E. R. The iterative calculation of a few of the lowest eigenvalues and corresponding eigenvectors of large real-symmetric matrices. *J. Comput. Phys.* **1975**, 87–94.

(29) Windus, T. L.; Pople, J. A. Pinnacle: An approach toward object oriented quantum chemistry. *International Journal of Quantum Chemistry* **1995**, *56*, 485–495.

(30) Epifanovsky, E.; Wormit, M.; Kuś, T.; Landau, A.; Zuev, D.; Khistyaev, K.; Manohar, P.; Kaliman, I.; Dreuw, A.; Krylov, A. I. New implementation of high-level correlated methods using a general block tensor library for high-performance electronic structure calculations. *J. Comput. Chem.* **2013**, *34*, 2293–2309.

(31) Solomonik, E.; Matthews, D.; Hammond, J. R.; Stanton, J. F.; Demmel, J. A massively parallel tensor contraction framework for coupled-cluster computations. *Journal of Parallel and Distributed Computing* **2014**, *74*, 3176–3190.

(32) Tennyson, J. Electron-molecule collision calculations using the R-matrix method. *Phys. Rep.* **2010**, *491*, 29–76.

(33) Da Costa, R. F.; Varella, M. T. N.; Bettega, M. H. F.; Lima, M. a. P. Recent advances in the application of the Schwinger multichannel method with pseudopotentials to electron-molecule collisions. *The European Physical Journal D* **2015**, *69*, 159.

(34) *Computational Methods for Electron-Molecule Collisions*; Huo, W. M., Gianturco, F. A., Eds.; Springer: New York, 1993.

(35) Taylor, H. S. Models, Interpretations, and Calculations Concerning Resonant Electron Scattering Processes in Atoms and Molecules. *Adv. Chem. Phys.* **1970**, *18*, 91–147.

(36) Hazi, A. U.; Taylor, H. S. Stabilization method of calculating resonance energies: Model problem. *Phys. Rev. A* **1970**, *1*, 1109–1120.

(37) Simons, J. Resonance state lifetimes from stabilization graphs. *J. Chem. Phys.* **1981**, *75*, 2465.

(38) McCurdy, C. W.; Turner, J. L. Wave packet formulation of the boomerang model for resonant electronmolecule scattering. *J. Chem. Phys.* **1983**, *78*, 6773–6779.

(39) Frey, R.; Simons, J. Resonance state energies and lifetimes via analytic continuation of stabilization graphs. *J. Chem. Phys.* **1986**, *84*, 4462–4469.

(40) McCurdy, C. W.; Lauderdale, J. G.; Mowrey, R. C. Complex self-consistent-field calculations on shape resonances in electron-Mg and electron-Ca scattering. *J. Chem. Phys.* **1981**, *75*, 1835.

(41) Aguilar, J; Combes, J. A Class of Analytic Perturbations for One-body Schrtidinger Hamiltonians. *Commun. Math. Phys.* **1971**, *22*, 269–279.

(42) Balslev, E; Combes, J. Spectral properties of many-body Schrödinger operators with dilatation-analytic interactions. *Commun. Math. Phys.* **1971**, *294*, 280–294.

(43) Simon, B. Quadratic form techniques and the Balslev-Combes theorem. *Commun. Math. Phys.* **1972**, *27*, 1–9.

(44) Simon, B. The definition of molecular resonance curves by the method of exterior complex scaling. *Phys. Lett. A* **1979**, *71A*, 211–214.

(45) Moiseyev, N.; Corcoran, C Autoionizing states of H_2 and H_2^- using the complex-scaling method. *Phys. Rev. A* **1979**, *20*, 3–6.

(46) McCurdy, C.; Rescigno, T. Extension of the method of complex basis functions to molecular resonances. *Phys. Rev. Lett.* **1978**, *41*, 1364–1368.

(47) Rom, N.; Engdahl, E.; Moiseyev, N. Tunneling rates in bound systems using smooth exterior complex scaling within the framework of the finite basis set approximation. *The Journal of Chemical Physics* **1990**, *93*, 3413–3419.

(48) Jolicard, G.; Austin, E. J. Optical potential stabilisation method for predicting resonance levels. *Chem. Phys. Lett.* **1985**, *121*, 106–110.

(49) Riss, U.; Meyer, H. Calculation of resonance energies and widths using the complex absorbing potential method. *J. Phys. B: At., Mol. Opt. Phys.* **1993**, *26*, 4503–4536.

(50) Santra, R.; Cederbaum, L. S. An efficient combination of computational techniques for investigating electronic resonance states in molecules. *J. Chem. Phys.* **2001**, *115*, 6853.

(51) Muga, J.; Palao, J.; Navarro, B; Egusquiza, I. Complex absorbing potentials. *Phys. Rep.* **2004**, *395*, 357–426.

(52) Moiseyev, N. Quantum theory of resonances: calculating energies, widths and cross-sections by complex scaling. *Phys. Rep.* **1998**, *302*, 211–293.

(53) Kukulin, V.; Krasnopolsky, V. Description of few-body systems via analytical continuation in coupling constant. *J. Phys. A: Gen. Phys.* **1977**, *10*, 32–37.

(54) Krasnopolsky, V.; Kukulin, V. Theory of resonance states based on analytical continuation in the coupling constant. *Physics Letters* **1978**, *69*, 251–254.

(55) Horáček, J.; Mach, P.; Urban, J. Calculation of S-matrix poles by means of analytic continuation in the coupling constant: Application to the $^2\Pi_g$ state of N_2^-. *Phys. Rev. A* **2010**, *82*, 032713.

(56) White, A. F.; Head-gordon, M.; Mccurdy, C. W. Complex basis functions revisited: Implementation with applications to carbon tetrafluoride and aromatic N-containing heterocycles within the static-exchange approximation. *J. Chem. Phys.* **2015**, *142*, 054103.

(57) White, A. F.; McCurdy, C. W.; Head-Gordon, M. Restricted and unrestricted non-Hermitian Hartree-Fock: Theory, practical considerations, and applications to molecular anions. *J. Chem. Phys.* **2015**, *143*, 074103.

(58) White, A. F.; Head-gordon, M.; Mccurdy, C. W. Stabilizing potentials in bound state analytic continuation methods for electronic resonances in polyatomic molecules. *J. Chem. Phys.* **2017**, *146*, 044112.

(59) Reinhardt, W. Complex coordinates in the theory of atomic and molecular structure and dynamics. *Annu. Rev. Phys. Chem.* **1982**, *33*, 223–255.

(60) Brändas, E The method of complex scaling. *Int. J. Quantum Chem.* **1986**, *30*, 119–127.

(61) Moiseyev, N., *Non-Hermitian Quantum Mechanics*; Cambridge University Press: 2011.

(62) Lipkin, N.; Moiseyev, N.; Brändas, E Resonances by the exterior-scaling method within the framework of the finite-basis-set approximation. *Phys. Rev. A* **1989**, *40*, 549–553.

(63) Moiseyev, N. Derivations of universal exact complex absorption potentials by the generalized complex coordinate method. *J. Phys. B: At., Mol. Opt. Phys.* **1998**, *31*, 1431–1441.

(64) Riss, U.; Meyer, H. Reflection-free complex absorbing potentials. *J. Phys. B: At., Mol. Opt. Phys.* **1995**, *28*, 1475–1493.

(65) Jagau, T.; Zuev, D.; Bravaya, K. B.; Epifanovsky, E.; Krylov, A. I. A Fresh Look at Resonances and Complex Absorbing Potentials: Density Matrix-Based Approach. *J. Phys. Chem. Lett.* **2013**, *5*, 310–315.

(66) Sajeev, Y; Sindelka, M.; Moiseyev, N. Reflection-free complex absorbing potential for electronic structure calculations: Feshbach type autoionization resonance of Helium. *Chem. Phys.* **2006**, *329*, 307–312.

(67) Sajeev, Y; Moiseyev, N. Reflection-free complex absorbing potential for electronic structure calculations: Feshbach-type autoionization resonances of molecules. *J. Chem. Phys.* **2007**, *127*, 034105.

(68) McCurdy, C. W.; Rescigno, T. N.; Davidson, E. R.; Lauderdale, J. G. Applicability of self-consistent field techniques based on the complex coordinate method to metastable electronic states. *J. Chem. Phys.* **1980**, *73*, 3268.

(69) McCurdy, C. W.; Rescigno, T. Complex-basis-function calculations of resolvent matrix elements: Molecular photoionization. *Phys. Rev. A* **1980**, *21*, 1499–1505.

(70) Rescigno, T.; Orel, A.; McCurdy, C. W. Application of complex coordinate SCF techniques to a molecular shape resonance: The $^2\Pi_g$ state of N_2^-. *J. Chem. Phys.* **1980**, *73*, 6347–6348.

(71) McCurdy, C. W.; Mowrey, R. Complex potential-energy function for the $^2\Sigma_u^+$ shape resonance state of H_2^- at the self-consistent-field level. *Phys. Rev. A* **1982**, *25*, 2529–2538.

(72) McNutt, J.; McCurdy, C. W. Complex self-consistent-field and configuration-interaction studies of the lowest ^{2}P resonance state of Be^-. *Phys. Rev. A* **1983**, *27*, 132–140.

(73) Lauderdale, J. G.; McCurdy, C. W.; Hazi, A. U. Conversion of bound states to resonances with changing internuclear distance in molecular anions. *J. Chem. Phys.* **1983**, *79*, 2200–2205.

(74) Yabushita, S.; McCurdy, C. W. Feshbach resonances in electron-molecule scattering by the complex multiconfiguration SCF and configuration interaction procedures: The $^1\Sigma_g^+$ autoionizing states of H_2. *J. Chem. Phys.* **1985**, *83*, 3547.

(75) Honigmann, M.; Hirsch, G.; Buenker, R. J.; Petsalakis, I. D.; Theodorakopoulos, G. Complex coordinate calculations on autoionizing states of HeH and H_2. *Chem. Phys. Lett.* **1999**, *305*, 465–473.

(76) Honigmann, M.; Buenker, R. J.; Liebermann, H.-P. Complex self-consistent field and multireference single- and double-excitation configuration interaction calculations for the $^2\Pi_g$ resonance state of N_2^-. *J. Chem. Phys.* **2006**, *125*, 234304.

(77) Honigmann, M.; Buenker, R. J.; Liebermann, H.-P. Complex multireference configuration interaction calculations employing a coupled diabatic representation for the $^2\Pi_g$ resonance states of N_2^-. *J. Chem. Phys.* **2009**, *131*, 034303.

(78) Honigmann, M.; Buenker, R. J.; Liebermann, H.-P. Complex configuration interaction calculations of the cross section for the dissociative electron attachment process $e^- + F_2 \rightarrow F_2^- \rightarrow F + F^-$ using the complex basis function method. *J. Comput. Chem.* **2012**, *33*, 355–62.

(79) Zuev, D.; Jagau, T.-C.; Bravaya, K. B.; Epifanovsky, E.; Shao, Y.; Sundstrom, E.; Head-Gordon, M.; Krylov, A. I. Complex absorbing potentials within EOM-CC family of methods: Theory, implementation, and benchmarks. *J. Chem. Phys.* **2014**, *141*, 024102.

(80) Kaprálová-Ždánská, P. R.; Šmydke, J. Gaussian basis sets for highly excited and resonance states of helium. *J. Chem. Phys.* **2013**, *138*, 024105.

(81) Matsuzaki, R.; Asai, S.; McCurdy, C. W.; Yabushita, S. Construction of complex STO-NG basis sets by the method of least squares and their applications. *Theor. Chem. Acc.* **2014**, *133*, 1521.

(82) Brändas, E; Froelich, P. Continuum orbitals, complex scaling problem, and the extended virial theorem. *Phys. Rev. A* **1977**, *16*, 2207–2210.

(83) Moiseyev, N.; Certain, P.; Weinhold, F Resonance properties of complex-rotated hamiltonians. *Mol. Phys.* **1978**, *36*, 1613–1630.

(84) Moiseyev, N. Resonance states by the generalized complex variational method. *Mol. Phys.* **1982**, *47*, 585–598.

(85) Morgan, J.; Simon, B. The calculation of molecular resonances by complex scaling. *J. Phys. B: At., Mol. Opt. Phys.* **1981**, *14*, L167–L171.

(86) Schlessinger, L Use of Analyticity in the Calculation of Nonrelativistic Scattering Amplitudes. *Phys. Rev.* **1968**, *36*, 1411–1423.

(87) Moiseyev, N.; Friedland, S.; Certain, P. Cusps, trajectories, and the complex virial theorem. *J. Chem. Phys.* **1981**, *74*, 4739–4740.

(88) Shao, Y. et al. Advances in molecular quantum chemistry contained in the Q-Chem 4 program package. *Mol. Phys.* **2015**, *113*, 1–32.

(89) Sanderson, C. *Armadillo: An open source C++ linear algebra library for fast prototyping and computationally intensive experiments*; tech. rep.; NICTA, 2010, pp 1–16.

(90) Taketa, H.; Huzinga, S.; O-Ohata, K. Guassian-Expansion Methods for Molecular Integrals. *J. Phys. Soc. Jpn.* **1966**, *21*, 2313–2334.

(91) Head-Gordon, M.; Pople, J. A method for two-electron Gaussian integral and integral derivative evaluation using recurrence relations. *J. Chem. Phys.* **1988**, *89*, 5777–5786.

(92) Adams, T. R.; Adamson, R. D.; Gill, P. M. W. A tensor approach to two-electron matrix elements. *J. Chem. Phys.* **1997**, *107*, 124.

(93) Obara, S; Saika, A Efficient recursive computation of molecular integrals over Cartesian Gaussian functions. *J. Chem. Phys.* **1986**, *84*, 3963–3974.

(94) McMurchie, L.; Davidson, E. One- and Two-Electron Integrals over Cartesian Gaussian Functions. *J. Comput. Phys.* **1978**, *26*, 218–231.

(95) Gill, P. M. W.; Johnson, B.; Pople, J. Two-electron repulsion integrals over Gaussian s functions. *Int. J. Quantum Chem.* **1991**, *40*, 745–752.

(96) Ishida, K. Accurate and fast algorithm of the molecular incomplete gamma function with a complex argument. *J. Comput. Chem.* **2004**, *25*, 739–748.

(97) Woon, D. E.; Dunning, T. H. Gaussian basis sets for use in correlated molecular calculations. IV. Calculation of static electrical response properties. *J. Chem. Phys.* **1994**, *100*, 2975.

(98) Dunning, T. H. Gaussian basis sets for use in correlated molecular calculations. I. The atoms boron through neon and hydrogen. *J. Chem. Phys.* **1989**, *90*, 1007.

(99) Christophorou, L. G.; Olthoff, J. K.; Rao, M. V. V. S. Electron Interactions with CF_4. *J. Phys. Chem. Ref. Data* **1996**, *25*, 1341.

(100) Ómarsson, F. H.; Szymanska, E.; Mason, N. J.; Krishnakumar, E.; Ingólfsson, O. Quantum Superposition of Target and Product States in Reactive Electron Scattering from CF_4 Revealed through Velocity Slice Imaging. *Phys. Rev. Lett.* **2013**, *111*, 063201.

(101) Xia, L.; Zeng, X.-J.; Li, H.-K.; Wu, B.; Tian, S. X. Orientation Effect in the Low-Energy Electron Attachment to the Apolar Carbon Tetrafluoride Molecule. *Angew. Chem.* **2013**, *125*, 1047–1050.

(102) Varella, M.; Winstead, C.; McKoy, V.; Kitajima, M.; Tanaka, H. Low-energy electron scattering by CH_3F, CH_2F_2, CHF_3, and CF_4. *Phys. Rev. A* **2002**, *65*, 022702.

(103) Huo, W. M. Electron-CF_4 elastic scattering in the static-exchange approximation. *Phys. Rev. A* **1988**, *38*, 3303–3309.

(104) Modelli, A.; Scagnolari, F.; Distefano, G.; Jones, D.; Guerra, M. Electron attachment to the fluoro-, bromo-, and iodomethanes studied by means of electron transmission spectroscopy and Xα calculations. *J. Chem. Phys.* **1992**, *96*, 2061.

(105) Winstead, C.; Sun, Q.; McKoy, V. Low-energy elastic electron scattering by tetrafluoromethane (CF_4). *J. Chem. Phys.* **1993**, *98*, 1105.

(106) Pisanias, M. N.; Christophorou, L. G.; Carter, J. G.; McCorkle, D. L. Compound-negative-ion resonance states and threshold-electron excitation spectra of N-heterocyclic molecules: Pyridine, pyridazine, pyrimidine, pyrazine, and sym-triazine. *J. Chem. Phys.* **1973**, *58*, 2110.

(107) Nenner, I.; Schulz, G. Temporary negative ions and electron affinities of benzene and N-heterocyclic molecules: pyridine, pyridazine, pyrimidine, pyrazine, and s-triazine. *J. Chem. Phys.* **1975**, *62*, 1747–1758.

(108) Mathur, D; Hasted, J. Temporary Negative-Ion States in Pyridine and Diazine Molecules. *Chem. Phys.* **1976**, *16*, 347–352.

(109) Mathur, D; Hasted, J. Resonant scattering of slow electrons from benzene and substituted benzene molecules. *J. Phys. B: At., Mol. Opt. Phys.* **1976**, *9*, 31–37.

(110) Song, J. K.; Lee, N. K.; Kim, S. K. Photoelectron spectroscopy of pyrazine anion clusters. *J. Chem. Phys.* **2002**, *117*, 1589.

(111) Winstead, C.; McKoy, V. Resonant Channel Coupling in Electron Scattering by Pyrazine. *Phys. Rev. Lett.* **2007**, *98*, 113201.

(112) Mašín, Z.; Gorfinkiel, J. D. Elastic and inelastic low-energy electron collisions with pyrazine. *J. Chem. Phys.* **2011**, *135*, 144308.

(113) Palihawadana, P.; Sullivan, J.; Brunger, M.; Winstead, C.; McKoy, V.; Garcia, G.; Blanco, F.; Buckman, S. Low-energy elastic electron interactions with pyrimidine. *Phys. Rev. A* **2011**, *84*, 062702.

(114) Mašín, Z.; Gorfinkiel, J. D. Shape and core excited resonances in electron collisions with diazines. *J. Chem. Phys.* **2012**, *137*, 204312.

(115) Palihawadana, P; Sullivan, J. P.; Buckman, S. J.; Brunger, M. J. Electron scattering from pyrazine: elastic differential and integral cross sections. *J. Chem. Phys.* **2012**, *137*, 204307.

(116) Sütay, B.; Tekin, A.; Yurtsever, M. Intermolecular interactions in nitrogen-containing aromatic systems. *Theor. Chem. Acc.* **2012**, *131*, 1120.

(117) Barbosa, A. S.; Pastega, D. F.; Bettega, M. H. F. Shape resonances in the elastic scattering of slow electrons by pyridine. *Phys. Rev. A* **2013**, *88*, 022705.

(118) Sieradzka, A; Blanco, F; Fuss, M. C.; Mašín, Z; Gorfinkiel, J. D.; García, G Electron scattering from pyridine. *J. Phys. Chem. A* **2014**, *118*, 6657–63.

(119) Junker, B. Recent computational developments in the use of complex scaling in resonance phenomena. *Advances in Atomic and Molecular Physics* **1982**, *18*, 207–263.

(120) Mishra, M.; Öhrn, Y.; Froelich, P. Self-consistent field theory of dilated atomic hamiltonians: Some remarks. *Phys. Lett. A* **1981**, *84*, 4–8.

(121) Frye, D; Armstrong, L. Complex-rotated Hartree-Fock method and its application to the Be- shape resonance. *Phys. Rev. A* **1986**, *34*, 1682–1685.

(122) Bentley, M. Fully numerical complex-coordinate Hartree-Fock calculations for the He 2s2p ^{1,3}P autodetaching states. *Phys. Rev. A* **1990**, *42*, 3826–3829.

(123) Whitenack, D.; Wasserman, A. Density functional resonance theory of unbound electronic systems. *Phys. Rev. Lett.* **2011**, *107*, 163002.

(124) Zhou, Y.; Ernzerhof, M. Calculating the lifetimes of metastable states with complex density functional theory. *J. Phys. Chem. Lett.* **2012**, *3*, 1916–1920.

(125) Zhou, Y.; Ernzerhof, M. Open-system Kohn-Sham density functional theory. *J. Chem. Phys.* **2012**, *136*, 094105.

(126) Larsen, A. H.; De Giovannini, U.; Whitenack, D. L.; Wasserman, A.; Rubio, A. Stark Ionization of Atoms and Molecules within Density Functional Resonance Theory. *J. Phys. Chem. Lett.* **2013**, *4*, 2734–2738.

(127) Yeager, D. L.; Mishra, M. K. Algebraic modifications to second quantization for non-Hermitian complex scaled hamiltonians with application to a quadratically convergent multiconfigurational self-consistent field method. *Int. J. Quantum Chem.* **2005**, *104*, 871–879.

(128) Samanta, K.; Yeager, D. L. Obtaining Positions and Widths of Scattering Resonances from a Complex Multiconfigurational Self-Constent Field State Using the M1 Method. *Int. J. Quantum Chem.* **2010**, *110*, 798–812.

(129) Žd'Ánská, P. R.; Moiseyev, N. Hartree-Fock orbitals for complex-scaled configuration interaction calculation of highly excited Feshbach resonances. *J. Chem. Phys.* **2005**, *123*, DOI: 10.1063/1.2110169.

(130) Zhang, S. B.; Yeager, D. L. A complex scaled multi-reference configuration interaction method to study Li and Li-like cations (Be, B, C, N, O) Auger resonances 1s2s2 2S and 1s(2s2p 3P) 2P. *J. Mol. Struct.* **2012**, *1023*, 96–100.

(131) Zhang, S. B.; Yeager, D. L. Complex-scaled multireference configuration-interaction method to study Be and Be-like cations' (B, C, N, O, Mg) Auger resonances 1s2s22p ^{1,3}P. *Phys. Rev. A* **2012**, *85*, 032515.

(132) Bravaya, K. B.; Zuev, D.; Epifanovsky, E.; Krylov, A. I. Complex-scaled equation-of-motion coupled-cluster method with single and double substitutions for autoionizing excited states: theory, implementation, and examples. *J. Chem. Phys.* **2013**, *138*, 124106.

(133) Sajeev, Y.; Ghosh, a.; Vaval, N.; Pal, S. Coupled cluster methods for autoionisation resonances. *Int. Rev. Phys. Chem.* **2014**, *33*, 397–425.

(134) Roothaan, C. Self-Consistent Field Theory for Open Shells of Electronic Systems. *Rev. Mod. Phys.* **1960**, *32*, 179–185.

(135) Davidson, E.; Stenkamp, L. SCF Methods for Excited States. *Int. J. Quantum Chem.* **1976**, *31*, 21–31.

(136) Plakhutin, B. N.; Gorelik, E. V.; Breslavskaya, N. N. Koopmans' theorem in the ROHF method: Canonical form for the Hartree-Fock Hamiltonian. *J. Chem. Phys.* **2006**, *125*, 204110.

(137) Pople, J. a.; Nesbet, R. K. Self-Consistent Orbitals for Radicals. *J. Chem. Phys.* **1954**, *22*, 571.

(138) Harris, F. E.; Pohl, H. a. Split-Shell Molecular Orbitals for Sigma-Bonded Systems: Hydrogen Halides. *J. Chem. Phys.* **1965**, *42*, 3648–3651.

(139) Small, D. W.; Sundstrom, E. J.; Head-Gordon, M. Restricted Hartree Fock using complex-valued orbitals: A long-known but neglected tool in electronic structure theory. *J. Chem. Phys.* **2015**, *142*, 024104.

(140) Gilbert, A. T. B.; Besley, N. a.; Gill, P. M. W. Self-consistent field calculations of excited states using the maximum overlap method (MOM). *J. Phys. Chem. A* **2008**, *112*, 13164–13171.

(141) Pulay, P Ab initio calculation of force constants and equilibrium geometries in polyatomic molecules. *Mol. Phys.* **1969**, *17*, 197–204.

(142) Head-Gordon, M.; Grana, A. M.; Maurice, D.; White, C. a. Analysis of Electronic Transitions as the Difference of Electron Attachment and Detachment Densities. *J. Phys. Chem.* **1995**, *99*, 14261–14270.

(143) Hazi, A.; Rescigno, T.; Kurilla, M. Cross sections for resonant vibrational excitation of N_2 by electron impact. *Phys. Rev. A* **1981**, *23*, 1089–1099.

(144) Meyer, H.-D. Optical potentials for electron-molecule scattering: A comparative study on the N_2 $^2\Pi_g$ resonance. *Phys. Rev. A* **1989**, *40*, 5605–5613.

(145) Mahalakshmi, S.; Venkatnathan, A.; Mishra, M. K. Application of higher order decouplings of the dilated electron propagator to $^2\Pi_g$ CO^-, $^2\Pi_g$ N_2 - and $^2\Pi_g$ C_2H_2 - shape resonances. *J. Chem. Phys.* **2001**, *115*, 4549–4557.

(146) Falcetta, M. F.; Difalco, L. A.; Ackerman, D. S.; Barlow, J. C.; Jordan, K. D. Assessment of Various Electronic Structure Methods for Characterizing Temporary Anion States: Application to the Ground State Anions of N_2, C_2H_2, C_2H_4 and C_6H_6. *J. Phys. Chem. A* **2014**, *118*, 7489–7497.

(147) Berman, M.; Estrada, H.; Cederbaum, L. S.; Domcke, W. Nuclear dynamics in resonant electron-molecule scattering beyond the local approximation: The 2.3-eV shape resonance in N_2. *Phys. Rev. A* **1983**, *28*, 1363–1381.

(148) Levin, D. A.; Fliflet, A. W.; McKoy, V. Low-energy e^--CO scattering in the static-exchange approximation. *Phys. Rev. A* **1980**, *21*, 1202–1209.

(149) Donnelly, R. a. Second-order calculation on the doublet pi CO shape resonance. *Int. J. Quantum Chem.* **1985**, *28*, 363–368.

(150) Ehrhardt, H.; Langhans, L.; Linder, F.; Taylor, H. S. Resonance scattering of slow electrons from H_2 and CO angular distributions. *Phys. Rev.* **1968**, *173*, 222–230.

(151) Lucchese, R. R.; McKoy, V. Study of electron scattering by CO_2 at the static-exchange level. *Phys. Rev. A* **1982**, *25*, 1963–1967.

(152) Lee, C.-H.; Winstead, C.; McKoy, V. Collisions of low-energy electrons with CO_2. *J. Chem. Phys.* **1999**, *111*, 5056.

(153) Sanche, L. Electron transmission spectroscopy: Resonances in triatomic molecules and hydrocarbons. *J. Chem. Phys.* **1973**, *58*, 479.

(154) Rescigno, T.; McCurdy, C. W.; Schneider, B. Accurate Ab Initio Treatment of Low-Energy Electron Collisions with Polyatomic Molecules: Resonant Electron-Formaldehyde Scattering. *Phys. Rev. Lett.* **1989**, *63*, 248–251.

(155) Mahalakshmi, S; Mishra, M. The 2B1 shape resonance in electron-formaldehyde scattering: an investigation using the dilated electron propagator method. *Chem. Phys. Lett.* **1998**, *296*, 43–50.

(156) Kaur, S.; Baluja, K. L. -Matrix Method. *J. Phys. B: At., Mol. Opt. Phys.* **2005**, *38*, 3917–3933.

(157) Benoit, C.; Abouaf, R. Low-energy electron collisions with formaldehyde: interference phenomena in the differential vibrational excitation cross section. *Chem. Phys. Lett.* **1986**, *123*, 134–138.

(158) Isaacs, W.; McCurdy, C.; Rescigno, T. Theoretical support for a Ramsauer-Townsend minimum in electron-CF_4 scattering. *Phys. Rev. A* **1998**, *58*, 309–313.

(159) Curik, R; Gianturco, F. a.; Sanna, N Electron and positron scattering from halogenated methanes: a comparison of elastic cross sections. *J. Phys. B: At., Mol. Opt. Phys.* **2000**, *33*, 615–635.

(160) Bjarnason, E. H.; Ómarsson, F. H.; Hoshino, M.; Tanaka, H.; Brunger, M. J.; Limão Vieira, P.; Ingólfsson, O. Negative ion formation through dissociative electron attachment to the group IV tetrafluorides: Carbon tetrafluoride, silicon tetrafluoride and germanium tetrafluoride. *Int. J. Mass Spectrom.* **2013**, *339-340*, 45–53.

(161) Yoon, J. S.; Song, M. Y.; Kato, H.; Hoshino, M.; Tanaka, H.; Brunger, M. J.; Buckman, S. J.; Cho, H. Elastic cross sections for electron collisions with molecules relevant to plasma processing. *J. Phys. Chem. Ref. Data* **2010**, *39*, 033106.

(162) Jagau, T.-c.; Krylov, A. I. Complex Absorbing Potential Equation-of-Motion Coupled-Cluster Method Yields Smooth and Internally Consistent Potential Energy Surfaces and Lifetimes for Molecular Resonances. *J. Phys. Chem. Lett.* **2014**, *5*, 3078–3085.

(163) Herzenberg, A Oscillatory energy dependence of resonant electron-molecule scattering. *Journal of Physics B* **1968**, *1*, 548–558.

(164) Dubé, L.; Herzenberg, A. Absolute cross sections from the "boomerang model" for resonant electron-molecule scattering. *Phys. Rev. A* **1979**, *20*, 194–213.

(165) Junker, B. R. Complex-coordinate method. II. Resonance calculations with correlated target-state wave functions. *Phys. Rev. A* **1978**, *18*, 2437–2442.

(166) Samanta, K.; Yeager, D. L. Investigation of P be shape resonances using a quadratically convergent complex multiconfigurational self-consistent field method. *J. Phys. Chem. B* **2008**, *112*, 16214–16219.

(167) Tsednee, T.; Liang, L.; Yeager, D. L. Electron-atom resonances: The complex-scaled multiconfigurational spin-tensor electron propagator method for the ^{2}P Be shape resonance problem. *Phys. Rev. A* **2015**, *91*, 022506.

(168) Ghosh, A.; Vaval, N.; Pal, S. Equation-of-motion coupled-cluster method for the study of shape resonance. *J. Chem. Phys.* **2012**, *136*, 234110.

(169) Ghosh, A.; Vaval, N.; Pal, S.; Bartlett, R. J. Complex absorbing potential based equation-of-motion coupled cluster method for the potential energy curve of CO2 anion. *J. Chem. Phys.* **2014**, *141*, 164113.

(170) Landau, A.; Haritan, I.; Kapralova-Zdanska, P. R.; Moiseyev, N. Advantages of complex scaling only the most diffuse basis functions in simultaneous description of both resonances and bound states. *Mol. Phys.* **2015**, *113*, 3141–3146.

(171) Purvis, G. D.; Bartlett, R. J. A full coupled-cluster singles and doubles model: The inclusion of disconnected triples. *J. Chem. Phys.* **1982**, *76*, 1910–1918.

(172) Nooijen, M.; Bartlett, R. J. Equation of motion coupled cluster method for electron attachment. *J. Chem. Phys.* **1995**, *102*, 3629.

(173) Knowles, P. J.; Andrews, J. S.; Amos, R. D.; Handy, N. C.; Pople, J. A. Restricted Moller-Plesset theory for open-shell molecules. *Chem. Phys. Lett.* **1991**, *186*, 130–136.

(174) Bartlett, R. J.; Musiał, M. Coupled-cluster theory in quantum chemistry. *Rev. Mod. Phys.* **2007**, *79*, 291–352.

(175) Krylov, A. I. Equation-of-motion coupled-cluster methods for open-shell and electronically excited species: the Hitchhiker's guide to Fock space. *Annu. Rev. Phys. Chem.* **2008**, *59*, 433–62.

(176) Dunning Jr, T. H. Gaussian basis sets for use in correlated molecular calculations. V. Core-valence basis set for boron through neon. *J. Chem. Phys.* **1995**, *103*, 4572–4585.

(177) Sommerfeld, T.; Tarantelli, F Ab initio calculation of energies and lifetimes of metastable dianions: The C22 resonance. *J. Chem. Phys.* **2000**, *112*, 6635–6642.

(178) Izmaylov, A. F.; Adamson, S. O.; Zaitsevskii, A. Multipartitioning many-body perturbation theory calculations on temporary anions: applications to N_2 and CO. *J. Phys. B: At., Mol. Opt. Phys.* **2004**, *37*, 2321–2329.

(179) Sommerfeld, T.; Ehara, M. Short-range stabilizing potential for computing energies and lifetimes of temporary anions with extrapolation methods. *J. Chem. Phys.* **2015**, *142*, 034105.

(180) Ehara, M.; Sommerfeld, T. CAP/SAC-CI method for calculating resonance states of metastable anions. *Chem. Phys. Lett.* **2012**, *537*, 107–112.

(181) Eliezer, I; Taylor, H. S.; Williams, J. K. Resonant States of H_2^-. *J. Chem. Phys.* **1967**, *47*, 2165.

(182) Stibbe, D. T.; Tennyson, J. Electron- scattering resonances as a function of bond length. *J. Phys. B: At., Mol. Opt. Phys.* **1998**, *31*, 815–844.

(183) Bardsley, J. N.; Cohen, J. S. Variational calculations of resonant states of H_2^-. *J. Phys. B: At., Mol. Opt. Phys.* **1978**, *11*, 3645–3654.

(184) Mundel, C.; Berman, M.; Domcke, W. Nuclear dynamics in resonant electron-molecule scattering beyond the local approximation: Vibrational excitation and dissociative attachment in H_2 and D_2. *Phys. Rev. A* **1985**, *32*, 181–193.

(185) Krylov, A. I. Size-consistent wave functions for bond-breaking: The equation-of-motion spin-flip model. *Chem. Phys. Lett.* **2001**, *338*, 375–384.

(186) Andersen, T. Atomic negative ions: Structure, dynamics and collisions. *Phys. Rep.* **2004**, *394*, 157–313.

(187) Gopalan, A.; Bömmels, J.; Götte, S.; Landwehr, A.; Franz, K.; Ruf, M. W.; Hotop, H.; Bartschat, K. A novel electron scattering apparatus combining a laser photoelectron source and a triply differentially pumped supersonic beam target: Characterization and results for the He^- (1s2s2) resonance. *Eur. Phys. J. D* **2003**, *22*, 17–29.

(188) Brunt, J. N. H.; King, G. C.; Read, F. H. Resonance structure in elestic electron scattering from helium, neon, and argon. *J. Phys. B: At., Mol. Opt. Phys.* **1977**, *10*, 1289–1301.

(189) Kennerly, R. E.; Van Brunt, R. J.; Gallagher, A. C. High-resolution measurement of the helium $1s2s^2$ ^2S resonance profile. *Phys. Rev. A* **1981**, *23*, 2340–2442.

(190) Buckman, S. J.; Hammond, P.; Read, F. H.; King, G. C. Highly-excited double Rydberg states of He^-. *J. Phys. B: At., Mol. Opt. Phys.* **1983**, *11*, 4039–4047.

(191) Dube, D.; Tremblay, D.; Roy, D. Analysis of the first Feshbach resonances in electron collisions in rare gases. *Phys. Rev. A* **1993**, *47*, 2893–2903.

(192) Bylicki, M. The Hermitian representation of the complex-rotation method and its application to the $ls2s^2$ ^2S resonance of He^-. *J. Phys. B: At., Mol. Opt. Phys.* **1991**, *24*, 413–421.

(193) Gil, T.; McCurdy, C. W.; Lengsfield, B. H. Convergence of the projected optical potential in a complex Kohn calculation of elastic e-He scattering. *J. Phys. B: At., Mol. Opt. Phys.* **1993**, *26*, 509–516.

(194) Jordan, K. D.; Voora, V. K.; Simons, J. Negative electron affinities from conventional electronic structure methods. *Theor. Chem. Acc.* **2014**, *133*, 1–5.

(195) Kukulin, V. I.; Krasnopolsky, V. M.; Horáček, J., *Theory of Resonances: Principles and Applications*; Kluwer Academic: 1989.

(196) Schneider, B. R-matrix theory for electron-atom and electron–molecule collisions using analytic basis set expansions. *Chem. Phys. Lett.* **1975**, *31*, 237–241.

(197) Lucchese, R. R.; Watson, D.; McKoy, V. Iterative approach to the Schwinger variational principle for electron-molecule collisions. *Phys. Rev. A* **1980**, *22*, 421–426.

(198) Schneider, B. I.; Rescigno, T. N. Complex Kohn variational method: Application to low-energy electron-molecule collisions. *Phys. Rev. A* **1988**, *37*, 3749–3754.

(199) Winkler, P. Calculation of Electron Hydrogen Scattering Resonances by the Coordinate-Rotation Method. *Zeitschrift für Physik A Atoms and Nuclei* **1977**, *160*, 149–160.

(200) Nestmann, B; Peyerimhoff, S. D. Calculation of the discrete component of resonance states in negative ions by variation of nuclear charges. *J. Phys. B: At. Mol. Phys.* **1985**, *18*, 615–626.

(201) Nestmann, B. M.; Peyerimhoff, S. D. CI method for determining the location and width of resonances in electron-molecule collision processes. *J. Phys. B: At. Mol. Phys.* **1985**, *18*, 4309–4319.

(202) Papp, P.; Matejčík, Š.; Mach, P.; Urban, J.; Paidarová, I.; Horáček, J. Analytical continuation in coupling constant method; application to the calculation of resonance energies and widths for organic molecules: Glycine, alanine and valine and dimer of formic acid. *Chem. Phys.* **2013**, *418*, 8–13.

(203) Horáček, J.; Paidarová, I.; Čurík, R. On a simple way to calculate electronic resonances for polyatomic molecules. *J. Chem. Phys.* **2015**, *143*, 184102.

(204) Čurík, R.; Paidarová, I.; Horáček, J. The 2Πg shape resonance of acetylene anion: an investigation with the RAC method. *Euro. Phys. J. D.* **2016**, *70*, 146.

(205) Bessis, D. Padé approximations in noise filtering. *J. Comput. Appl. Math.* **1996**, *66*, 85–88.

(206) Baker, G. A.; Graves-Morris, P., *Padé Approximants*; Cambridge University Press: 1996.

(207) Horáček, J.; Paidarová, I.; Curik, R Determination of the Resonance Energy and Width of the $^2B_{2g}$ Shape Resonance of Ethylene with the Method of Analytical Continuation in the Coupling Constant. *J. Phys. Chem. A* **2014**, *118*, 6536–6541.

(208) Adamson, R.; Dombroski, J.; Gill, P. Efficient calculation of short-range Coulomb energies. *J. Comput. Chem.* **1999**, *20*, 921–927.

(209) Besley, N. A.; Peach, M. J. G.; Tozer, D. J. Time-dependent density functional theory calculations of near-edge X-ray absorption fine structure with short-range corrected functionals. *Physical Chemistry Chemical Physics* **2009**, *11*, 10350–10358.

(210) Tao, L.; McCurdy, C. W.; Rescigno, T. N. Grid-based methods for diatomic quantum scattering problems: A finite-element discrete-variable representation in prolate spheroidal coordinates. *Physical Review A - Atomic, Molecular, and Optical Physics* **2009**, *79*, 1–9.

(211) Tao, L.; McCurdy, C. W.; Rescigno, T. N. Grid-based methods for diatomic quantum scattering problems. II. Time-dependent treatment of single- and two-photon ionization of H_2^+. *Physical Review A - Atomic, Molecular, and Optical Physics* **2009**, *80*, 1–7.

(212) Tao, L.; McCurdy, C. W.; Rescigno, T. N. Grid-based methods for diatomic quantum scattering problems. III. Double photoionization of molecular hydrogen in prolate spheroidal coordinates. *Physical Review A - Atomic, Molecular, and Optical Physics* **2010**, *82*, 1–9.

(213) Guberman, S. L.; Giusti-Suzor, A. The generation of O(1S) from the dissociative recombination of O_2^+. *J. Chem. Phys.* **1991**, *95*, 2602–2613.

(214) Miller, W. H.; Morgner, H. A unified treatment of Penning ionization and excitation transfer. *J. Chem. Phys.* **1977**, *67*, 4923–4930.

(215) Sánchez, I.; Martín, F. The doubly excited states of the H_2 molecule. *J. Chem. Phys.* **1997**, *106*, 7720–7730.

(216) Morales, F.; McCurdy, C. W.; Martín, F. Validity of the isolated resonance picture for H_2 autoionizing states. *Phys. Rev. A* **2006**, *73*, 014702.

(217) Domcke, W Analytic theory of resonances and bound states near Coulomb thresholds. *J. Phys. B: At. Mol. Phys.* **1983**, *16*, 359.